Czech Technical University in Prague

Faculty of Electrical Engineering

Doctoral Thesis

February 2015

Jakub SVATOŠ

Czech Technical University in Prague

Faculty of Electrical Engineering
Department of Measurement

Advanced Instrumentation for Polyharmonic Metal Detectors

Doctoral Thesis

Jakub Svatoš

Prague, *February 2015*

Ph.D. Programme: *Electrical Engineering and Information Technology*
Branch of study: *Measurement and Instrumentation*

Supervisor: ***Assoc. Prof. Josef Vedral, CSc.***
Supervisor-Specialist: ***Assoc. Prof. Jan Holub, Ph.D.***

Poděkování

Na tomto místě bych předně rád poděkoval svému školiteli doc. Ing. Josefu Vedralovi, CSc. za poskytnutý námět, konzultace a odborné vedení při tvorbě této disertační práce a také školiteli specialistovi doc. Ing. Janu Holubovi, Ph.D. Dále bych rád poděkoval všem, kdo se cennými radami podíleli na vzniku této práce, jmenovitě doc. Ing. Petru Kašparovi, CSc., doc. Ing. Radislavu Šmídovi, Ph.D. a prof. Ing. Vladimíru Haaszovi, CSc.

Další poděkovaní patří všem kolegům z katedry měření na ČVUT a katedry elektrotechniky a automatizace na ČZU, kteří svými konzultacemi pomohli vyřešit spoustu dílčích problémů. Speciálně bych rád poděkoval p. Kočové za její ochotu a vstřícnost při řešení administrativních činností.

V neposlední řadě bych rád srdečně poděkoval své rodině za vytvoření výborných podmínek, za trpělivost a za plnou podporu při tvorbě této disertační práce.

Čestné prohlášení

Čestně prohlašuji, že disertační práci na téma „Advanced Instrumentation for Polyharmonic Metal Detectors“ jsem vypracoval samostatně a použil k tomu úplný výčet citací z literatury uvedené v seznamech na konci každé jednotlivé kapitoly této práce. Nemám námitek proti půjčování nebo zveřejňování mé disertační práce, nebo jejích částí. Taktéž nemám námitek proti využití výsledků této práce Elektrotechnickou fakultou ČVUT, a to se souhlasem katedry měření.

Abstrakt

Předmětem této disertační práce je užití polyharmonických signálů pro detekci kovů. Zásadním problémem všech běžných detektorů kovů pracujících na bázi vířivých proudů je omezená možnost identifikace detekovaných předmětů. To je způsobeno tím, že většina detektorů kovů s diskriminační schopností používá jako buzení pouze jeden kmitočet. Informace o detekovaném předmětu je tudíž obsažena jen v jedné frekvenci, respektive v její fázi. Vzhledem k tomu, že některé objekty mají podobnou odezvu, je diskriminační schopnost těchto detektorů omezena. Hledá-li operátor specifický materiál (např. zlato), může nastat situace, že tento může být zaměněn za materiál s podobnou odezvou (např. alobal). Další oblast, kde je třeba zlepšit schopnost diskriminace detektorů, jsou humanitární organizace zabývající se odminováváním oblastí. Detekci jedné miny předchází až tisíc falešných poplachů.

Budicí signál a jeho zpracování detektorem by proto mělo být provedeno tak, aby lépe charakterizoval detekovaný objekt. Užití polyharmonických signálů a jejich pokročilé zpracování nabízí příležitost, jak zlepšit detekční schopnosti detektorů. Tato disertační práce se zabývá použitím těchto netradičních polyharmonických signálů jako budicích signálů pro detektory kovů pracujících na bázi vířivých proudů. V práci jsou popsány principy detektorů kovů, jak z fyzikálního, tak i z technologického hlediska. Uvedeny jsou dva základní typy aktivních detektorů kovů. Pozornost je věnována také běžným konfiguracím hledacích hlav detektorů. Chování elektromagnetické indukce je vysvětleno pomocí jednoduchého obvodového modelu. Odezva pro specifický tvar objektu – koule, pro oba typy materiálů – feromagnetických a neferomagnetických, je také prezentována v teoretické části práce.

V praktické části práce jsou vyhodnoceny změřené výsledky tří různých budicích multifrekvenčních signálů. Tyto budicí signály jsou step sweep sine-wave signál, chirp signál a sinc signál. Práce je orientována hlavně na signál sinc. Výsledky z experimentálního měření jsou zpracovány, jak v časové, tak ve frekvenční oblasti. V časové oblasti jsou prezentovány výsledky dosažené pomocí standardních integrálních parametrů signálu. Ve frekvenční oblasti jsou prezentovány amplitudová a fázová spektra spolu s polárními grafy. V rámci práce byla na základě experimentálních měření provedena klasifikace měřených objektů. Klasifikace, jak do tříd feromagnetických a neferomagnetických materiálů, tak do tříd jednotlivých testovaných materiálů. Závěrem byla provedena klasifikace odhadu velikosti objektu. Jako klasifikátor byl spolu s dalšími primárně použit ‘support vektor‘ klasifikátor.

Díky použití více frekvencí je odezva detekovaného předmětu změřena v širším frekvenčním pásmu. V takovéto odezvě je informace o detekovaném předmětu nesena ve více frekvencích, respektive jejich amplitudách a fázích. To umožňuje lépe charakterizovat detekovaný předmět ve srovnání s klasickou metodou použití pouze jedné frekvence. Experimentální výsledky ukázaly, že použití vhodného polyharmonického signálu může zlepšit identifikaci předmětu, v porovnání s běžnými metodami, vyžívající pouze jednu frekvenci.

Abstract

The dissertation concerns the application of polyharmonic signals in devices for metal object detection. A basic problem of conventional eddy current metal detectors (induction devices in general) lies in its limited possibilities of discrimination or identification of detected objects. It is due to the fact that most of eddy current metal detectors with some limited discrimination ability use only one frequency excitation signal. Therefore the information about detected object is carried only in one frequency, in its phase shift respectively. It leads to limited discrimination ability due to the fact that some of detected objects have similar response in this case. For example if an operator looks for a specific material (e.g. gold) the response can be misinterpreted for material which has similar one (e.g. tinfoil). Another area where improvement of detectors identification ability is useful is humanitarian demining. There is usually a great amount (in average about 1000) of false alarms to one detected mine.

To better characterize the detected object, the excitation signal and the following signal processing in the detector should be done. Application of polyharmonic excitation signal and its processing could bring an opportunity to improve the determination ability. Therefore the dissertation deals with finding some suitable polyharmonic signals applicable for this purpose. The two types of active metal detectors using various types of their search head /coils configuration) were introduced. Behavior of electromagnetic induction is explained using a Simple circuit model. Response function for specific cases of the object`s shape (the homogenous sphere for two types of materials, ferromagnetic and non-ferromagnetic) is introduced.

Three different excitation polyharmonic signals for an eddy currents metal detector were evaluated. Step sweep sine-wave signal, chirp signal, and a sine cardinal (sinc) signal were taken into account. The work was mainly focused to the modifying sinc signal. Experimental measurements were processed in both time and frequency domain. Spheres of different diameters and from different ferrous and non-ferrous materials were used as specimens. In the time domain, standard integral parameters of the response (RMS and peak value and crest factor) were calculated. In the frequency domain amplitude and phase spectra were calculated and presented together with polar graphs. As part of the work, classifications of ferrous and non-ferrous materials were done based of measured data as well as classification of individual ferrous including non-ferrous materials and estimation of the size of the classified object. Support vector classifier was primarily used for data classification (together with other classifiers).

Thanks to multiple frequencies a response of detected object is measured in a wide band. In the response, information about detected object is carried by multiple phases and amplitudes and one gets more detailed information about a detected object than by using classical single-tone methods. Experimental results verified that application of a suitable multifrequency signal can bring more accurate identification of property of detected metal object than by using classical single-tone methods.

List of Abbreviations

ADC	Analogue-to-Digital Converter
AP	Anti-Personnel
ATMID	All Terrain Mine Detector
BFO	Beat-Frequency Oscillator
CF	Crest Factor
CMAC	Cambodian Mine Action Centre
CROMAC	CROatian Mine Action Centre
CW	Continuous Wave
DDS	Direct Digital Synthesizer
DFT	Discrete Fourier Transformation
ENOB	Effective Number Of Bits
EM	ElectroMagnetic
EMF	ElectroMotive Force
FFT	Fast Fourier Transform
FIR	Finite Impulse Response
GPR	Ground Penetrating Radar
KNN	k-Nearest Neighbors
KNNC	k-Nearest Neighbors Classifier
LDA	Linear Discriminant Analysis
MAG	Mines Advisory Group
NMC	Nearest Mean Classifier
PCA	Principal Component Analysis
PI	Pulse Induction
RX	Receiving
SGS	Specialist Ghurkha Services
SINAD	SIgnal-to-Noise And Distortion ratio
SNR	Signal-to-Noise Ratio
SVM	Support Vector Machines
SVC	Support Vector Classifier
TTL	Transistor-Transistor Logic
TADS	Technical Assistance to Demining Service
TX	Transmitting
UXO	UneXploded Ordnance
VLF	Very Low Frequency

Contents

1. Introduction 3
1.1. Mine Clearance 3
1.2. Archeology and Treasure Hunting 4
1.3. Security 5
1.4. Summary 5
2. State of the Art 7
2.1. Types of Metal Detectors 7
2.1.1. Time Domain Metal Detectors 7
2.1.2. Frequency Domain Metal Detectors 9
2.2. Search Head – Coil Basic 14
2.2.1. Search Coil Size and Shapes 14
2.2.2. Search Coils Configuration 15
2.3. Ground Balancing 17
2.4. All Terrain Mine Detector 18
2.5. Summary 20
3. Objectives 23
4. Proposed Methods 25
4.1. Theoretical Background 25
4.2. Modeling of Electromagnetic Induction 27
4.3. All Terrain Mine Detector Searching Head 34
4.4. Polyharmonic Signal Limitations 38
4.5. Summary 39
5. Measured and Processed Data 41
5.1. Step Sweep Sine-wave Signal 41
5.2. Linear Frequency Sweep - Chirp Signal 51
5.3. Sinc Signal 56
5.3.1. Signal Processing in Time Domain 60
5.3.2. Signal Processing in Frequency Domain 66

5.4. Summary 76
6. Data Classification 79
6.1. Data Preprocessing 81
6.2. Support Vector Machines Classifier 85
6.3. Data Classification 87
6.3.1. Classification of Ferrous and Non-ferrous Materials 91
6.3.2. Classification of Individual Non-ferrous Materials 92
6.3.3. Classification of Individual Ferrous Materials 94
6.3.4. Objects Sizes Classification 96
6.4. Summary 98
7. Conclusion 101
7.1. Future Research 104
8. List of Publications 105
8.1. Related with Thesis 105
8.1.1. Publications in Journals with Impact Factor 105
8.1.2. Publications in ISI 105
8.1.3. Other Publications 105
8.2. Non-related with Thesis 106
8.2.1. Publications in Journals with Impact Factor 106
8.2.2. Publications in ISI 106
8.2.3. Other Publications 107

1. Introduction

Metal detectors are an important part of our lives in present time. There are used at the airports or in important buildings, where walk-through security metal detectors serve to improve the security. Amateur treasure hunters or archaeologists use detectors to detect ancient artefacts and old coins. Metal detection and classification is also widely used in pharmacy, food, beverage or chemical industries and military. Last but not least, metal detectors are used in humanitarian demining, where a handheld metal eddy current detectors plays a key role during land clearance from explosives remnants of wars.

There are many methods to detect metal object or mine [1] but eddy current metal detectors are still the most popular detectors in humanitarian demining, for hobbyist treasure hunters and for archeologist because of their low cost. Ground penetrating radars (GPR), which are much better in detection and discrimination capabilities, are extremely expensive [2] and [3]. Metal detectors based on the eddy current principle typically convert the complex received signal into an acoustic signal. This acoustic output signal reports the presence of a metallic object to the user (treasure hunter, archeologist or deminer). Accurate locating in the two-dimensional positioning (pinpointing) of a detected buried metal object is easily possible for a qualified deminer [4].

Main problem remains in identifying of detected object. If the operator finds any object there is still doubt what kind of target is found. Even with discrimination ability, there is still a challenge to avoid undesirable metal materials. This is due to the fact that some of them have similar response (for example tinfoil and gold). Thus, improperly setting of discrimination ability of certain metal materials increases the risk of ignoring the objects. For this reason, better discrimination ability should be undertaken [5].

1.1. Mine Clearance

The World War and World War II had a significant impact on metal detectors. Many new types of metal detectors were further improved for military purposes, especially for land mine detection. After these wars detectors were used for humanitarian demining to clear unexploded buried land mines.

Nowadays large numbers of land mines are buried in the soil. That causes significant problem across the world. They are placed manually or by special mining vehicles approximately 40 cm deep into the ground. The greatest danger they present is their invisibility not only for soldiers but also for civilians. Removal of the mines following a military conflict is a difficult task. Probably, the antipersonnel land mines are the biggest problem. There are about sixty to seventy billion antipersonnel mines buried in seventy countries [6] and [7]. There

are two types of land mines: antitank and antipersonnel (AP). Antitank mines are much larger and more powerful than AP mines. However, AP mines are the most common type of mines and also the most difficult to find. AP mines kill or cripple 26 thousand people each year. The statistics say that half of these victims are civilians, mostly children younger than sixteen years of age. Effective demining of land mines means that close to 100 % of the mines in the demined area must be detected as fast as possible and with minimum number of false alarms (mistaking a different objects for a buried mine). Nowadays there is no existing land mine detection system which meets these criteria. Reasons for this failure are especially the variety of environments in which the mines are buried and the limits or flaws of current technology [8] and [9].

Another obstacle in removing buried mines is nature itself. Even if accurate maps about distribution of mines can be made, they could not be taken for granted because of floods, quicksand, and other phenomena which can completely invalidate the contents of such records. This problem does not only concern mines but all unexploded ordnance (UXO). Detonation is typically triggered by pressure or in some cases by activating a tripwire or similar mechanisms. Therefore a land mine detector must work without physically contacting the mine. Also a detector must be able to locate all types of mines in different environments.

1.2. Archeology and Treasure Hunting

In recent times, the development of archaeology brought a significant rise of treasure (or relic) hunting like "artifact seeking", "site looting", "coin shooting" or looking for valuable metals in their natural forms. Coin shooters are looking for present day coins which were lost after events where many people are involved, like festivals or concerto. Advanced “hunters” may look for any old coins, bullets, ancient weapons or conduct historical research to locate an archeological or historical site. This led to a large increase in use of metal detectors.

The first recorded use of a metal detector by an archeologist is dated in 1958 by military historian Don Rickey, who used metal detector to detect the firing lines at Little Big Horn [10]. Recently, cooperation between professional archeologists and metal detecting hobbyists have begun even though archaeologists oppose the use of metal detectors by hobbyists or "site looters" whose activities disrupt or even damage archaeological sites. Because treasure hunting, is becoming more and more popular in these days this result in more producers, who researching new technologies and methods in metal detection. Manufacturers generally try to put on additional features, such as discrimination - metal detector can be muted for a specific material and remain silent when situated upon it. Notching discrimination is another new feature which can distinguish between different objects. But these features are inaccurate. An attractive goal for manufacturers is to improve discrimination ability of detectors.

Another possible function is Ground Balancing which is either automatic or manually adjustable. This function is based on filtering the selected phase shift, which may have a negative effect - the loss of information on the searched subject [11].

1.3. Security

Metal detectors are widely used as a security screening at the airports, in governor buildings or at important events or meetings, especially after recent increase of terrorist attacks. In common with the developments in mine clearance or treasure hunting uses of metal detectors, both pulse and continuous wave systems are used. Construction of these detectors can be handheld or walk-through. Targeted objects, such as weapons (e.g. guns and knives), should be consistently and accurately detected, while personal items (e.g. keys, coins, belts) should pass through without causing an alarm.

1.4. Summary

Electromagnetic detectors remain the most commonly used type of metal detectors, though it has its shortcomings - detectors poorly recognize or discriminate specific materials or mines. For example in humanitarian demining, there is still done major detection and clearance work using manual methods. This method is accurate but very slow – the rate usually does not exceed 100 m^2 per deminer per day [8]. After a war the soil is contaminated by large amounts of shrapnel, metal scraps, etc., and this leads to false alarms – depending on location between 100 and 1,000 false alarms for each real mine. The decrease of these false alarms is therefore desirable [12].

The excitation signal and signal processing in the detector should be done in a way to avoid false alarms. Also the detectors should be able to work properly in challenging conditions, but mainly they should detect any dangerous objects. Use of multi-tone excitation signal can be considered. Such signals should be composed of suitable frequencies and the resulting received signal spectrum can be evaluated.

[1] Bielecki, Z., Janucki, J., et al, 2012. Sensors And Systems For The Detection Of Explosive Devices – An Overview, *Metrology and Measurement Systems*, vol. XIX, no. 1, pp. 3-28.

[2] Amazeen, C. A., Locke M. C., 1998. Developmental Status of The U.S. Army's New Handheld Standoff Mine Detection System (Hstamids), *U.S. Army Communications and Electronics Command Night Vision and Electronic Sensors Directorate (NVESD)*, USA.

[3] Doheny, R. C., Burke, S., Cresci, R., Ngan, P.: Walls, R., 2008. Handheld Standoff Mine Detection System (HSTAMIDS) Field Evaluation in Thailand, *Assistant Secretary of Defense, (Special Operations and Low - Intensity Conflict)*.

[4] Composite Autors, 1997. *Metal Detector Basic and Theory*, Fortress Technology Inc.

[5] Krüger, H., Ewald, H., 2008. Handheld metal detector with online visualisation and classification for the humanitarian mine clearance, *IEEE SENSORS 2008 Conference*, pp. 415–418.

[6] Brooks, J., W., 2000. *The Detection of Buried Non-Metallic Anti-Personnel Land Mines*, Dissertation thesis, Huntsville, The University of Alabama in Huntsville.

[7] Haupt, W. R., et al., 2006. *Standoff Acoustic Laser Technique to Locate Buried Land Mines*, Lincoln Laboratory, Massachusetts Institute of Technology, Massachusetts.

[8] Azevedo, S. G.: Stull S., 1997. Making Land-Mine Detection and Removal Practical, *Science & Technology review*, Lawrence Livermore National Laboratory, pp. 19–20.

[9] Composite Autors, 2004. *Metal Detector – In Particular Mine Detector*, U.S. Pat. 7265551 B2.

[10] Connor, M., Scott, D. D., 1998. Metal Detector Use in Archaeology: An Introduction, *Historical Archaeology*, vol. 32, no. 4, pp. 76-85.

[11] Bruschini, C., 2004. On the Low Frequency EMI Response of Coincident Loops Over a Conductive and Permeable Soil and Corresponding Background Reduction Schemes, *IEEE Trans. Geoscience & Remote Sensors*, vol. 42, no. 8, pp. 1706–1719.

[12] The Mine Action Support Group, [online] Available at <http://mineaction.org/>.

2. State of the Art

Currently, eddy current methods are still major techniques in detection. The available information indicates that the majority of producers of eddy current metal detectors use one frequency (about 10 kHz) in the cheaper (and thus more readily available) metal detectors and metallic objects are mainly recognized by phase shift. But this method has some disadvantages for example something that look like one large object could be several objects close to each other and even from different materials.

In the more expensive models, manufacturers currently use multiple frequencies (most often two or three) and the user can switch between them depending on where and what objects is the user searching for. It is known that lower frequencies are less affected by ground effect, because metal detectors are dependent on the magnetic susceptibility of the soil. They also suppress skin effect of the material. These frequencies penetrate deeper into the soil, but on the other hand, higher frequencies have a higher resolution. Therefore, manufacturers must make a compromise between these frequencies or use multiple frequency systems.

Recently Minelab came to the market with their new broadband technology, where the excitation signal range is composed of 28 frequencies from 1 kHz to 100 kHz and full band technology with sweep signal from 1.5 kHz to 25.5 kHz [13] – [19].

2.1. Types of Metal Detectors

Electromagnetic induction devices or metal detectors can be generally divided into passive and active metal detectors. Passive detectors trace the background and detect magnetic fields. Active detectors generate a time varying low frequency magnetic field which changes when a metallic objects is present. Active metal detectors can be also divided into two groups - frequency domain and time domain metal detectors [20].

2.1.1. Time Domain Metal Detectors

Time domain metal detectors or Pulse induction (PI) system usually use a single coil for transmitting and receiving or may have different coils for transmitting and receiving. This technology sends powerful, short repeated bursts (typically 1 kHz) of current pulses, taking care to minimize the current switch-off time. Duty cycle of current pulses is typically about 4% [21]. As the current pulse shuts off, due to rapid change of current, a very large voltage spike of opposite polarity is induces (counter EMF). An *eddy currents* are induced if a conductive object is present. These *eddy currents* generate a secondary magnetic field which is induced in the coil. The exponential decay of the secondary field is slower than

that of the primary field. The time constant of eddy current decay depends on the object's conductivity, permeability and size. The received pulses are measured by an integrator and after that are converted to an audio tone as an indication.

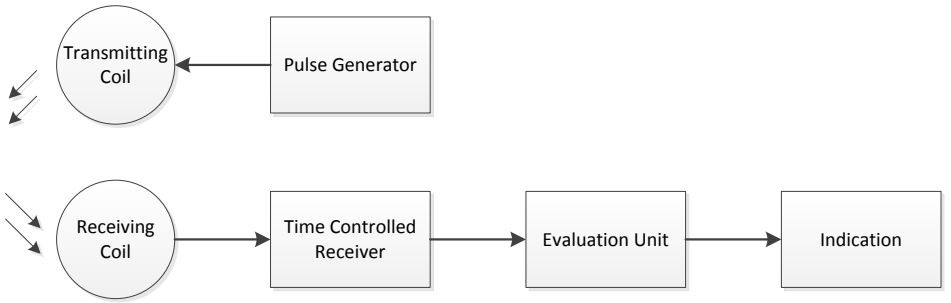

Fig. 2.1: Simple block diagram of the PI system

Since reflected pulses could have the same lengths for various metals, it is not easily distinguishable. In that case PI detectors are not good at discrimination.

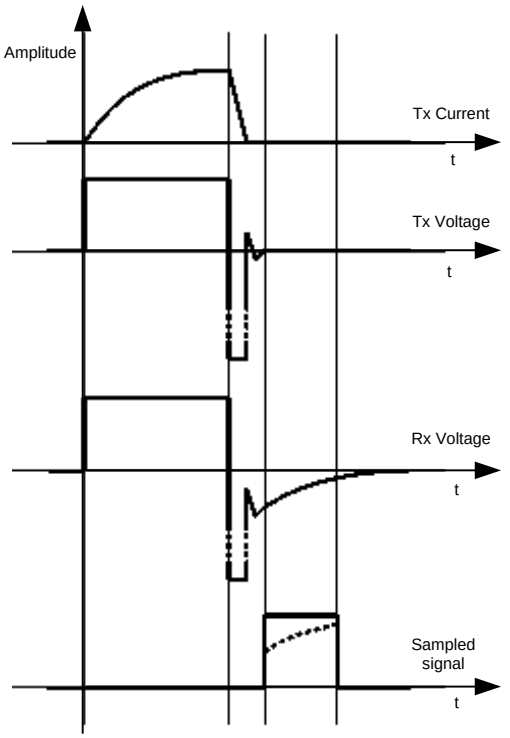

Fig. 2.2: Transmitted and received signals of PI metal detector

By increasing the period between transmitter pulses shut-off and pulses delay, specific metal objects can be rejected. For example the first will be aluminum foil, followed by nickel and gold. There have been attempts to design PI detectors with better discrimination capabilities but with limited results [21]. Response of a Pulse Induction detector for a conductor present and without any target (no metal) is presented in Fig. 2.3.

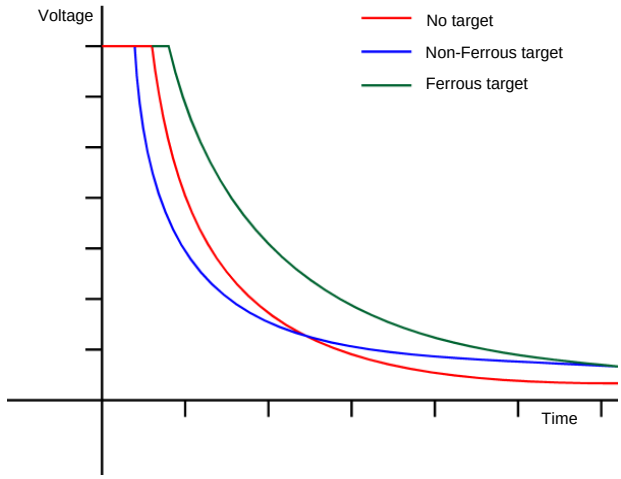

Fig. 2.3: Response of different targets

PI detectors are useful in some areas which are strongly mineralized or near salt water. Also, PI detectors can often detect metal much deeper in the ground than other systems.

2.1.2. Frequency Domain Metal Detectors

Frequency domain metal detectors use single coil, or separate transmitting (TX) and receiving (RX) coils and usually operates at one or more sinusoidal signals, very often just one. Real and imaginary parts (or amplitude and phase) of the received signal contain information about detected objects when the detector passes near objects.

Operating frequencies of the detectors are usually in the range from 1 kHz to 120 kHz. The lowest possible frequency is determined by the size of the search coil (low energy of the emitted electromagnetic field). The amount of emitted energy is proportional to the third power of the frequency. The maximum usable frequency is determined by the properties of the soil. The penetration depth (skin depth) in case when of incident planar wave is given by formula:

$$\delta = \sqrt{\frac{2\rho}{\omega\mu_0\mu_r}} = \sqrt{\frac{1}{\pi f \mu_0 \mu_r \sigma}} \tag{2.1}$$

where ρ is resistivity, ω is angular frequency, μ_0 is permeability of the vacuum ($4\pi \times 10^{-7}$ NA^{-2}), μ_r is relative permeability, σ is conductivity and *f* is frequency.

In accordance with this formula, depth of penetration into the ground decreases when frequency increases as well as the influence of the soil capacitance character. *"From the point of view of sensitivity there is a tendency to move towards higher operating frequencies, which can be probably explained by thinking of the quality factor Q improvement of a resonant (LC) circuit, and also by the fact that the induced voltage U is proportional, according to Faraday's law, to the rate of change of the magnetic flux Φ passing through the receiver coil"* [22]. However it is also known (in accordance with formula (2.1) for skin depth δ) that lower frequencies penetrate better than higher frequencies and skin effect is reduced too. Also the ground effect is lesser. Therefore manufacturers are compelled to find a compromise between these frequencies. Some of them use multiple frequencies where the system can switch between different frequencies. At present, there is a trend to use multi-frequency technologies by manufacturers.

Frequency change

The simple system works on change of frequency principle. A single coil can be used in this system. The system is based on is oscillator with the operating frequency given by resonant circuit. Operating resonant frequency f_R is given by well-known Thomson formula (2.2).

$$f_R = \frac{1}{2\pi\sqrt{LC}}, \tag{2.2}$$

where *L* is inductance of the coil and *C* is capacitance of parallel capacitor.

Fig. 2.4: Simple block diagram of Frequency change system

When the detector passes near a metallic object the impedance of the coil is changed. It causes that the oscillator oscillates at slightly different frequency. Frequency of the oscillator can be either increased, which is usually caused by non-ferrous metals, or decreased by a presence of ferrous material. But it is not

possible to distinguish between different materials in practice. That is because metal objects of different shapes and sizes causing a different frequency changes. The inability to discriminate different metals is the reason this system is not commonly used.

Beat-frequency Oscillator

Another simple technology is based on beat-frequency oscillator (BFO). BFO system could work with one or two coils (separate TX and RX coil). The principle of BFO system is similar to well-known superheterodyn receivers i.e. mixing of the two slightly different frequencies. By this way small changes in frequency can be indicated. The system uses two identical oscillators which oscillate at the same frequency (kHz). One of the oscillators is coupled with the coil. Second oscillator which oscillates with constant frequency is used as a reference. Both oscillators are connected to a mixer. The mixer is basically multiplier in which signals from oscillators are multiplied resulting in difference of both frequencies. The result from this operation is an acoustic beat (Fig 2.5).

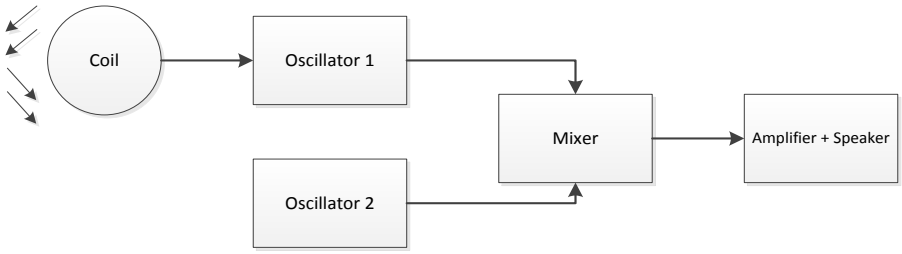

Fig. 2.5: Simple block diagram of BFO

If the coil in the search head passes over a metal object, the object's magnetic field changes the frequency of the oscillator. Ratio of the frequency change based on the change of self-inductance is given by formula (2.3).

$$\frac{\Delta f}{f_0} = \frac{1}{2}\frac{\Delta L}{L}, \tag{2.3}$$

where Δf is frequency change, f_0 is frequency of the oscillator, ΔL is inductance change and L is inductance of the coil.

As the pickup frequency deviates from the reference oscillator frequency, the frequency of acoustic beats (tone) changes depending on the type of metal. Despite its simplicity this system is still used in some applications, for example in traffic light controls via a loop buried under the surface [22].

Very Low Frequency

Very low frequency (VLF) metal detectors (also known as induction balance) are the most widely used detector technology in use today. System can be divided into transmitting part and receiving part. These parts are connected only by mutual inductance *M* between TX and RX coils [Transmitter Receiver – Induction Balance system]. The system uses separate transmitting and receiving coils which operates at single frequency typically from range of 1 kHz to 50 kHz. The shape and position of the coils is arranged in a way to have as low mutual inductance as possible when a metal object is not present. This is the reason for the contrast between the presence and absence of an object.

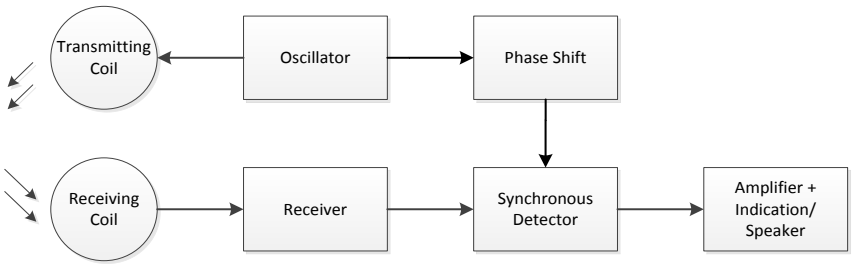

Fig. 2.6: Simple block diagram of VLF

A block diagram of VLF metal detector is showed in Fig 2.6. The oscillator generates a signal with frequency *f* and excites the TX coil which generates time varying electromagnetic field. Phase shift block can be set to prevent false detection or discriminate specific type of metal.

Voltage V_T in TX coil can be described by formula

$$V_T = I_T e^{j\omega t}, \tag{2.4}$$

where I_T is current driven through TX coil, ω is radian frequency ($\omega = 2\pi f$), and *t* is time.

Voltage V_R inducted at RX coil is given by formula

$$V_R = -j\omega M I_T e^{j\omega t}, \tag{2.5}$$

where *M* is mutual inductance.

When the receive coil passes over an object, this object thanks to the primary field, produce a secondary magnetic field (due to eddy currents induced in object by primary field) and it causes a change in the voltage V_R induced in RX coil. The coils become unbalanced and it changes a mutual inductance *M* between the TX and the RX coils.

The received signal which corresponds to secondary magnetic field could be formulated as complex value. The received signal consists of a signal which is in phase with the transmitted one V_{Real} (in-phase/resistive) and signal which is dephased by 90 degrees V_{Imag} (quadrature-phase/reactive) (Fig. 2.7).

$$V_R(t) = A \cdot \sin(\omega t + \varphi) = V_{Real} \sin(\omega t) + V_{Imag} \cos(\omega t), \qquad (2.6)$$

where $V_{Real} = A \cdot \cos(\varphi)$, and $V_{Imag} = A \cdot \sin(\varphi)$, φ is phase shift between transmitted and received signal and A is amplitude,

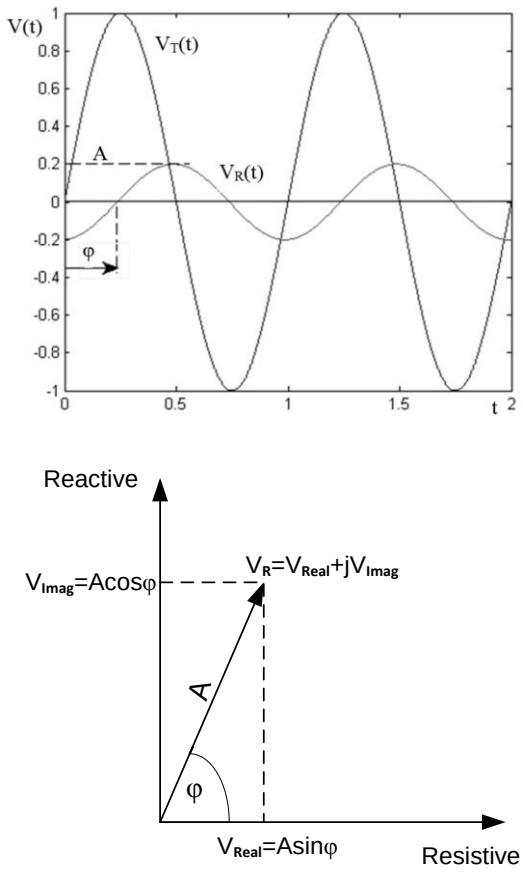

Fig. 2.7: Transmitted and received signals waveform and phase vector of the received signal in the complex plane

Separation of these two components of the signal is usually done by synchronous demodulator. The frequency and phase of reference signal for the synchronous demodulator must be controlled quite precisely – thermal stability and insignificant drift are required.

When the detector moves upon a target the amplitude *A* and the phase shift φ will vary. Therefore information about the object nature is contained in their changes. Based on the character of the secondary magnetic field, these metal detectors can approximately determine some information about the target, for example how deep the object of a specific size is. Because of the phase shift, VLF detectors can distinguish between different types of metal materials. The signal phase shift depends on the conductivity and permeability of an object. Basically objects with high conductivity have a larger phase shift. The signal phase shift depends on the conductivity and permeability of an object.

Since most metals differ in conductivity and permeability and therefore have a different phase shift, VLF metal detectors provide the possibility to discriminate between them. Another discrimination feature of VLF detectors is called notching. A notch is a discrimination filter for a particular segment of the phase shift and in principle it is low-pass filter on the output of mixer. The discrimination and notching have one big disadvantage - the inability to distinguish between objects with similar conductivity and permeability or between objects which aren't similar in case of conductivity and permeability but have the same phase shift response [4], [8] and [23].

2.2. Search Head – Coil Basic

2.2.1. Search Coil Size and Shapes

The diameter of a coil can influence the detection depth and sensitivity of a detector. The signal from a larger coil covers wider area and penetrantes deeper, but with less sensitivity to small target. Also separation of multiple targets in its path is more difficult. Smaller diameter soil is more sensitive, but the detection depth is reduced. Small diameter coil allows to maneuver through common debries to locate desired targets. It is lighter in weight, easier to control and may be chosen for their ability to cope with difficult terrain or undergrowth. Small coils are considered those with diameter less than 150 mm, large ones with diameter greater than 250 mm.

Generally, search coils are circular or elliptical in shape; exceptionally in a special 2-box shape configuration they could have square shape. This kind of configuration is used for detection of large, deeply buried targets. Elliptical shape concentrates the field towards the centre thus has good pinpointing ability. However, a circular search coil has slightly deeper detection depth and sensitivity in non-mineralized soil. It’s the most commonly used shape [24], [25] nad [26].

2.2.2. Search Coils Configuration

A search head consists of TX and RX coil(s). In addition to various search coil sizes and shapes, a variety of search coil configurations are available. Each of them provides different advantages for specific applications.

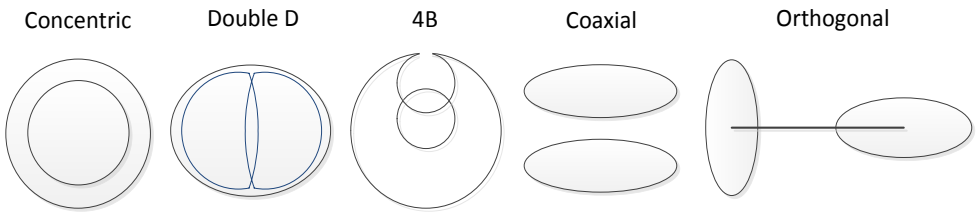

Fig. 2.8: Some possible search head configurations

The coil configuration is chosen according to size of objects and soil properties. There are basically three coplanar configurations (Concentric, Mono and Double-D) and two non-coplanar (Coaxial and Orthogonal). The majority of metal detectors used for mine detection use coplanar configuration. Coplanar searching heads have various shapes – elliptical, square coils or diferential setups (Double-D, 4B).

Mono-coil

A mono-coil or mono-loop configuration is used only in Pulse Induction detectors and is a one of the type of concentric configuration. This head can be made as a single coil acting both as TX and RX coil. The signal shape of the Mono-loop coil is cone thus is not good in precise localization (pinpoint) of the target. Mono-coil configuration and its signal shape is shown in Fig 2.9 (black color represents the search head while white color represents coil itself).

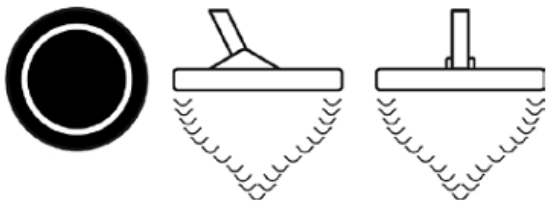

Fig. 2.9: Mono-coil configuration field shape [25]

Concentric

The concentric configuration consists of a transmitting coil and a receiving coil which are usually circular. A RX coil has usually smaller diameter than a TX coil. The signal is sent out from a transmitting coil in conical shape (Fig. 2.10). Concentric coils receive more interference from mineralized soil [25]. Advantage of this coil configuration is it provides the most symmetrical field allowing pinpointing an object easily. Concentric configuration has also better discrimination ability.

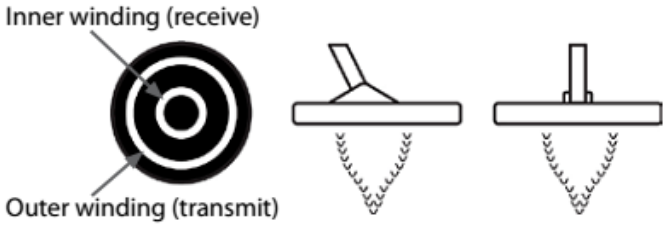

Fig. 2.10: Concentric coils confuguration field shape [25]

Double-D

Double-D coils have two overlapping coils in the shape of two D's (Fig. 2.11). This configuration is designed to significantly reduce mineralized soil effect and recover the performance lost by a concentric coil especially in mineralized soil.

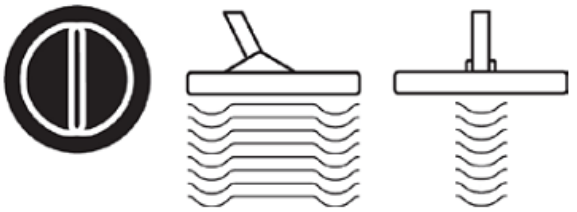

Fig. 2.11: Concentric coils confuguration field shape [25]

Because of its small positive detection field, the Double-D is little bit less sensitive than a Concentric search head of the same size, over non-mineralized ground. Advantages of a Double-D coil are stability in mineralized ground, good depth, sensitivity and pinpointing of the target [24].

The other two configurations belong to non-coplanar configurations – coaxial and orthogonal. A coaxial or imagining configuration of a search coil is an enhanced version of the concentric configuration with an additional RX coil(s) and is more complex. This extra coil(s) provides the detector with additional target information like object depth and object size but is also affected by mineralized soil and has small detection depth. Because of its specific design, this type is used only in the smallest coils [27].

The orthogonal or 2-Box setup uses physically separated TX and RX. This setup is often used with larger coils for very deep detection of large objects. Disadvantage of this configuration is that because of its large detection field, it ignores objects smaller than about 60 mm in diameter.

Some of the head configurations use a differential setup of the RX coils. A TX coil is located around the whole perimiter and the receive coils are located inside symetrically in form of Double-D. If a metal object is not present in the primary field, the differential setup causes that the votage induced in the coils has the same amplitude but the opposite polarity so it cancels out. Immediately after an object gets under the receiving coils a different voltage will be induced. In this case the differential voltage will not be zero and coils detect the object's presence. The advantage of this setup is that it makes pinpointing much easier. Disadvantages are lowered sensitivity, due to RX coil being splited into two halfs, and strict mechanical tolerances on construction. Big disadvantage is also zero sensitivity in perpendicular direction because of dividing the signal equally from both coils.

2.3. Ground Balancing

Signal from soil itself could be appreciable when searching for objects is performed in highly mineralised soils. In this case a problem occurs with intrusive background signal. Other intrusive signals like electromagnetic background, drift effects can be eliminated by the design of a searching coils and electronics, eventually in advanced systems, by signal processing. The most important problem is the effect of soil itself especially in highly mineralized regions (bauxite, magnetite) or beaches (salt). Susceptibility, conductivity and permeability (magnetite has a relative permeability $\mu_r = 5$) of the soil have influence on the signal and cause false alarms. It is known that some soil types can reduce sensitivity, generate false alarms or even render a detector unusable. Ground properties can change greatly from area to area even in relatively small areas.

The interference of the signal could be significant if the soil is more conductive or permeable and the objects are small or deep, or are less conductive or permeable and in addition the soil is inhomogeneous. This signal from the soil

is small but in much larger volume in contrast to small metal objects. The resulting signal may not correspond with reality. For this case, modern metal detectors offers some form of background rejection. Manual ground balancing of metal detectors is becoming a thing of the past. The most of the present metal detectors have automatic ground balancing. As mentioned in [11] one of the most common way of implementing background rejection is to measure the ground signal alone and then suppress it. This method could be implemented by measuring the phase shifts related to the ground signal and shift from received signal related to presence of metal object using of a synchronous demodulator or advanced signal processing using digital signal processor.

2.4. All Terrain Mine Detector

The ATMID™ All Terrain Mine Detector is the mine clearance detector developed by Schiebel company, Austria. The ATMID is a military standard detector which can be used unaffected by climatic variations. It is designed to be highly effective in detecting minimum-metal-content objects in all areas, even in heavily mineralized soils. The ATMID can operate either in the continuous wave mode (8.17 kHz and 10 Vp-p of amplitude) or pulse mode depending on the type of search head. Both modes work combined with ground-compensating technology.

Fig. 2.12: Search head of the ATMID

As mentioned above, ATMID metal detector works on operating frequency f = 8.17 kHz. Therefore coil is balanced/tuned for this operating frequency by capacitor (0.47 μF) which is placed in electronic unit [28] and small ferromagnetic core placed in the search head (Fig 2.13). Number of turns of transmitting coil is 17 and receiving coil is approx. 190 turns.

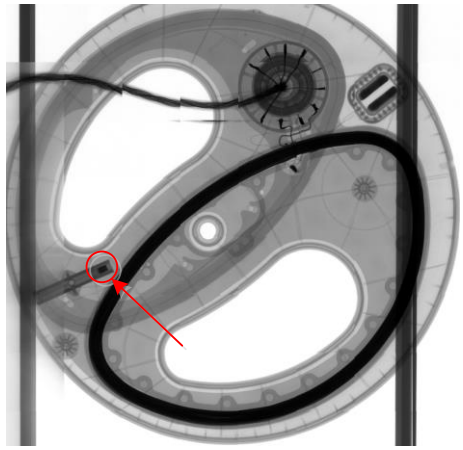

Fig. 2.13: Ferromagnetic core placed in head of the ATMID

The coil is unbalanced for other frequencies and induced voltage has a nonzero value. This situation is describes in Fig. 2.14. When operating frequency at 8.17 kHz, the coil is balanced and the output voltage is minimal or zero. If the search head only without its electronic will be used and if operates on different frequencies, coils became unbalanced and the output voltage won't be minimal. This effect can be used for comparing signal from a target with a signal without any target present.

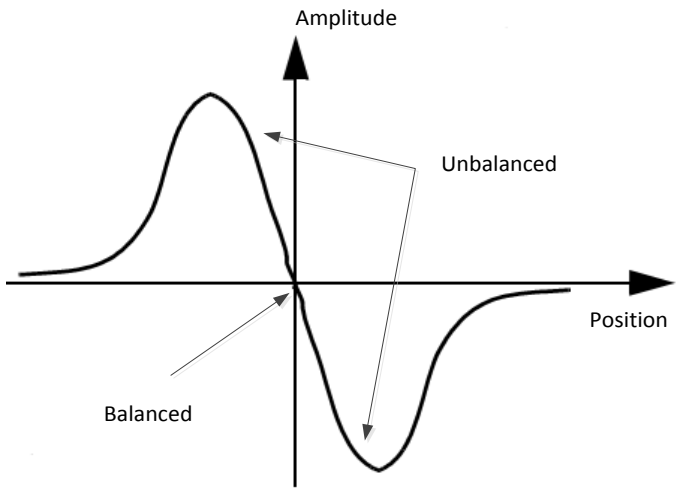

Fig. 2.14: Unbalanced and balanced signal from Double-D head type

As reported by Geneva International Centre for Humanitarian Demining, the ATMID detector has been used in service for more than 10 years and there are

now more than 4,000 in use worldwide, for example in Cambodia, Croatia, Ecuador, Laos, Lebanon, Mozambique, Peru, Slovenia, Taiwan, the U.S. and Vietnam. They are being used by armed forces from a number of countries (Cambodia, Sweden, US, etc.), humanitarian demining organizations (CMAC, CROMAC, MAG, etc.) and commercial demining companies (SGS, RONCO, Milsearch, TADS, etc.) [29], [30] and [31].

2.5. Summary

Eddy current metal detectors are still major devices used in detection. There are two types of active metal detectors; frequency domain and time domain eddy current metal detectors. Time domain metal detectors use pulse induction principles. Its advantages include large depth of detection and an ability to operate in strongly mineralized soils, but it is outweighed by inability of discrimination. Most capable frequency domain metal detectors are VLF detectors, which process real and imaginary part of the received signal to detect and discriminate objects. Their limitation is in ability to discriminate objects which have similar electromagnetic properties (conductivity and permeability) or objects which could have similar response. An inseparable part of a metal detector is also its search head. There are differenet coils sizes and coils configuration. Generally, configuration selection strongly depends on the main purpose of the detector. The ideal searching head should cover the largest ground area with the best pinpointing ability for all terrain situations with maximal sensitivity. The best compromise is offered by concentric or Double-D configuration. In addition, Double-D configuration offers the better functionality in mineralized ground.

[13] Garrett Metal Detectors, [online] Available at <http://www.garrett.com>.

[14] Minelab Metal Detectors, [online] Available at <http://www.minelab.com>.

[15] Fischer Research Labs Detecting and Underground Locating Equipment, [online] Available at <http:// http://www.fisherlab.com>.

[16] Teknetics Metal Detectors, [online] Available at <http://www.tekneticst2.com>

[17] Metal Detector Reviews, [online] Available at <http://metaldetectorreviews.net>

[18] Tom's Personal Metal Detector and Treasure Hunting Web Page, [online] Available at <http://www.thomasathomas.com>

[19] White's Metal detectors, [online] Available at <http://whites.co.uk>

[20] Gaudin, C., Sigrist, Ch., Bruschini, C., 2003. *Metal Detectors for Humanitarian Demining: a Patent Search and Analysis*, EUDEM2 Technology Survey.

[21] White's Metal detectors, How Metal Detectors Work, [online] Available at <http://www.whiteselectronics.com/the-hobby/knowledge-base/field-reports/how-metal-detectors-work>

[22] Bruschini, C., 2002. *A Multidisciplinary Analysis of Frequency Domain Metal Detectors for Humanitarian Deminig*, Dissertation thesis, Vrije Universiteit Brusse.

[23] Lewis, A., M., et al., 2004. *Multisensor Mine Signatures – Final Report*, Joint Research Centre - European Commission (JRC/EC).

[24] Concentric vs Double D and then there's, [online] Available at <http://detectordepot.com/2013/01/concentric-vs-double-d/>

[25] Minelab, 2012. Coil Selection Guide. [pdf] KNOWLEDGE BASE ARTICLE, Available at <www.minelab.com/FKBA_02-1_Coil_Selection_Guide.pdf>.

[26] Garrett Metal Detectors, [online] Available at <http://www.garrett.com/hobbysite/hbby_searchcoil_tech_sheet.aspx>.

[27] Metal Detecting World, [online] Available at <http://www.metaldetectingworld.com/search_coil_types.shtml>.

[28] Siegenfeld, A., 2003. *ATMID – Technologie und Schaltungsbeschreibung*, Schiebel.

[29] Geneva International Centre for Humanitarian Demining, [online] Available at <http://www.gichd.org/mine-action-resources/equipments/detectors/ equipment/schiebel-atmid-all-terrain-mine-detector/#.U7pc1LFHZI0>.

[30] Geneva International Centre for Humanitarian Demining, [online] Available at <http://www.gichd.org/mine-action-resources/organisations/detail/ organisation/schiebel-mine-detection-gmbh/#.U7pc1bFHZI0>.

[31] Strategic Defence Intelligence, [online] Available at <http://www.strategicdefenceintelligence.com/article/gksBMAttDJQ/ 2013/10/22/schiebels_atmid_mine_detector_tested_in_peru/>.

3. Objectives

The aim of this work is to improve discrimination or recognition of detected objects by eddy current metal detectors. Low frequency magnetic fields, which penetrate deeper into the ground, are less affected by magnetic or mineralized soils and also a skin effect is reduced. On the other hand high frequencies offer better resolution and sensitivity. The received signal could then be processed either separately for each individual frequency or as a whole spectrum - for the entire frequency range. These methods should be implemented in a way allowing to use them in real-time. It could be achieved by using of a microprocessor fast enough for a signal processing or a gate array.

The main goal of the thesis is to analyze and verify possibilities of using a polyharmonic signal to improve the identification of located objects. To achieve it, it is necessary:

- to analyze properties of system excited by a polyharmonic signals
- to verify the system properties using an excitation by a multiple frequency signal
- to measure experimental data for different objects
- to process measured data in both time and frequency domains
- to classify different measured objects into classes
- to compare advantages and disadvantages of a polyharmonic excitation signals with standard methods

The partial goals mentioned above enables an opportunity to explore polyharmonic signals, which cover large spectrum of frequencies. For their application in metal detectors there are three different ways how to generate such a signal with multiple frequencies. The first method uses step sweep signal which changes its frequency by defined steps. Parameters of the step sweep signal depend on the quality of the used generator and the lock-in amplifier. The possibility of using synchronous demodulator is the main advantage of the signal. Thanks to that the great sensitivity can be reached. Disadvantage is in the time demandingness of individual measurements. However this signal cannot be considered as polyharmonic. The second method uses chirp or linear frequency sweep signal. This type of signal is easily defined and covers wide spectrum of frequencies at once. The spectrum of such signal is a rectangular function. It can be an asset. A drawback is the inability to use synchronous detection. The last one uses a signal which is a combination of the both signals mentioned above. A signal consists of multiple harmonic frequencies, where each frequency is clearly defined, and all frequencies are applied ‘at once’. There are several waveforms which meet these criteria but signal described by cardinal sine function or sinc having the Fourier transform of rectangular shape $rect(f)$ enables to define easily the frequency range and number of individual frequencies.

All three methods of signal generation mentioned above offer possibilities of processing in both frequency and time domains. In the frequency domain a Fourier transform with amplitude and frequency spectrum can be done. For better interpretation polar graphs can be used. Along with Fourier transform another integral transformation come into consideration, the Hilbert transform. Data processing of polyharmonic continuous excitation signal in the time domain offers nontraditional methods used in metal detection such as standard integral parameters; RMS of the signal, maximal value of the signal or its relations such as Crest Factor. Main drawback of time domain methods is loss of information concerning individual frequencies. Therefore time domain methods can be considered as additional ones to frequency domain methods. Obtained results should be used for an object identification using selected classification method. Classification should be done in a way to utilize all used frequencies or relations between individual frequencies.

All types of excitation signals mentioned above can be defined and programmed in mathematical software e.g. in MATLAB and can be generated by a common arbitrary generator which can generate very low frequencies (1 kHz – 50 kHz). The signal induced in the receiving coil will be digitized by a convenient digitizer for further processing. It can be performed either in gate array or digital signal processor, or in personal computer with a mathematical tool such as MATLAB.

Last but not least is to consider the possibility using of existing metal detector or its search head. For example the All Terrain Mine Detector (ATMID) metal detector has been used in service for more than 10 years and there are now more than 4,000 in use worldwide. The search head of ATMID metal detector uses Double-D coil configuration.

4. Proposed Methods

4.1. Theoretical Background

Metal detectors - Electromagnetic induction devices - are systems generating a low frequency electromagnetic field. Any magnetic or electrically conductive object that enters this field will cause changes in the field strength around it. All metals have either one or both of these electromagnetic properties and will be detectable if the signal changes are large enough.

The detectors usually consist of a search head containing one or more coils – TX and RX. TX coils carry a time varying electric current I_{prim}. This AC current generates a time varying magnetic field B_{prim}. The primary magnetic field interacts with the electromagnetic properties of metallic objects. This can be explained by Ampere's Law (4.1).

$$\oint_{\delta l} B_{prim} dl = \mu_0 I_{prim}, \tag{4.1}$$

where μ_0 is permeability of vacuum ($4\pi 10^{-7}$ Hm^{-1}), l is length of closed curve.

The object reacts by generating a secondary magnetic field B_{sec}. This process occurs because of *eddy currents* (Fig. 4.1) which are induced in metal objects affected by the primary magnetic field. The characteristic of the secondary magnetic field depends on various parameters. It depends on object's orientation and distance from the source, on object's properties – size, shape, conductivity and permeability, and also on the soil (if the soil is mineralized or not).

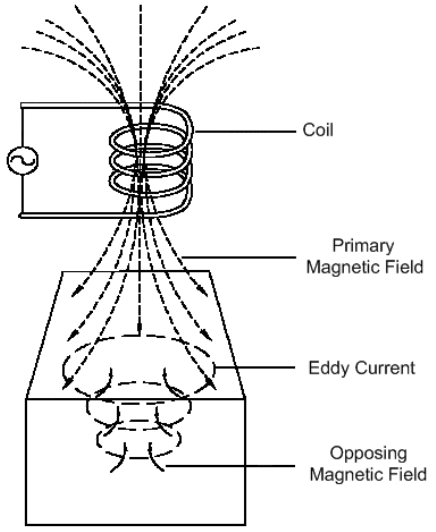

Fig. 4.1: Eddy Currents

Eddy currents generate magnetic field opposed to the primary one. Low conductive metals (alloys, steel) are in principle more difficult to detect. However, for ferromagnetic objects, due to its high value of relative permeability μ_r, the response of the detector is magnified. *Eddy currents* circulate primarily on the surface of metallic objects - current density near the surface of the conductor is greater than at its core. This is called the *Skin Effect*. The electric current tends to flow at the "skin" of a conductor. The electromagnetic field in a conductor decreases exponentially with depth from the surface. The distance from surface (diameter), where density of current drops to 1/*e*, is called *skin depth* δ (2.1).

Examples of *skin depth* of representative materials are presented in Table 4.1.

Tab. 4.1. Skin depth of selected materials

Material	**Conductivity σ (Sm^{-1})**	**Relative permeability μ_r (-)**	**Skin Depth δ (mm) at *f* = 1 kHz**	**Skin Depth δ (mm) at *f* = 25 kHz**
brass	1,500	1	4,11	0,82
bronze	0,740	1	5,85	1,17
INOX AISI 316	0,137	1,02	13,46	2,69
INOX AISI 420	0,139	600	0,55	0,11
AISI 100Cr6	0,465	300	0,43	0,08

Secondary magnetic field is detected by the RX coil(s) in the search head. This magnetic field induces a voltage in the RX coil(s) according to the Maxwell-Faraday equation

$$\oint_{\delta l} Edl = -\frac{\delta \Phi_{B,S}}{\partial t}, \tag{4.2}$$

where *E* is intensity of electric field, Φ is a magnetic flux and *t* is time

The equation of the Ampere's Law for a circular coil with radius *a* can be reformulated using the Biot-Savart's Law. This allows describing the magnetic field at a distance *d* along the axis of the coil.

$$B = \frac{\mu_0}{4\pi} \oint \frac{Idl\ cos\theta}{a^2} \tag{4.3}$$

After solving the Biot-Savart's Law the important equation is obtained (4.4), where *N* is the number of turns of the coil, M_M is the magnetic moment and *S* is the area of the coil ($M_M = N \cdot I \cdot S$).

$$B = \frac{N\mu_0 I}{2} \frac{a^2}{(r^2+d^2)^{\frac{3}{2}}} = \frac{\mu_0 M_M}{2\pi(r^2+d^2)^{\frac{3}{2}}} \tag{4.4}$$

$$B(0) = \frac{N\mu_0 I}{2a} \qquad B(d) = \frac{\mu_0 M_M}{2\pi d^3} \qquad (4.5, 4.6)$$

Equation (4.6) shows an important fact that magnetic field falls off rapidly with the cube of the distance *d* far away from the coil when $d >> a$. The *far field* does not depend on the shape of coil but only on its dipole moment M_M. The magnetic field $B(0)$ at distance $d = 0$, gets weaker as the coil gets larger but decreases less rapidly with the distance see Fig. 4.2, but smaller receiving coils pick up smaller secondary field. The magnetic field *B* was normalized to its maximal value and scaled for better comparison. Fig 4.2 also shows that smaller coils do not allow going as deep as larger coils but at closer ranges they have better sensitivity and area resolution.

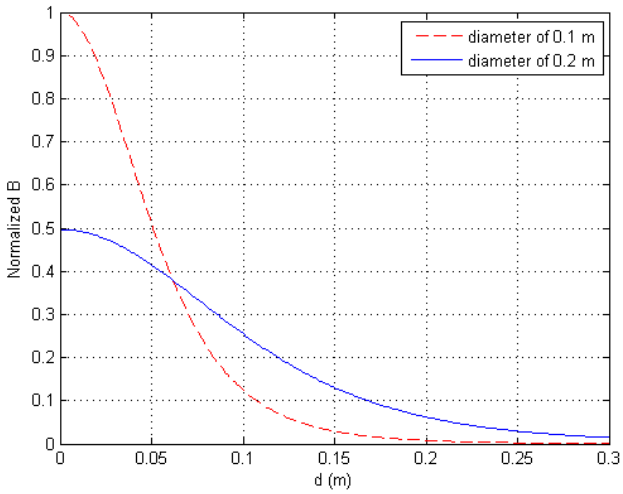

Fig. 4.2: Normalized relation between magnetic field, distance and diameter of the coil

The secondary magnetic field depends on the distance and orientation of an object, its shape and size, conductivity and permeability. It is also influenced by EM background and soil mineralization properties. Various shapes and configuration of the searching head are used to suppress ground effect (see chapter 2.1.) [8], [32], [33] and [34].

4.2. Modeling of Electromagnetic Induction

Firstly the response of *simple circuit model* is presented because a s*imple circuit model* helps to understand problems associated with modeling of electromagnetic induction. The electromagnetic field produced by an AC current flowing in a circular coil is generally quite complicated in the presence of a conducting material.

A conductive object is exposed to a time-varying magnetic field produced by a current-carrying transmitting coil. The *eddy currents* that are induced in the metal object produce a secondary time-varying magnetic field which is detected by a receiving coil.

At first, a *simple circuit model* is presented, it can helps to understand the behavior of a metal detector with an inductive response. The possibilities how to distinguish between different objects and identify an object by its characteristic phase response are presented in this chapter. A simple model consists of separated transmit and receive coils with operating frequency ω and a conductive object is used as a target (short circuit wire loop with the properties of a lumped resistance *R* and inductance *L*). The transmit coil is driven by the current *I*. There are several ways how to describe quasimagnetostatic transfer function of a *simple circuit model*. The method described in [35] is used. Different approach with the same results can be found for example in [22]. The Voltage V_{Target} inducted in the loop is proportional to the magnetic flux passing through the loop and its frequency according to Faraday law (4.2). The magnetic flux is also proportional to the excitation current I_{Trans}, which is driven through the transmitting coil. If a time differentiation is replaced by multiplication by $j\omega$ in the frequency domain equation (4.7) is obtained.

$$V_{Target}(j\omega) \sim j\omega I_{Trans}(j\omega) \tag{4.7}$$

Conductive isolated object can be modeled for low frequencies by lumped resistance *R* and inductance *L*. Then the impedance $\mathbf{Z}_{\text{Target}}$ of the target is given by (4.8)

$$\mathbf{Z}_{Target} = R + j\omega L \tag{4.8}$$

and the current passing through the loop is according to Ohm's law:

$$\mathbf{I}_{Target} \sim \frac{V_{Target}(j\omega)}{\mathbf{Z}_{Target}(j\omega)} = \frac{j\omega I_{Trans}(j\omega)}{\mathbf{Z}_{Target}(j\omega)} \tag{4.9}$$

Voltage V_{Receive} induced in the receiving coil is again according to Faraday law

$$\mathbf{V}_{\text{Receive}}(j\omega) \sim j\omega \mathbf{I}_{Target} = \frac{(j\omega)^2 I_{Trans}(j\omega)}{\mathbf{Z}_{Target}(j\omega)} \tag{4.10}$$

In this case *Loop Transfer Function G*(jω) can be defined as the ratio of voltage V_{Receive} induced in receiving coil to voltage V_{Target} induced in target.

$$G(j\omega) = \frac{\mathbf{V}_{Receive}(j\omega)}{V_{Target}(j\omega)} \sim \frac{j\omega}{\mathbf{Z}_{Target}(j\omega)} = \frac{j\omega}{R + j\omega L} \tag{4.11}$$

Loop Transfer Function of *Response Function* $G(j\omega)$ depends on the operating frequency f and lumped resistance R and inductance L. If parameter α is defined as $\alpha = \omega L/R$ and then *Response Function* is defined by (4.12).

$$G(\alpha) = \frac{\alpha^2 + j\alpha}{1 + \alpha^2} = \frac{\alpha^2}{1 + \alpha^2} + j\frac{\alpha}{1 + \alpha^2} \tag{4.12}$$

Coefficient α is rewritten as a *Response Function* $G(\alpha)$ in [22] and is split into real and imaginary parts. Real part represents *eddy currents* and hysteresis losses and imaginary part represents the target's susceptibility.

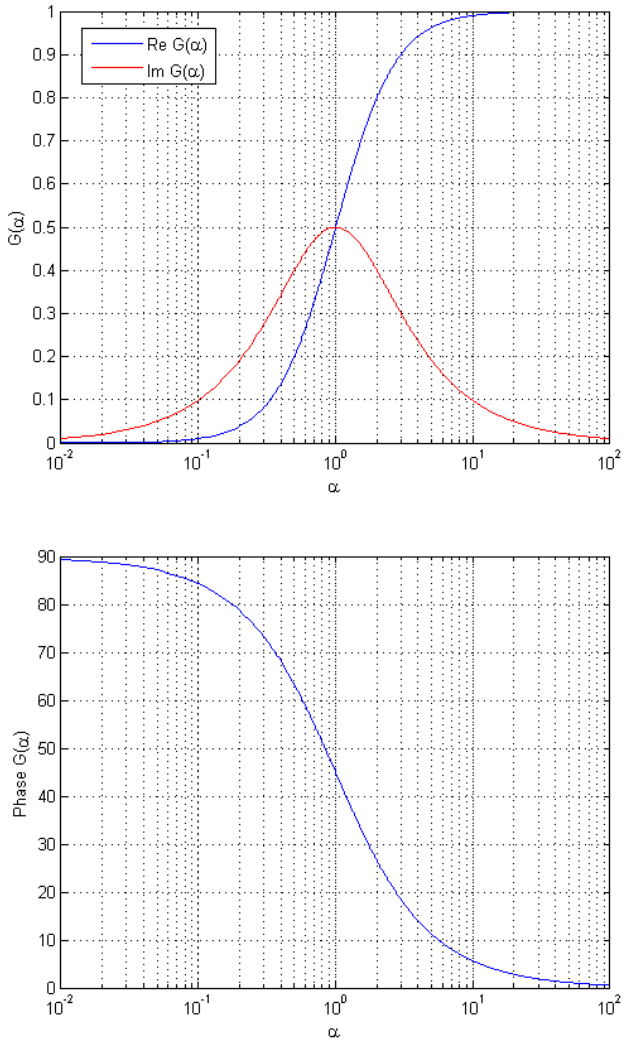

Fig. 4.3: *Response Function* for a simple model

When α limits to infinity, real part of the *Response Function* goes to 1 and imaginary to 0. This is for highly conductive (low *R*) or inductive (high *L*) targets or if the detector operates at high frequencies – this case is called the Inductive limit. On the other hand when α goes to zero the *Response Function* is imaginary and this case is called the Resistive limit. The target conductivity is low or we are operating at a low frequency.

When α is 1 the real and imaginary components are equal (1/2). This case is called crossover frequency f_{cross}. *Response Function* phase is 45°. Thus phase goes from 90° to 0° as shown in Figure 4.3 and 4.4.

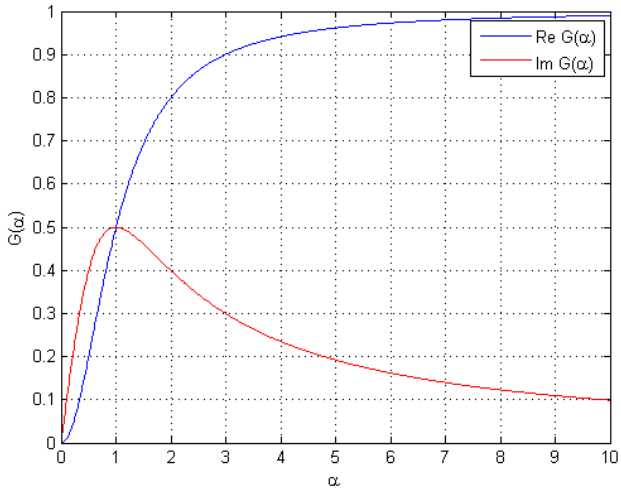

Fig. 4.4: Detail of the *Response Function* with crossover frequency

Simple circuit model showed a behavior of modeling of electromagnetic induction. Now a specific case of shape – homogenous sphere, which is more complicated, is presented. A homogenous sphere represents well an approximation of a common small object. Lots of studies of the response of homogenous sphere have been presented in many publications. Formulation from [36] is used. There are many possible scenarios of primary magnetic fields and surrounding medium. A sphere in a circular coil`s axis in full space (e.g. infinite external medium) is discussed in this case and quasi-static (low frequency) approximation will be considered. More details of quasi-static approximation can be found in [36] or [22], see section 3.4.

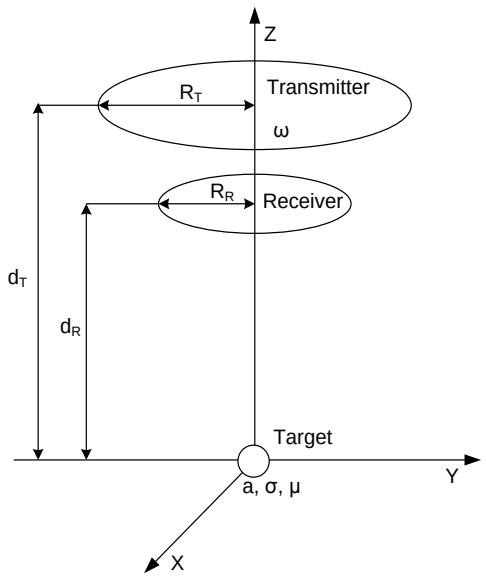

Fig. 4.5: Model of coaxial coils on the axis of a homogenous sphere

Fig 4.5 shows separated TX and RX coils. Transmitting coil is circular with a radius R_T and at a distance d_T from the target. The transmitting coil operates at frequency ω and is driven by current *I*. The circular receiving coil has a radius R_R and is at distance d_R from the object. A target is a homogenous sphere with radius *a* conductivity σ and permeability μ. Sphere is placed in the axis of both coils. With these conditions we can determine the induced voltage $V_{Receive}$.

The transmitting magnetic field is represented by spherical harmonics, and each harmonic generates a spherical harmonic in the receiving field for the same index *n* [36]. Induced voltage $V_{Receive}$ is the sum of the product of infinite geometric series and frequency dependent terms of the induced receive field which are generated by the transmitted field (4.13 and 4.14). This equation consists of a geometry dependent term (real) and *Response Function* (complex).

$$V_{Receive} = 2\pi\mu_0 j\omega I \frac{R_R R_T}{(d_T^2+R_T^2)^{\frac{1}{2}}} \sum_{n=1}^{\infty} \frac{a^{2n-1}}{2n(n+1)} \frac{P_n^1\left(\frac{d_T}{[d_T^2+R_T^2]^{\frac{1}{2}}}\right) P_n^1\left(\frac{d_R}{[d_R^2+R_R^2]^{\frac{1}{2}}}\right)}{(d_T^2+R_T^2)^{\frac{n}{2}}(d_R^2+R_R^2)^{\frac{(n+1)}{2}}} \chi_n(ka) \quad (4.13)$$

$$\chi_n(ka) = \frac{[(n+1)\mu_r+n]I_{n+\frac{1}{2}}(ka)-kaI_{n-12}(ka)}{n(\mu_r-1)I_{n+\frac{1}{2}}(ka)-kaI_{n-12}(ka)} = X_n(ka) + jY_n(ka), \quad (4.14)$$

where P_n^1 are associated Legendre polynomials and $I_{n\pm\frac{1}{2}}$ are modified Bessel functions of the first kind.

The term $\chi_n(ka)$ depends on frequency as well as on target properties and it is similar to the *Response Function G*(α) of a simple model circuit. The response coefficient α can be determined for quasi-static approximation from (4.15)

$$k^2a^2 = j\omega\mu\sigma a^2 = 2ja^2/\delta^2 = j\alpha. \tag{4.15}$$

It shows that response coefficient is purely imaginary and depends not only on object parameters but also on skin depth. It is also evident that induced voltage grows linearly with frequency.

The *Dipole Approximation* is investigated below. If the coil is at a larger distance from the sphere or the sphere is much smaller than the diameter of coils, the sphere acts like a magnetic dipole and only the first term (n = 1) is relevant. A magnetic dipole has a magnetic moment which is always aligned with the transmit field H_T. The phase responses of the sphere depend on sphere electromagnetic parameters, radius of the sphere and frequency but not on geometry of the model. If the sphere is placed into a homogenous transmitting magnetic field, induced voltage V_{Receive} using *Dipole Approximation* can be described by equation (4.16).

$$V_s = 2\pi\mu_0 j\omega I \frac{a^3}{4} \frac{{R_T}^2}{(d_T^2+R_T^2)^{\frac{3}{2}}} \frac{{R_R}^2}{(d_R^2+R_R^2)^{\frac{3}{2}}} X_1(ka) + jY_1(ka) \tag{4.16}$$

The *Response Function* of the sphere (in *Dipole Approximation*) placed in full space is then given by (4.17) (see [37]) and it is evident that it is independent of the system position, for more details see [38].

$$\chi_n(ka) = X_1(ka) + jY_1(ka) = \frac{[\mu_0(1+k^2a^2)+2\mu]\sinh(ka)-(2\mu+\mu_0)kacosh(ka)}{[\mu_0(1+k^2a^2)-\mu]\sinh(ka)+(\mu-\mu_0)kacosh(ka)} \tag{4.17}$$

If non-ferromagnetic object (μ_r = 1) is taken into account the *Response Function* (4.17) will be simplified to (4.18) and its plot is quantitatively similar to the *simple circuit model* (Fig. 4.3).

$$\chi_n(ka) = 3\left[\frac{1}{k^2a^2} + \frac{1}{3} - \frac{cosh(ka)}{ka\,sinh(ka)}\right], \qquad \text{for } \mu_r = 1 \tag{4.18}$$

The *Response Function* for ferromagnetic material in Dipole Approximation is derived from equation (4.13). Since relative permeability of ferromagnetic material is $\mu_r > 1$ the Response Function is dependent also on it. The case for n = 1 is depicted in Figure 4.7. Figs 4.6 and 4.7 shows that for α limiting to infinity the

absolute value of the response coefficient α of non-ferromagnetic objects saturates and the phase goes to -90° for both non-ferromagnetic and ferromagnetic objects.

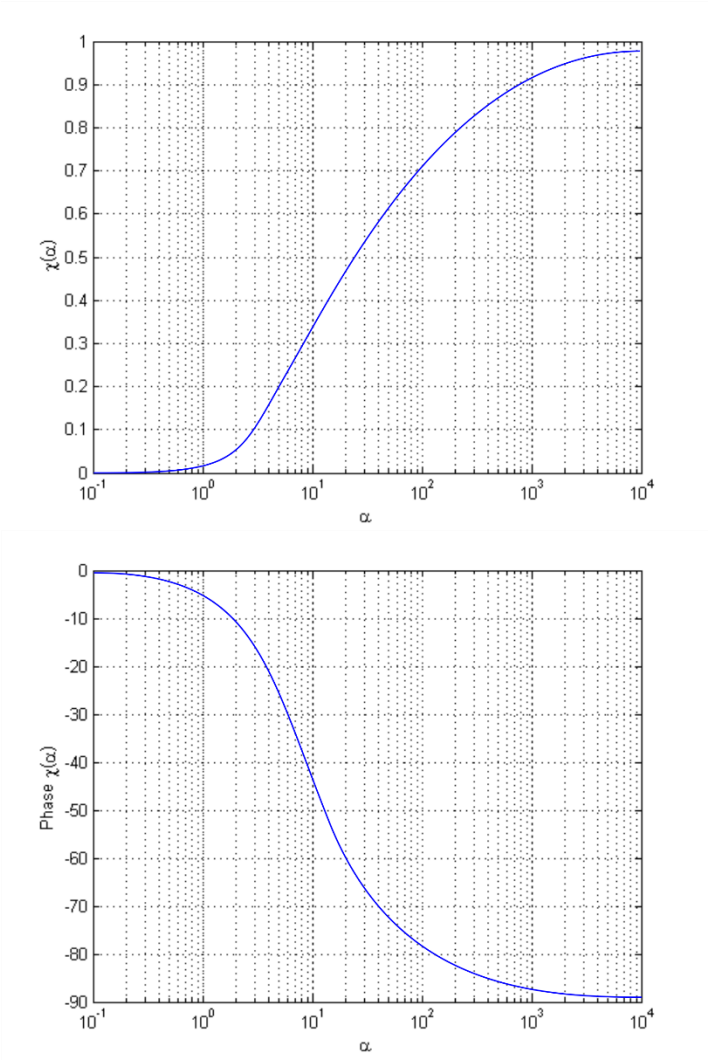

Fig. 4.6: Response Function of a non-ferromagnetic material

To be possible to recognize if the object (with negative phase response) is ferromagnetic or not, multiple frequencies have to be used. However, only ferromagnetic objects show a positive phase response.

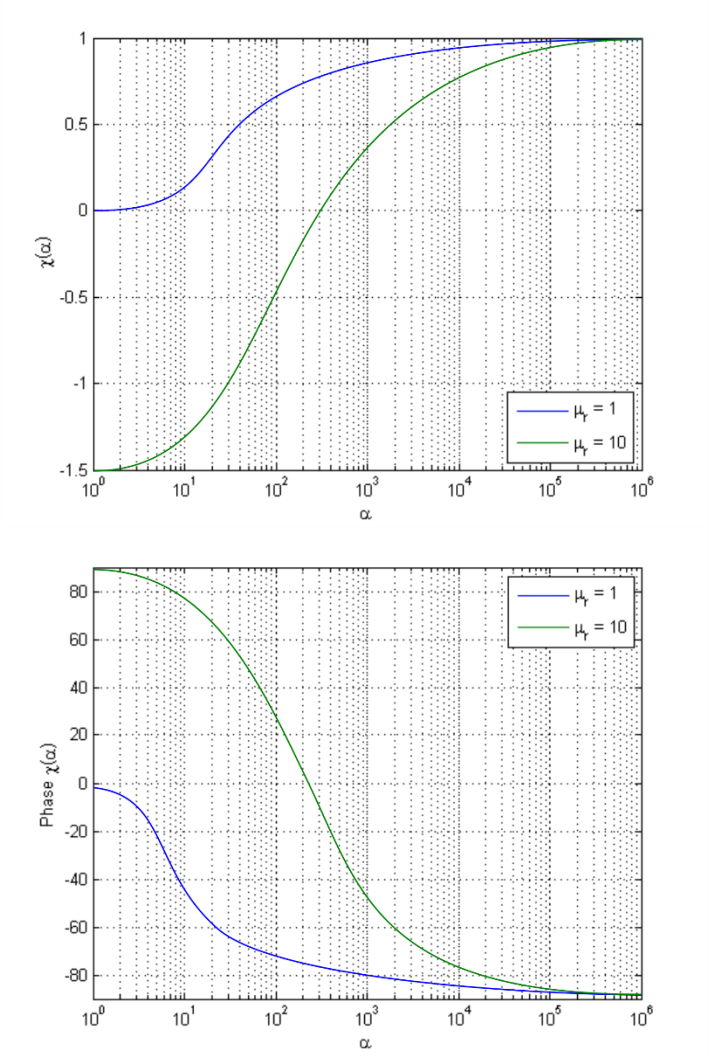

Figure 4.7: Comparison of Response Functions of a ferromagnetic material ($\mu_r = 10$) and non-ferromagnetic material ($\mu_r = 1$)

Electromagnetic induction modeling of simple phenomenological models (based on analytic solution for spheres) of different objects is described in [39].

4.3. All Terrain Mine Detector Searching Head

As mentioned above (the chapter 3) it would be advantageous to use the existing metal detector. One of the suitable detectors is All Terrain Metal Detector by Schiebel company [40]. In this case search head of the ATMID metal detector

is used only. The electronic unit of the detector is not used and should be replaced by a different measuring circuit which can process polyharmonic signals.

Following experiments only the search head of the ATMID detector (without the electronic unit) is used (Fig 2.12). The ATMID search head uses a Double-D coil configuration with a diameter of 260 mm and in can be used either in pulse mode or for continuous wave (CW) mode. Connection of the connector depends on the mode of the detector. Configuration of the ATMID search head connector is shown in Fig 4.8. All measurement with polyharmonic signals has been realized in CW configuration (Fig 4.9) [41].

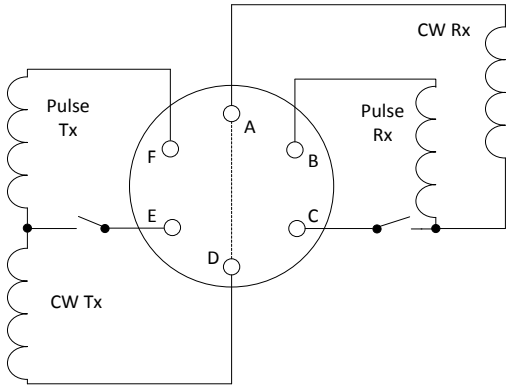

Fig. 4.8: ATMID connector of the searching head

If a CW mode is used pins D and E only are used for TX coil and pins A and C only are used for RX coil.

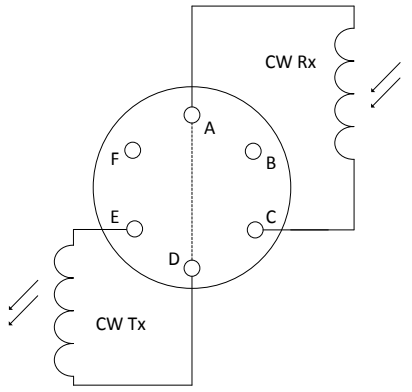

Fig. 4.9: Connection of the connector for CW configuration

The electrical equivalent circuit diagram of the Double-D coil in CW connection mode is presented in Fig. 4.10.

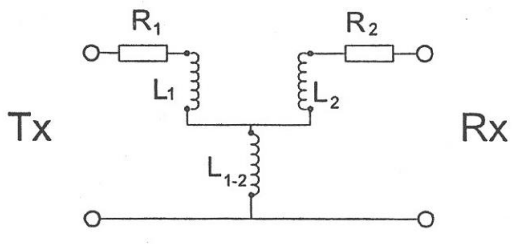

Fig. 4.10: Equivalent circuit diagram of the ATMID coil

R_1 is ohmic resistance and L_1 is inductance of TX coil, R_2 is ohmic resistance, L_2 is inductance of RX coil and $L_{1\text{-}2}$ corresponds to the mutual inductance between coils. T–shape configuration of inductances on Fig. 4.10 corresponds to transformer with inductances L_1 of primary and L_2 of secondary winding and mutual inductance M between both windings. Measured parameters for operating frequency of 8.17 kHz are listed in table 4.2. These parameter corresponds with parameters given by producer [28].

Tab. 4.2: Double-D coil parameters for operating frequency of 8.170 kHz

R_1 (Ω)	L_1 (mH)	R_2 (Ω)	L_2 (mH)	M (μH)
1.2	0.774	182	3.35	0.1

Frequency characteristics of TX and RX coils including mutual impedance are published following figures (Figs. 4.11 – 4.14).

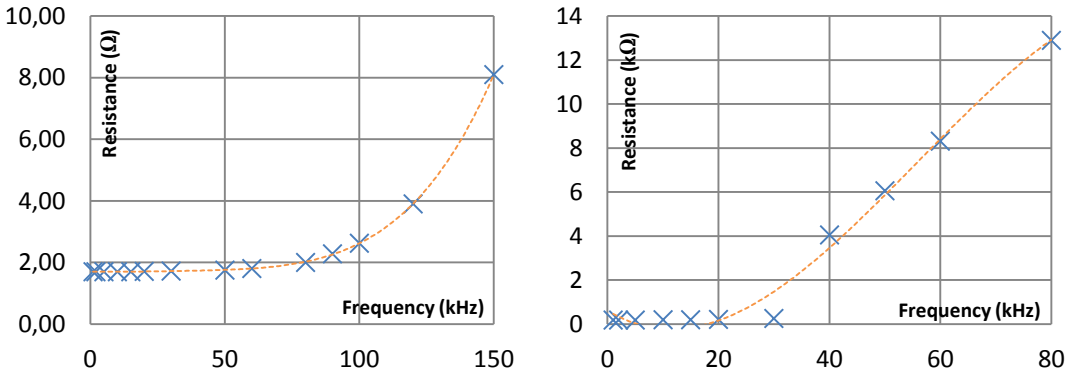

Fig. 4.11: Resistance frequency dependence of the transmitting and receiving coils

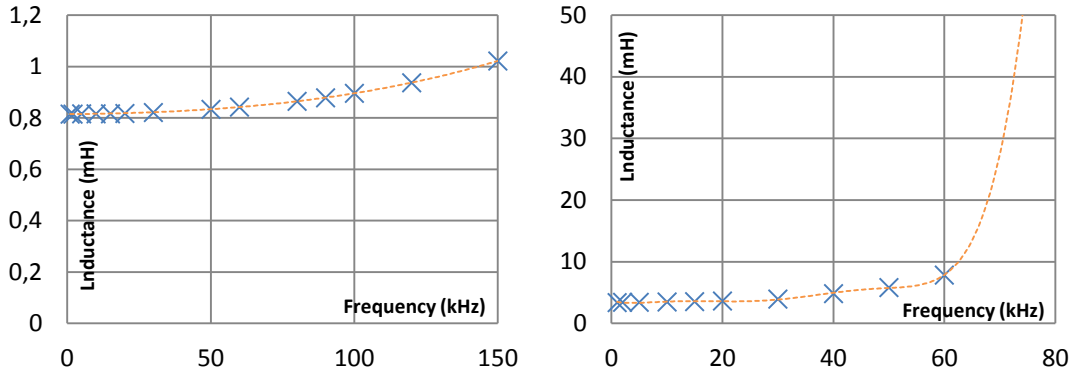

Fig. 4.12: Inductance frequency dependence of the transmitting and receiving coils

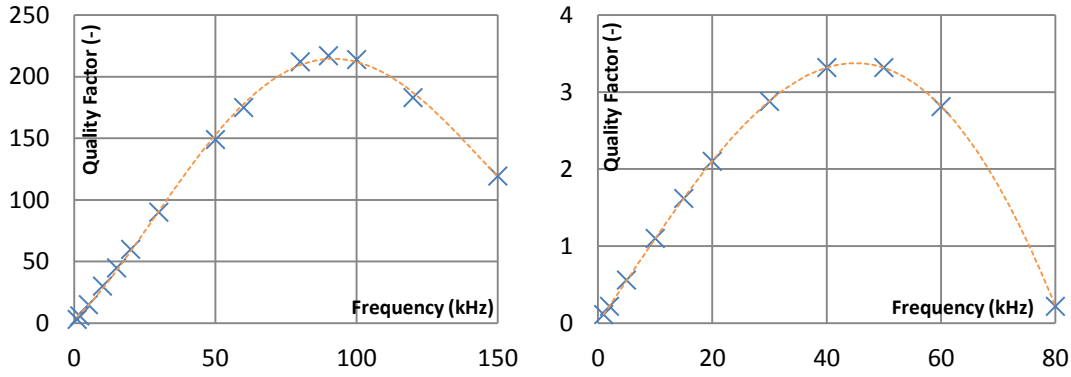

Fig. 4.13: Quality factor frequency dependence of the transmitting and receiving coils

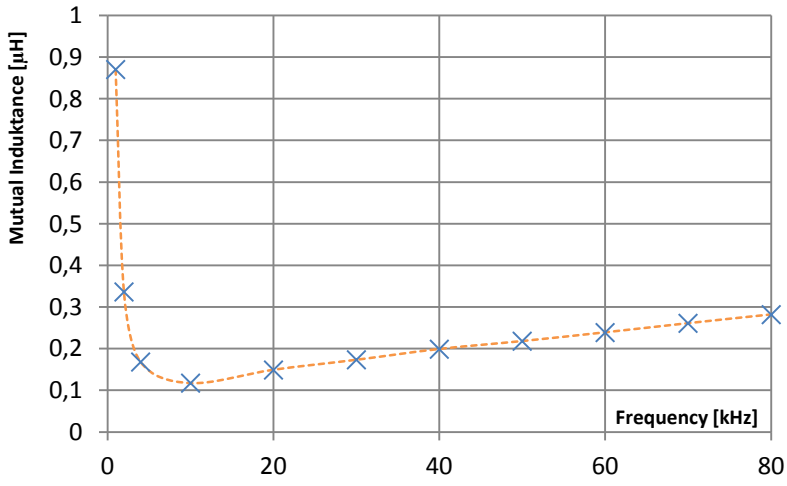

Fig. 4.14: Mutual inductance frequency dependence

How it follows from the frequency characteristic, usable frequency range for polyharmonic signals can be used at a range of 1 kHz to 30 kHz. The upper limit is given by resonant frequency of the receive coil which is about 45 kHz.

The behavior of the coil with small ferromagnetic core (as described in chapter 2.4) were verified on coil with similar parameters (number of turns of transmitting and receiving coils, diameters and coil configuration) the same results were achieved. The coil was excited by the same excitation signals as search head of ATMID.

4.4. Polyharmonic Signal Limitations

Inability to use analog switching synchronous demodulator is a main drawback of polyharmonic signals. Common analog switching synchronous demodulator allows to measure the periodic harmonic signal, which is drowned in noise with SNR = −100 dB [42]. Special synchronous demodulators offer even better SNR up to −120 dB. In this case sensitivity of a metal detector is reduced and is given by the quality of the used analogue to digital converter (ADC). Used ADC is always a compromise between number of bits *N* and sampling speed.

To achieve an identical result, a digitizer with Effective number of bits 19.6 bits should be used. Signal-to-noise and distortion ratio (SINAD) for *N* bit analogue to digital converter (ADC) is given by well-known formula (4.19).

$$ENOB = \frac{SINAD - 1.76}{6.02}\,[\text{bit}] \tag{4.19}$$

Successive approximation ADC with a resolution of $N = 18$ bits and maximal sampling frequency of 1Msample/s achieve SINAD = 97 dB, sigma-delta ADC with $N = 24$ bit and maximal sampling frequency of 627 ksample/s achieve SINAD = 109 dB at 256 oversampling. In real measuring chain consisting of ADC and preamplifier even less SINAD need to be considered.

For example 24-bit sigma delta ADC AD7762 (SINAD = 109 dB) with suggested preamplifier AD8021 (spectral noise density 2.1 nV/$\sqrt{Hz}$) has SNR ≈ 90 dB.

Band width B_W of the input signal corresponds to $B_W = 20$ kHz this give input noise $U_{Ain} = 297$ nV. Since the input range of the ADC is 2.5 V and measured signal from the receiving coil is in range of tens of millivolts signal has to be multiplied by gain of 250. It means that $U_{Aout} = 74.2$ μV. Noise of the ADC (SINAD = 109 dB) for 2.5 V on its input is $U_{ADCin} = 8.9$ μV. From this, total SNR [dB] of the measure chain can be computed using formula (4.20).

$$U_{chain} = \sqrt{U_{Aout}^2 + U_{ADCin}^2} \tag{4.20}$$

For U_{chain} = 75 μV and input voltage of 2.5 V the SNR ≈ 90 dB. From this analysis is clear that the major effect on the SNR of the measure chain has a noise of the preamplifier and its amplification, in comparison with the LeCroy HDO6104 Oscilloscope with its 15-bit ADC, which have SNR up to 80 dB. Although the achievable SNR is lower than SNR of the synchronous demodulator using a sinc signal as an excitation signal is favorable in terms of identifying of detected object.

4.5. Summary

The *Simple circuit model* helps to explain the behavior of electromagnetic induction. Loop *Response Function* of a target using *simple circuit model* has been defined. Model showed that *Response Function* depends on the electromagnetic properties of the target and on frequency. A model using a homogenous sphere can be used for approximation of a common small object. For a quasi-static an approximation the *Response Function G*(α) depends only on objects properties (μ, σ, *a*) and on operating frequency *f*. Behavior of *Response Function* of non-ferromagnetic objects is similar to the *Response Function* of any target using *simple circuit model*. Non-ferromagnetic material shifts the phase of the received signal to negative values only (from 0° to -90°) in contrast to ferromagnetic materials which shifts the phase of the received signal from +90° to -90°. Inducted voltage is defined as a sum of product of infinite geometry series, but for a *Dipole Approximation* higher order can be neglected and only the 1st term is relevant. Measurement of the parameters of ATMID search head shown that can be used for experiments at frequency range from 1 kHz to 30 kHz.

[32] Gaydecki, P., Quek, S., Miller, G., et al., 2002. Design and Evaulation of an Inductive Q-detection Sensor Incorporating Digital Signal Processing for Imagining of Steel Reinforcing Bars in Concret, *Measurement Science and Technology*, vol. 13, pp. 1327-1335.

[33] Guelle, D., et al., 2003. *Metal Detector Handbook for Humanitarian* Luxembourg ,*Deminig*, European Commision.

[34] Kaspar, P., Draxler, K., Ripka, P., 1998. *Magneticke prvky a mereni*, CVUT, Praha.

[35] Riggs, L. S., Mooney, J., E., 2001. Identification of Metallic Mine-Like Objects Using Low Frequency Magnetic Fields, *IEEE Transactions on Geoscience & Remote Sensing*, vol. 39, no. 1.

[36] J.E. McFee, 1989. *Electromagnetic Remote Sensing; Low Frequency Electromagnetics*, Defense Research Establishment Suffield, Ralston, Alberta, Canada, Suffield Special Publication no.124.

[37] A. A. Kaufman, and P. A. Eaton, 2001. *The Theory of Inductive Prospecting*. Amsterdam, NL, Elsevier.

[38] F. S. Grant and G. F. West, 1965. *Interpretation Theory in Applied Geophysics*. New York, McGrawHill.

[39] Miller, T., J., Bell, H., Soukup, J., 2001. Single Phenomenological Models for Wideband Frequency-Domain Electromagnetic Induction, *IEE Transactions on Geoscience & Remote sensing*, vol. 39, no. 6, pp. 1294–1298.

[40] Schiebel. ATMID Maintenance Manual MT5001/16/010E.

[41] Schiebel, [online] Available at < http://www.schiebel.net/Products/Mine-Detection-Systems/ATMID/ Introduction.aspx>.

[42] Hlavac, V., Sedlacek, M., 2005. Zpracovani signalu a obrazu, CVUT, Prague, ISBN: 80-01-031110-1.

5. Measured and Processed Data

To verify the presumption and methods discussed in chapter 4 the numbers of experiments were executed. The metal detector ATMID was used for all experiments. The frequency range of all measurements was below the resonant frequency of the coils (transmitting coil about 90 kHz receiving coil about 45 kHz). Homogenous spheres of different sizes from non-ferromagnetic or ferromagnetic materials were used as a test targets. Targets were placed on the axis of the greatest sensitivity (see Fig. 2.11 and Fig. 5.1) of the search head in open air. The targets were not placed into the ground to avoid the ground effect. The excitation signal was driven through the transmitting coil of ATMID metal detector. Measured data were mostly processed in MATLAB.

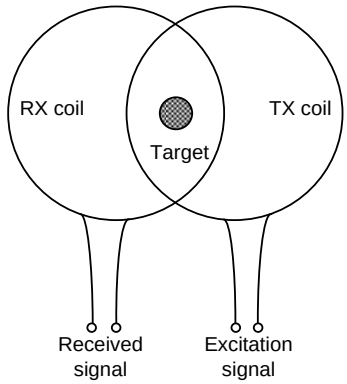

Fig. 5.1: Position of the target

5.1. Step Sweep Sine-wave Signal

The first verification of the behavior of the detector was done for individual frequencies in the desired frequency band. This should verify Models of Electromagnetic Induction described in chapter 4.2. Frequency step sweep signal which consists of multiple frequencies equally stepped from lower to higher frequencies can be used to measure the *Response Function* of the object. Through this way of excitation, a response over a wide frequency range can be obtained in comparison with the classical single frequency methods and also synchronous demodulation for each frequency step can be used. This means that the obtained results can be compared with the *Response Function* model.

Due to the resonant frequency of the receiving coil, a frequency range from 3 kHz to 25 kHz was chosen. This frequency range covers one decade of the *Response Function* for each target (see Fig. 4.6 for non-ferrous materials and

Fig 4.7 for ferrous materials). Measurement setup of the experiment is shown in Fig. 5.2.

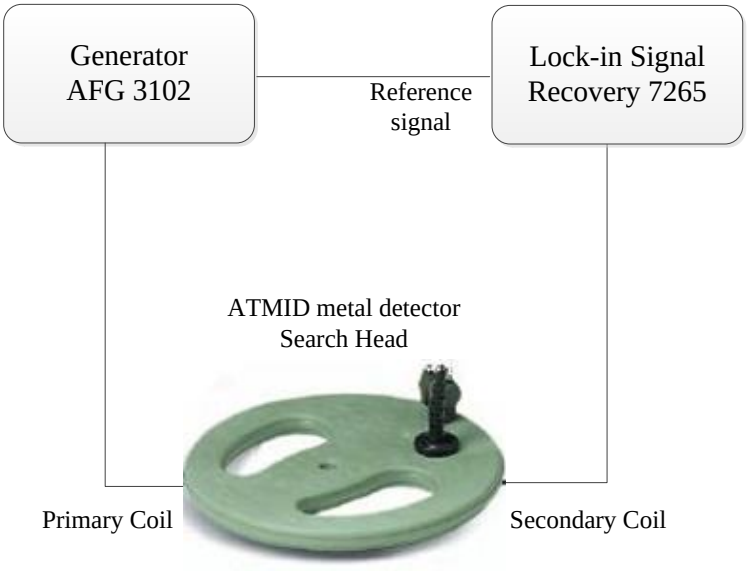

Fig. 5.2: Block diagram of the measurement setup

The transmitting coil is excited by a step sweep sinus signal of chosen range of frequencies (3 kHz – 25 kHz) with a step of 2 kHz and amplitude of 10 V generated by an AFG 3102 generator. AFG 3102 generator offers two outputs where the second one can be used as a reference signal for a lock-in amplifier. The same signal as a excitation signal but with amplitude of 1 V is connected to the reference input of the lock-in amplifier. The amplitude was lowered because of input requirement of the lock-in. Both amplitude and phase of the signal from the receiving coil were measured by the lock-in amplifier.

Target spheres of different diameters and from different materials were used. Four different materials and two different sizes of the spheres were chosen. Two non-ferromagnetic and two ferromagnetic materials – bronze and brass as non-ferromagnetic and stainless steel AISI 420 and chrome steel AISI 52100 100Cr6 as ferromagnetic material were presented. All materials were measured for two different diameters of spheres (diameter of 10 mm and 20 mm). Frequency dependency of the amplitude and phase are presented in next figures. These results can be compared with the *Response Function*s $G(\alpha)$ (chapter 4.2) of non-ferrous and ferrous materials. Experimental data and results were published in [43].

Results measured on spheres from chrome steel AISI 52100 100Cr6 with diameter of 10 mm and 20 mm is shown in Fig. 5.3. In the magnitude chart it is evident that induced voltage increases with increasing frequency and size/diameter of the spheres equally. The larger differences between induced voltages are noticeable on higher frequencies. The phase chart of the chrome steel AISI 52100 100Cr6 shows expected results. Absolute phase shift increases with the diameter of the target and it confirms that chrome steel sphere as ferrous material can shifts phase from positive values to negative if the sufficient range of Response coefficient α is measured (see Fig. 4.7).

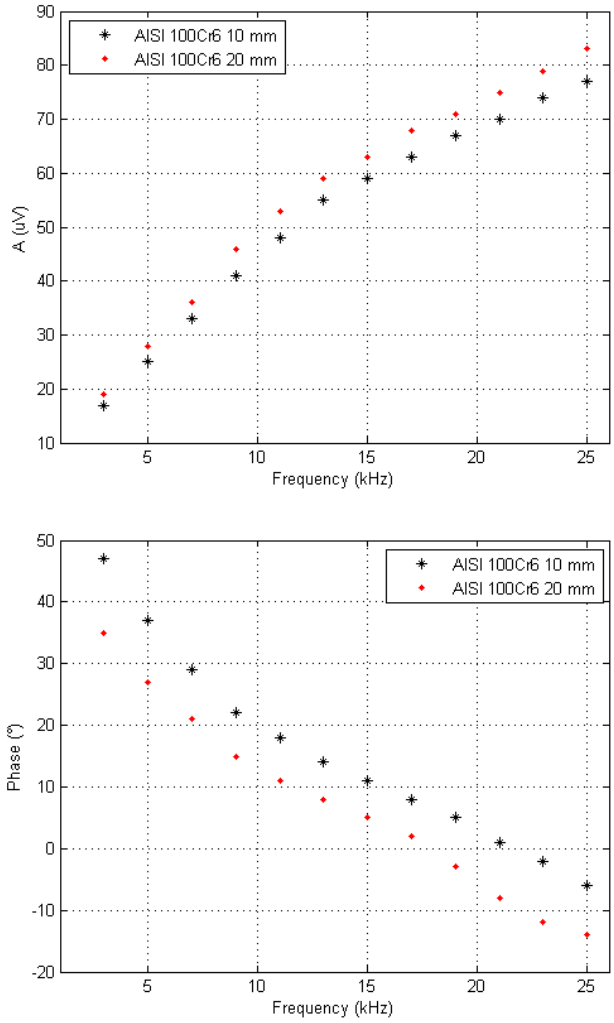

Fig. 5.3: Magnitude and phase of AISI 52100 100Cr6 spheres with diameters of 10 mm and 20 mm

A polar graph is presented for a better presentation and comparison of both sizes. Using a polar graph magnitude and phase dependency and differences between materials and diameters are better observable.

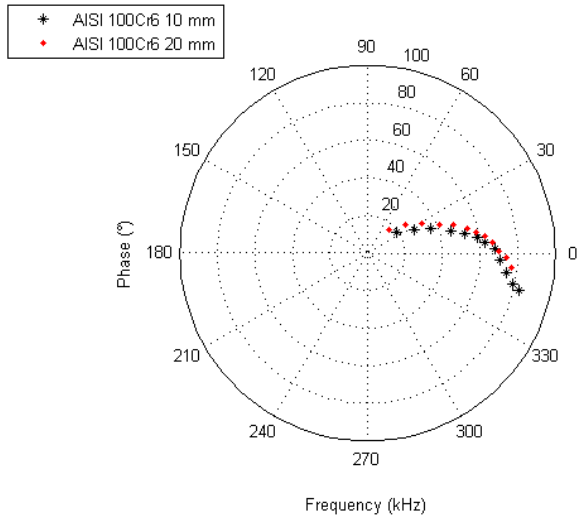

Fig. 5.4: Polar graph of AISI 52100 100Cr6 spheres with diameters of 10 mm and 20 mm

Spheres from ferromagnetic stainless steel INOX AISI 420 is presented here as a next example. The very same diameters of the spheres were measured and presented. AISI 420 spheres give similar charts as spheres from the material AISI 52100 100Cr6. Stainless steel AISI 420 has lower conductivity but higher relative permeability (see Tab. 1 in chapter 4.1) and the order of the Response coefficient α is similar. Measured results are presented in Figs 5.5 and 5.6.

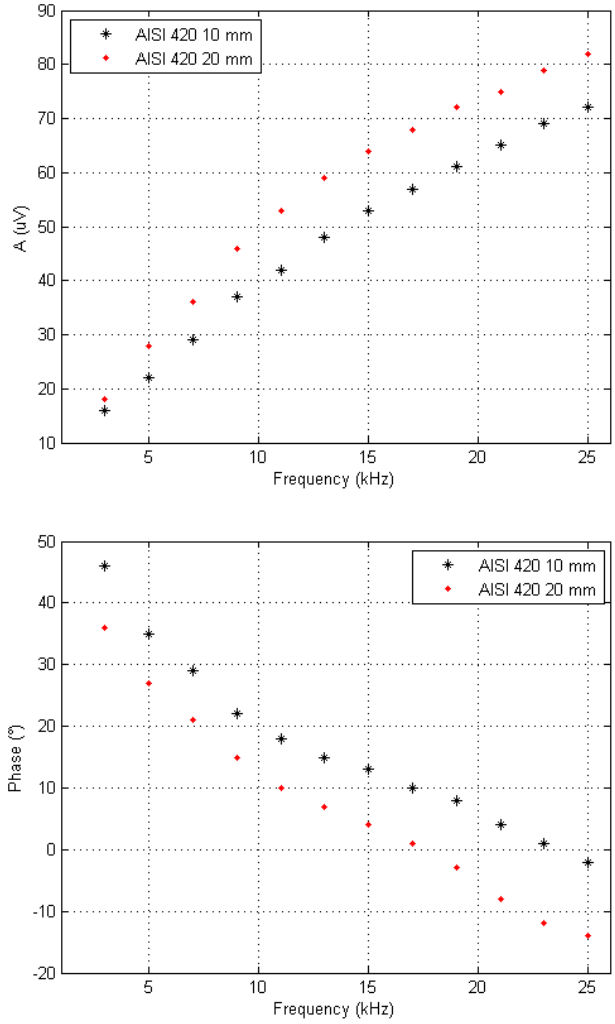

Fig. 5.5: Magnitude and phase of INOX AISI 420 spheres with diameters of 10 mm and 20 mm

Induced voltage has similar trend as for chrome steel and same trend for the phase which changes more with increasing greater diameter. The phase of the signal from stainless steel in comparison with chrome steel is similar. Differences are in units of degrees, which can be explained due to Response coefficient α, which has lower value thanks to the lower conductivity, for this material. The polar graph for spheres of two different diameters (d = 10 mm and d = 20 mm) is presented in Fig. 5.6.

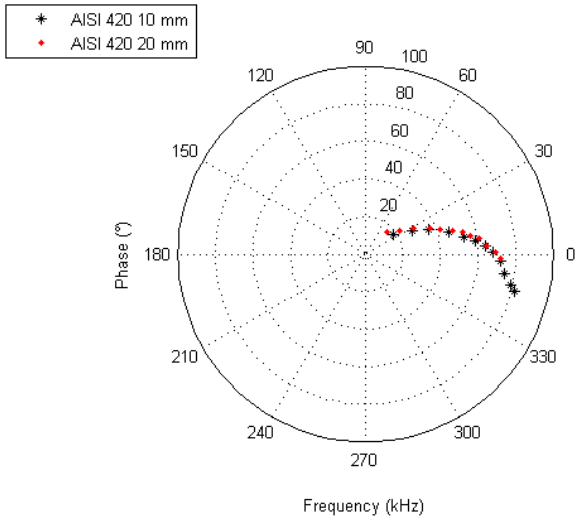

Fig. 5.6: Polar graph of INOX AISI 420 spheres with diameters of 10 mm and 20 mm

As non-ferromagnetic material representative, bronze spheres of diameters 10 mm and 20 mm were measured. Obtained results are presented in Fig. 5.7 and Fig. 5.8.

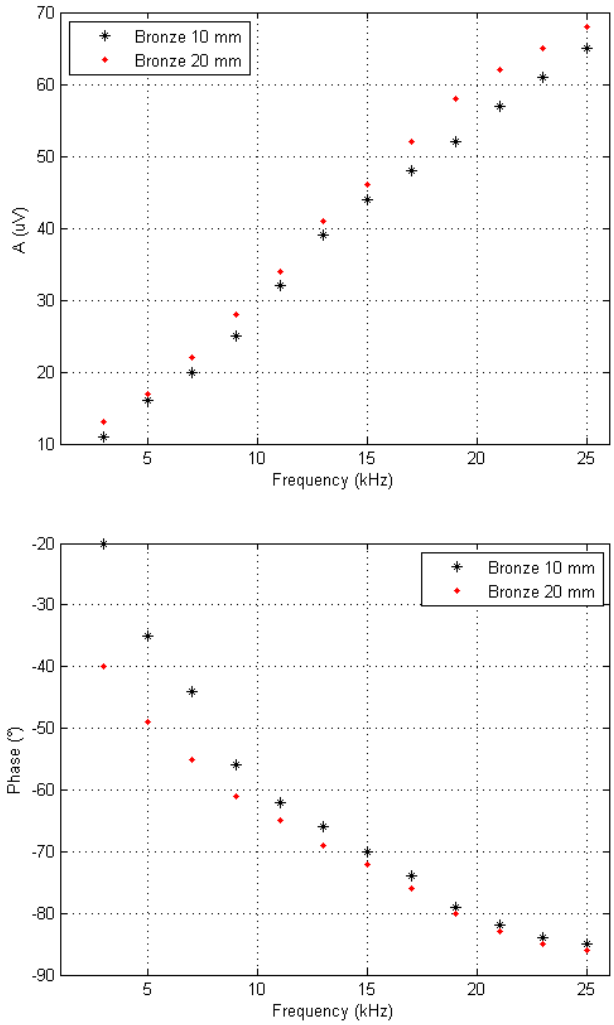

Fig. 5.7: Magnitude and phase of bronze spheres with diameters of 10 mm and 20 mm

An induced voltage is increasing with increasing frequency. Phase shift of bronze spheres goes to negative values unlike that of ferrous steels. It corresponds with the theory concerning ferrous and non-ferrous materials. Phase shift increases with diameter more at lower frequencies but decreases with increasing frequency. It can be explained due to Response coefficient α which is approaching to inductive limit and changes less significantly. Fig. 4.6 (chapter 4.2) shows that for higher values of Response coefficient α, the phase shift decreases. There is also a polar graph presented in Fig. 5.8.

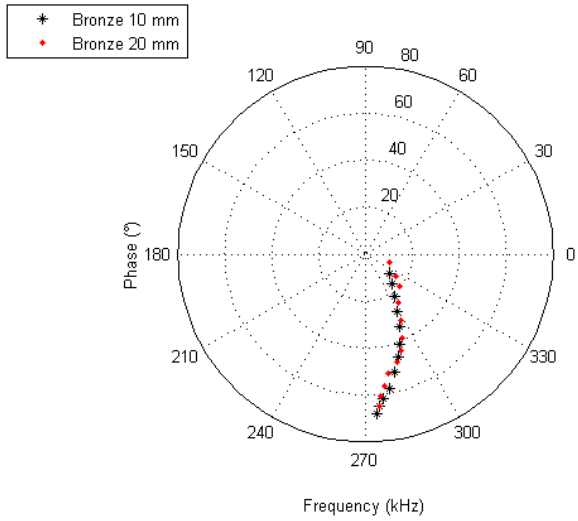

Fig. 5.8: Polar graph of bronze spheres with diameters of 10 mm and 20 mm

The second non-ferromagnetic material which was investigated is brass. Results concerning brass spheres of diameter 12 mm and 20 mm are presented in Figs. 5.9 and 5.10. Due to higher conductivity of the brass, induced voltage is also higher. The phase of bronze is decreasing with increasing frequency and diameter, which is similar to previous materials. The phase shift of brass sphere is also higher than that of bronze because of higher Response coefficient α.

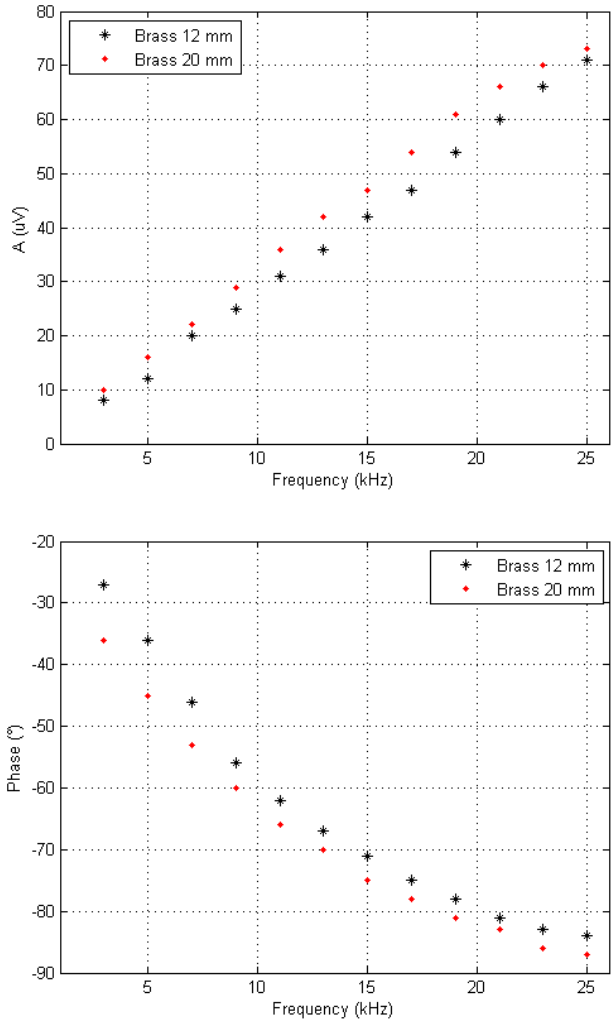

Fig. 5.9: Magnitude and phase of brass spheres with diameters of 10 mm and 20 mm

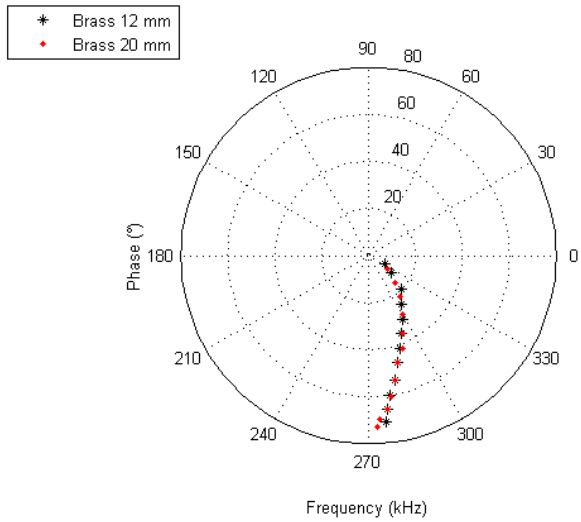

Fig. 5.10: Polar graph of brass spheres with diameters of 10 mm and 20 mm

Comparisons of all materials for spheres of diameters of 10 mm (12 mm) and 20 mm are presented in Figs 5.11 and 5.12. From these polar graphs it is evident that frequency dependencies of different ferromagnetic materials are similar but there are small differences in its *Response Function* through measured frequency. This can be also applied for non-ferromagnetic materials. Comparisons of all materials and both sizes of spheres are presented in polar graphs (Figs. 5.11 and 5.12).

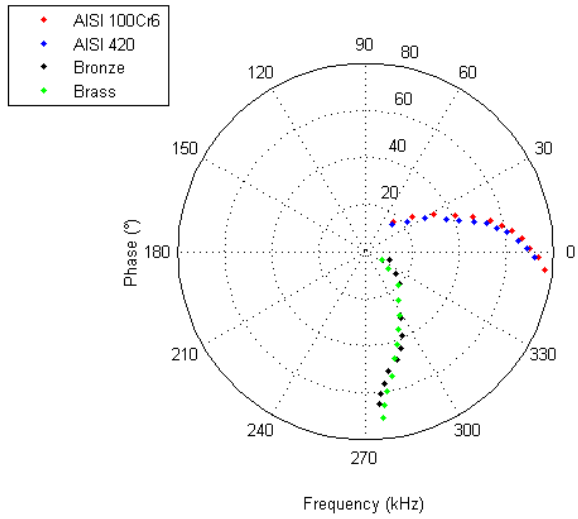

Fig. 5.11: Polar graph of all measured spheres with diameters of 10 mm

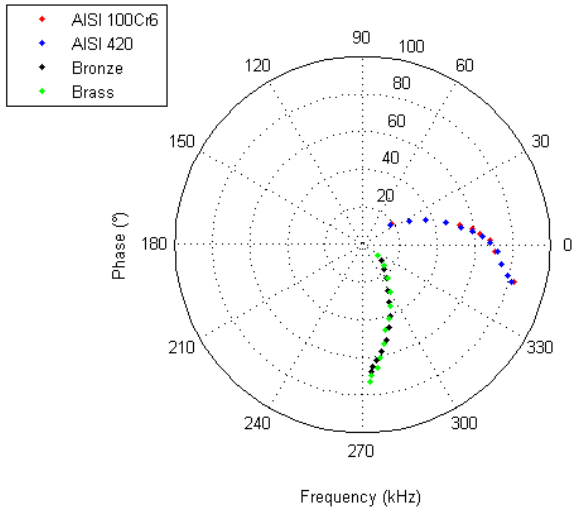

Fig. 5.12: Polar graph of all measured spheres with diameters of 20 mm

Frequency step sweep signal confirms the behavior of ferromagnetic and non-ferromagnetic materials for different materials and frequencies. Differences from theoretical models can be explained by using simplified functions (chapter 4.2.) in modelling of the *Response Function*. Since the frequency step sweep signal cannot be considered as polyharmonic, different excitation signals will be considered.

5.2. Linear Frequency Sweep - Chirp Signal

Frequency sweep signal or in short chirp signal is one of the common polyharmonic signals. Chirp signal is commonly used in many areas for example in audio applications, radar and sonar systems or communication. Its advantage, as all polyharmonic signals, is that can cover wide frequency range. Therefore there is an opportunity to use chirp signal as an excitation signal for metal detector to measure a *Response Function* (response coefficient α respectively) of detected object. As a disadvantage the impossibility of using synchronous demodulation have to be considered. Inability of using synchronous demodulation is drawback of all polyharmonic signals. Signals which are composed of multiple frequencies data must be digitized first and then processed using advanced signal processing.

Frequency of increasing linear frequency sweep signal varies linearly with the time

$$f(t) = f_0 + kt \quad \text{and} \quad k = \frac{f_1 - f_0}{T}, \tag{5.1}$$

where f_0 is starting (initial) frequency, f_1 is final frequency, T is sweep time, k is a sweep rate and t is the time.

The time domain function is defined (5.2), is shown in Fig. 5.13. The spectrum of chirp signal is rectangular function from frequency f_0 to f_1.

$$u(t) = sin\left[2\pi\left(f_0 + \frac{k}{2}t\right)t\right], \tag{5.2}$$

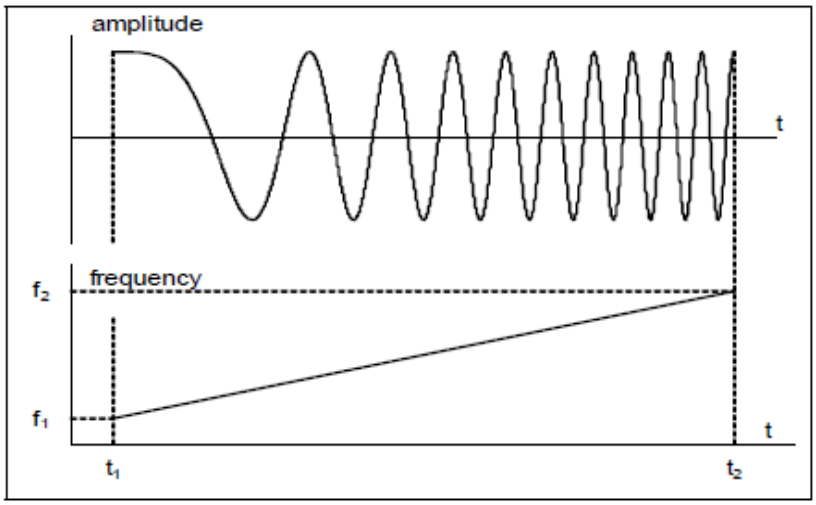

Figure 5.13: Linear frequency sweep

Several experiments using chirp excitation signal were done. These experiments were presented in [44] and [45]. However author of this work found out, that chirp signal has been already used by Minelab company, during these experiments [14]. Therefore all additional experiments have been discontinued. Experiments already done by the author are presented in [44]. Author no longer processed measured data and only basic signal processing has been done. The results below are demonstration only and were not been analyzed in depth.

Presented experiment were measured using AFG 3102 generator which das a resolution of 14-bit and oscilloscope MSO 4034 in hi-res mode (12-bit). Measurement setup is presented in Fig. 5.14. Sampling frequency of the digitizer was 1MSample per second. Following parameters of the excitation chirp signal generated by the formula (5.2) were used: frequency range of 1 kHz to 25 kHz, sweep time 10 ms and amplitude of 10 $V_{p\text{-}p}$.

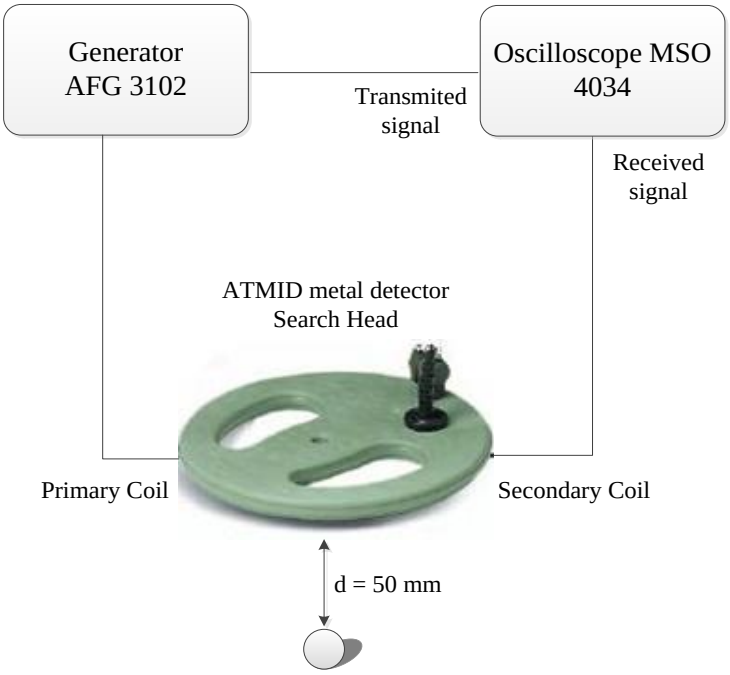

Fig. 5.14: Block diagram of the measurement setup

As targets the same spheres were used. Targets were placed in open air on the axis of the greatest sensitivity (Fig. 5.1) of the search head in distance d = 50 mm. Received signal was digitized and processed in MATLAB software. The measured spheres from bronze and ferromagnetic stainless steel AISI 52100 100Cr6 with the diameter of 10 mm are presented here only. The first one, as a specimen of non-ferromagnetic material and the second one, as a specimen of ferromagnetic material.

Measured data were filtered by band pass FIR filter of 300th order and Blackman-Harris window has been used. Lower frequency of the band pass filter was f_d = 1 kHz and upper frequency f_h = 30 kHz. Discrete Fourier Transformation (DFT) computed with a fast Fourier transform (FFT) algorithm from filtered signals was computed.

$$X(k) = \sum_{i=1}^{N} x(i)\omega_N^{(i-1)(k-1)} \tag{5.3}$$

$$\omega_N = e^{(-2\pi j)/N}, \tag{5.4}$$

where x(i) is sampled signal and N is number of samples.

FFT was computed for N = 1048578, which is nearest powers of two from 1M samples. Although the coherent sampling cannot be done the results is relevant because of the large number of samples N usage in signal processing.

Amplitude and phase spectra are presented. The presented phase spectra were computed and corrected as a difference between phase spectra of transmitted signal and received signal with the object. Figs. 5.15 and 5.16 show the amplitude and phase spectra as well as polar graphs of these two materials. They show processed data of AISI 52100 100Cr6 sphere and bronze sphere respectively.

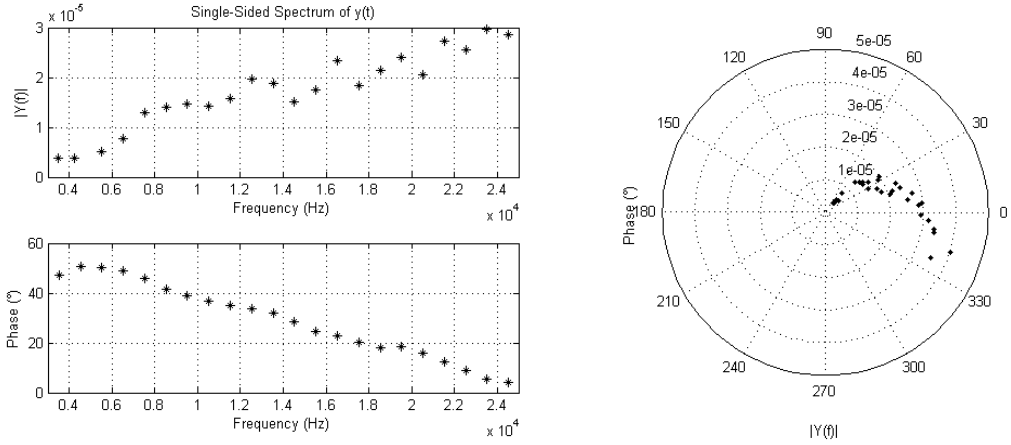

Fig. 5.15: Amplitude spectra and Phase spectra and polar graph of AISI 52100 100Cr6 sphere with diameters of 10 mm

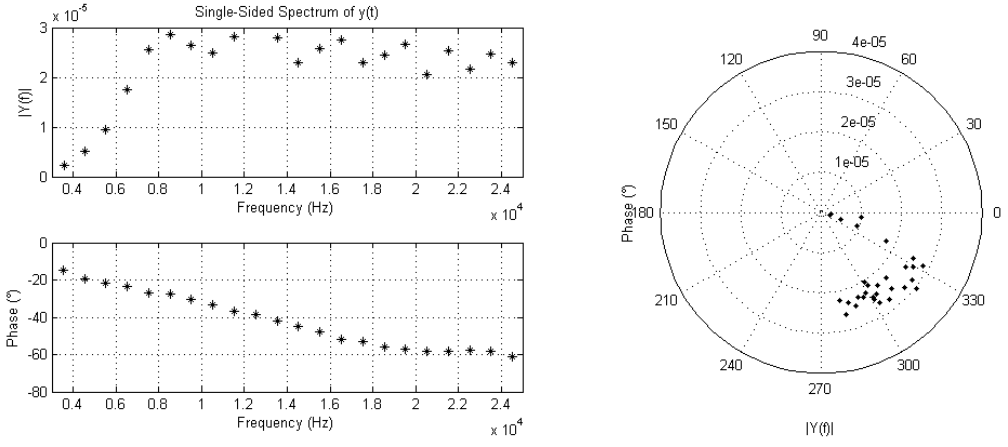

Fig. 5.16: Amplitude spectra and Phase spectra and polar graph of bronze sphere with diameters of 10 mm

The shape of amplitude spectra for both materials shows that material with higher relative permeability induced higher voltage at higher frequencies especially. It corresponds with step sweep sine-wave results and although with theory. However, noticeable difference is visible for measured data of bronze sphere where magnitude for higher frequencies (greater than 10 kHz) does not increase. This can be explained by very low level of the received signal or that the induced voltage reached the inductive limit.

Polar graph presented in Fig. 5.17 show comparisons of both materials.

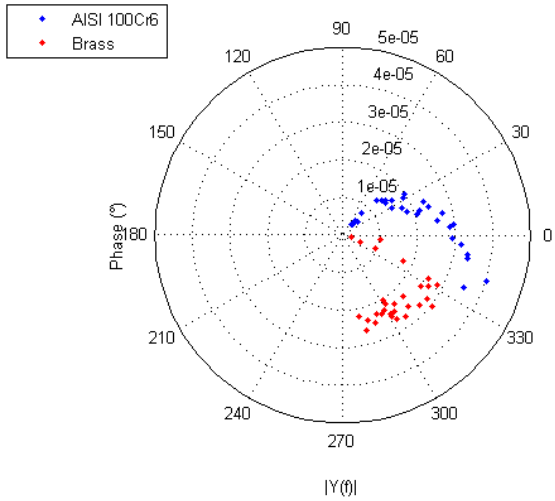

Fig. 5.17: Polar graph of both measured spheres

Phase spectra of both materials confirm what is to be expected; ferromagnetic materials has phase shift from positive values to negative and non-ferromagnetic materials (in this case bronze) have negative values phase shift only.

Experiment confirmed that materials with relative permeability higher than one changes their phase to positive values unlike materials with relative permeability equal to one. As mentioned above, no further verification measurement and advanced signal processing were done because of usage of this excitation signal by Minelab company. These results are not presented as meaningful and provide possibilities how to process a polyharmonic signal only.

The advantage of chirp signal or another similar polyharmonic signal lies in its ability to coverage of part of the detected objects *Response Function*. Since the similar excitation signal has been used by Minelab company already, all the entire future work is focused on other polyharmonic signal which have similar characteristic. As one of the suitable excitation signal sinc signal is offered.

5.3. Sinc Signal

The sine cardinal signal or commonly referred function sinc is one of polyharmonic signals which can be suitable for metal detector excitation to cover a wide range of the *Response Function* of the detected object. Recently, sinc signal is widely used in many areas, for example in analogue to digital converters testing [46] or high-impedance spectroscopy [47] and it is very perspective signal thanks to its spectrum. Also the spectrum of the sinc signal is similar to the spectrum of the chirp signal. The spectrum of the sinc function is appropriate for further spectral analysis of the *Response Function* of the detected object. The number and position of the spectral lines could be easily set and defined. Another advantage is that all frequencies are applied at once.

In digital signal processing normalized sinc function is defined by equation

$$sinc(x) = \frac{\sin(\pi t)}{\pi t}, \tag{5.5}$$

where $sinc(0) = 1$.

A modified sinc signal, which is used for next experiments, is composed of two sinc signals with the same parameters where the second half of the period is inverted (Fig 5.18). One period of the signal is described by the formula:

$$u(t) = H\left(t + \frac{T_1}{2}\right)\left[\frac{sin\left(\frac{2\cdot\pi\cdot t}{T_2}\right)}{\frac{2\cdot\pi\cdot t}{T_2}}\right] - H\left(t - \frac{T_1}{2}\right)\left[\frac{sin\left(\frac{2\cdot\pi\cdot t}{T_2}\right)}{\frac{2\cdot\pi\cdot t}{T_2}}\right], \tag{5.6}$$

where H is Heaviside function, which chops the segment of the sinc function in time range $< -T_{1/2}, T_{1/2})$. The anti-symmetrical signal covers full scale of digitizer and allows to continuous crossing between periods.

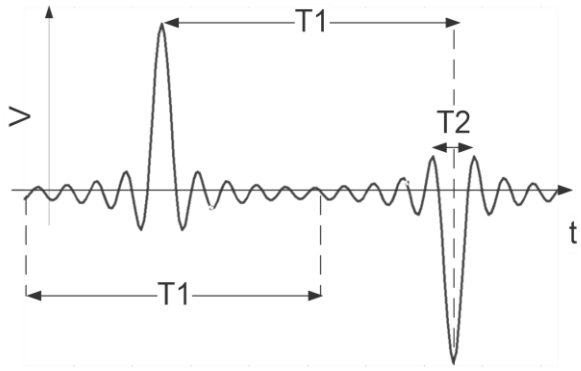

Fig. 5.18: Time plot of the modified sinc signal

Since the coil is excited by current i_L, its voltage u_L correspond to the first derivative (5.7).

$$u_L = L\frac{di_L}{dt}, \tag{5.7}$$

First derivative of the sinc signal is defined:

$$\frac{d}{dt}sinc(\pi t) = \frac{\pi t \cdot \cos(\pi t) - \sin(\pi t)}{(\pi t)^2}, \tag{5.8}$$

In this case time plots of sinc signals and its derivative normalized to its maximal value is shown in Fig. 5.19 (top) and time plots of the modified sinc signal (bottom).

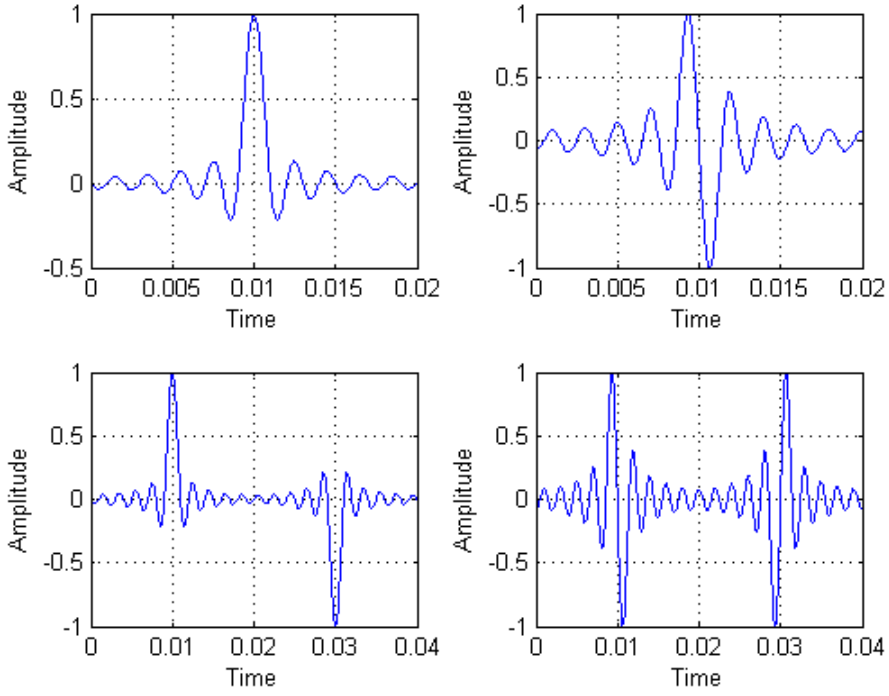

Fig. 5.19: Normalized time plot of the sinc signal and its derivative

Since the sinc signal is composed of all frequencies equally its spectrum has rectangular shape with equidistantly distributed frequencies. The number of spectral lines is given by ratio of the T_1 and T_2 (Fig 5.20). The first spectral line is at frequency $f_1 = 1/T_1$ and the last is at $f_2 = 1/T_2$. The spectrum of its derivative has an ascending shape which follows the derivative of the function, but the character of the spectrum is unchanged. I has been advantageous to use integral of sinc function. Antiderivative of sinc function is *Sine Integral* function Si(x). Since the

definition and generation of Si(x) is not simple modified sinc function has been used.

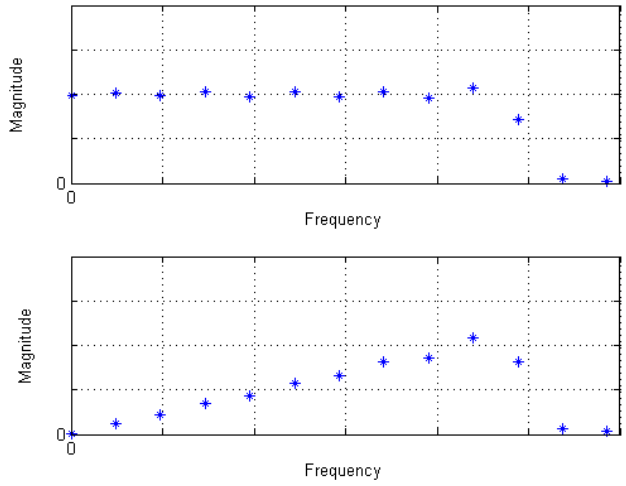

Fig. 5.20: Amplitude spectra of the sinc signal (top) and its derivative (bottom)

The measurement setup consisted of 14-bit programmable function generator AFG 3102 and Teledyne LeCroy HDO6104 High Definition Oscilloscope (15-bit digitizer) connected to PC. The generator used external synchronization from the oscilloscope. Trigger and Interpolator Jitter of the horizontal system was set less than 4 ps [48]. It means that the time uncertainty of the sample is $\Delta T = 4 \cdot 10^{-12}$ s. Digitized signal had maximum frequency of f_{max} = 21 kHz. Using formula (5.9), the phase error in degree is obtained.

$$Phase\ Error\ = \Delta T \cdot f_{max} \cdot 360 \quad (°) \tag{5.9}$$

After expressing the jitter and maximal frequency into (5.9), phase error had been calculated to $\approx 3 \cdot 10^{-5}$ degree. Thanks to this satisfactory phase resolution is ensured.

The detector operates on a non-magnetic construction in laboratory conditions and was excited by current sinc signal. Non-magnetic construction consists of platform where test targets were placed and adjustable arm with ATMID search head. Several experiments were done using the sinc signal on ATMID metal detector search head. Results were presented in [49] and [50]. Experiments showed that phase shift without using of lock-in amplifier is difficult to determine as a difference between transmitted and received signal. The possibility to measure phase shift between the background signal (measure without any object present) and signal measured with testing target present is offered. It was stated above (chapter 2.3), ATMID metal detector have small

ferromagnetic core placed in the search head (Fig 2.14). Thanks to that the reference signal can be obtained. Measured signals from testing targets can be than compared with it.

Evaluation of the received signal can be done both in time and frequency domains. Time domain evaluation offers nontraditional methods used in metal detection, such as correlation methods or fitting methods. Author of this work has an experience with fitting methods from previous research of analogue to digital converters testing, for example in [51], [52] and [53]. In the frequency domain an evaluation using Fourier transform (amplitude and frequency spectrum) will be done. As other integral transformations the Hilbert transform analysis come into consideration. Experimental results obtained with the sinc signal have been already presented in [54] and [55].

Block diagram of the measurement setup is in Fig 5.21.

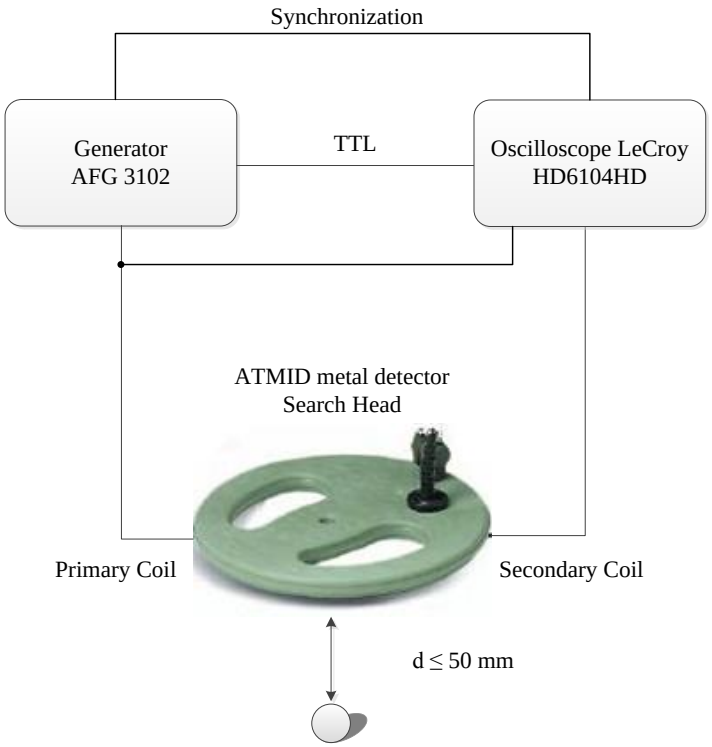

Fig. 5.21: Block diagram of the measurement setup

The generator was externally synchronized from the synchronization output of the oscilloscope. The digitizer was triggered by TTL signal from the generator. This is done to ensure the repeatability of the sinc signal generation.

As targets spheres of different diameters and materials were used. Five different materials, each with different sizes of the spheres diameters where chosen, three non-ferromagnetic and two ferromagnetic materials – bronze, brass and stainless steel AISI 316 spheres for non-ferromagnetic and stainless steel AISI 420 and chrome steel AISI 52100 100Cr6 spheres as a representatives of ferromagnetic materials. Stainless steel AISI 316 spheres represents material with relative permeability slightly larger than one; μ_r = 1.02. All materials were measured for at least three different diameters of spheres (diameter from 10 mm to 25 mm). Spheres were placed to maximal distance of 50 mm from the coil in the axis of greatest sensitivity.

The following parameters describe the used modified sinc signal, frequency $f_1 = 1/T_1$ = 0.5 kHz, $f_2 = 1/T_2$ = 10 kHz, 10 significant carrier frequencies, and amplitude of 10 V. From this parameters repeating frequency of f_R = 1 kHz follows and significant frequencies at each 2 kHz.

5.3.1. Signal Processing in Time Domain

As written above (chapter 3), in the time domain signal processing offers methods that are non-traditional in metal object detection. Significant drawback of time domain methods lies in loss of the information from individual frequencies; the signal has to be examined as a whole. Therefore the processing of the signal in time domain is not advantageous in comparison with frequency domain methods. But it can be used as a complement to frequency domain methods or as very simple methods which are not demanding for computation. After several experiments using correlation functions, only standard integral parameters of the signal such as RMS value and peak values of the signal and Crest Factor (5.10) were applied.

$$CF = \frac{u_{MAX}}{\sqrt{\frac{1}{T}\int_0^{0+T} u^2(t)dt}}, \tag{5.10}$$

where u is the signal and T is period.

Experimental data, measured on measurement setup presented in Fig. 5.21, from different targets, as stated above, had to be preprocessed. Firstly signal was filtered by designed band pass FIR filter of 300th order and Blackman-Harris window with lower filtered frequency f_d = 1 kHz and upper frequency f_h = 22 kHz. Moreover the one period of the signal was averaged from 1000 periods which corresponds to measurement time of one second. Time plot of the induced voltage without any metal object is shown in Fig 5.22.

As it was stated in chapter 2.4 and presented in Fig. 2.14, the output signal waveform from the receiving coil is not equaled to zero. This is caused by the ferromagnetic core. The coil is unbalanced.

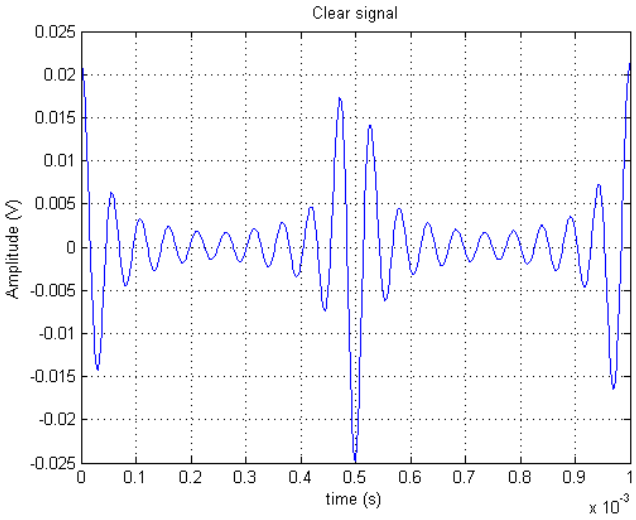

Fig. 5.22: Time plot of received signal without any object present

Waveforms of signal which corresponds to ferromagnetic and non-ferromagnetic object response is presented in Fig. 5.23.

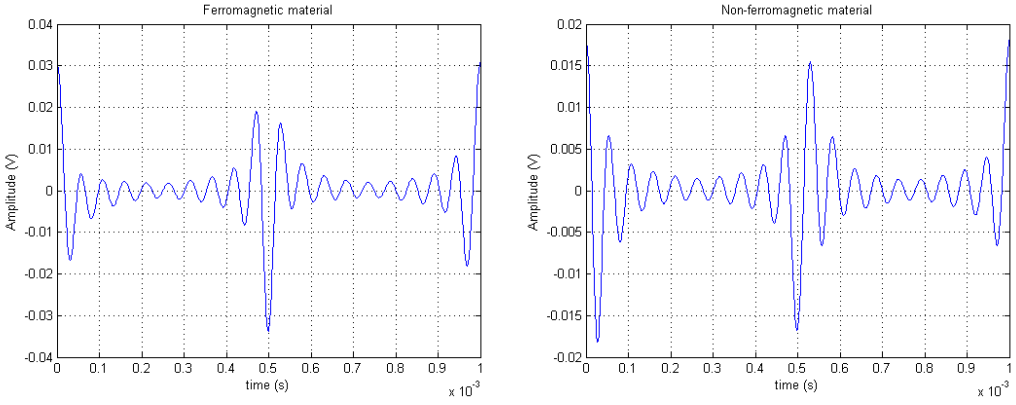

Fig. 5.23: Time plot of received signal from a ferromagnetic object and non-ferromagnetic object

Fig.5.23 shows signal waveforms correspond to ferrous chrome steel AISI 52100 100Cr6 sphere with diameter of 25 mm and signal correspond to non-ferrous Bronze sphere with the same diameter. These materials were chosen for demonstration of induced voltage behavior for the both types of materials (ferrous x non-ferrous). A ferrous material increases the value of induced voltage, which also corresponds to theory. A different situation occurs in the case of a non-ferrous material. The shape of the signal waveform is different. It is due to the opposite phase shift which is caused by non-ferromagnetic target. The induced voltage is smaller. Thanks to that the signal waveform of a non-ferrous material has a different shape.

Comparison of two different diameters of both ferrous and non-ferrous materials is presented in Figs. 5.24 and 5.25.

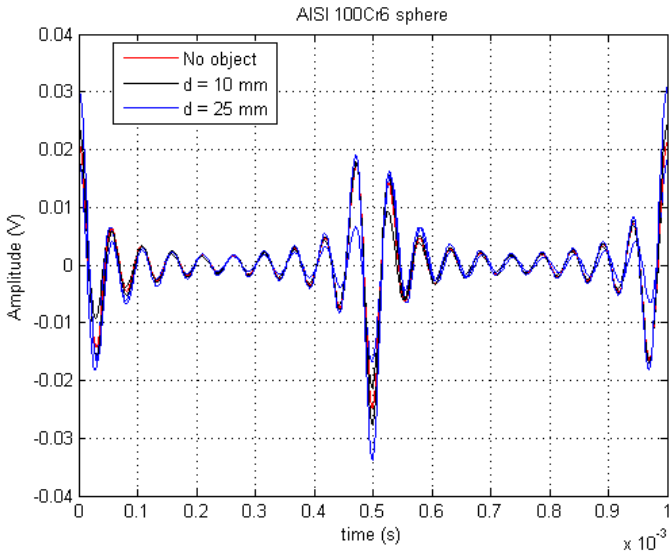

Fig. 5.24: Time plot of received signal from different sizes of AISI 52100 100Cr6 spheres

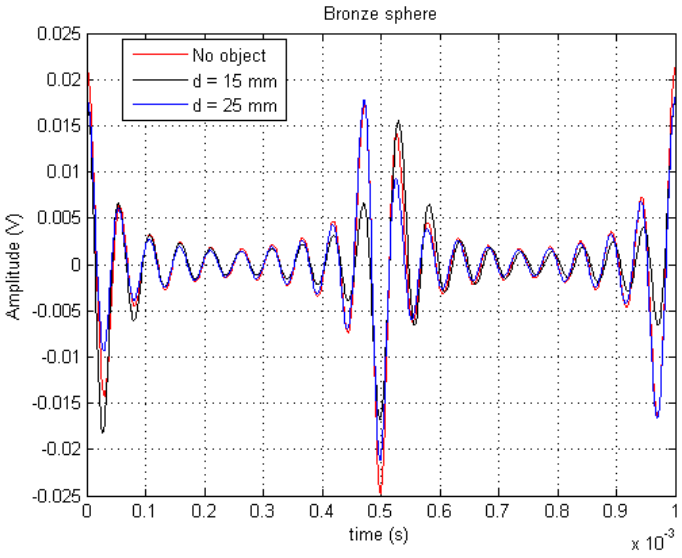

Fig. 5.25: Time plot of received signal from different sizes of bronze spheres

The value of induced voltage is proportional to the excitation frequency, the size and electromagnetic properties of the object. Therefore it can be seen the biggest increase of induced voltage on high frequencies is noticeable. From the both figures (5.24 and 5.25) it is clear that the shape of the waveform changes also with the sizes.

This can be used in determining the standard integral parameters of the induced signal. On the next two figures (Figs. 5.26 and 5.27) are shown effective and maximal values of various ferrous and non-ferrous materials of various sizes for two different distances l (l = 10 mm and l = 30 mm) from the coil compared with values if no object is present. Measured RMS, MAX, and Crest factor values corresponds to target spheres, are named after the material which is made of and the sphere diameter (e.g. bronze sphere of diameter d = 10 mm is named Bronze10).

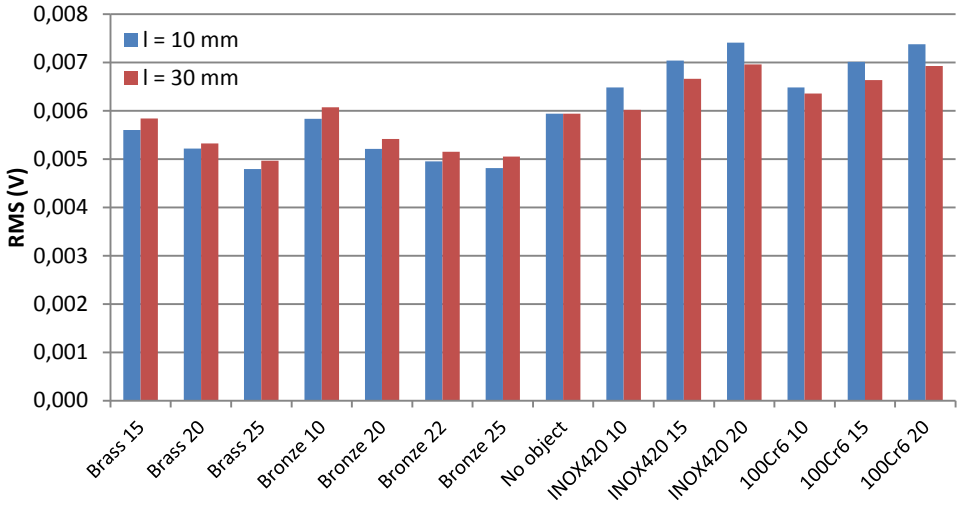

Fig. 5.26: RMS value corresponds to different materials, sizes (in mm) and distances

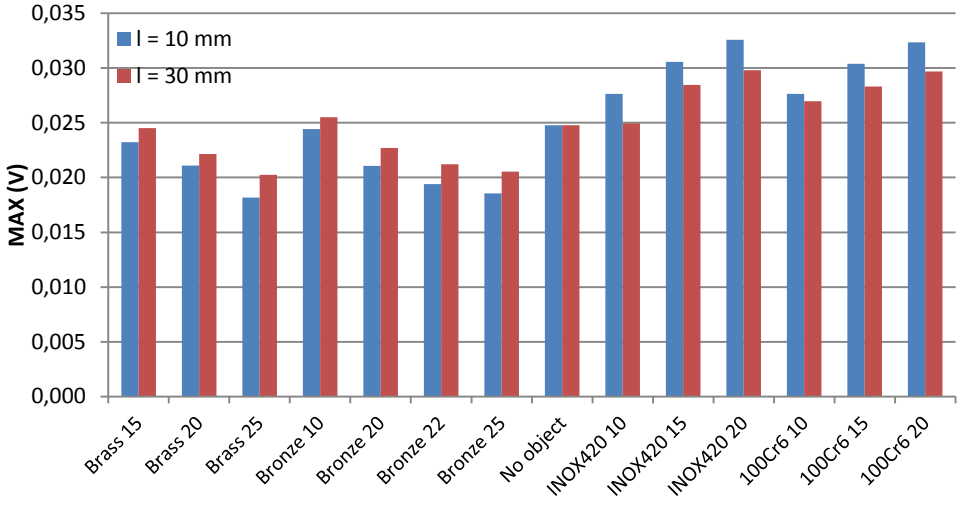

Fig. 5.27: MAX value corresponds to different materials, sizes (in mm) and distances

The change of the both RMS and maximal values can be observed from figures. Presence of ferrous materials increases the both values with increasing diameter of spheres. In contrast to non-ferrous materials, which decrease the both values with increasing diameter of the sphere. This only applies to the targets in close distances. For small diameters in larger distance non-ferrous materials behave like ferrous. Figures (5.26 and 5.27) also shows that with increasing

distance from the coil both RMS and MAX values of the measured objects are approaching evenly to the values of signal without measure object. Fig. 5.28 shows dependency of Crest Factors difference with and without measured metal object.

Crest factor difference were computed as a difference of crest factor of signals which corresponds to measured objects and crest factor when no object is present. Crest factors bar shows that if the signal from the detected object is strong enough (i.e. detected object is large enough or the distance from the coil is not large) differentiation between ferrous and non-ferrous materials can be done very simply and easily. On the other hand if the object is small and is not close to the coil non-ferrous materials act like ferrous.

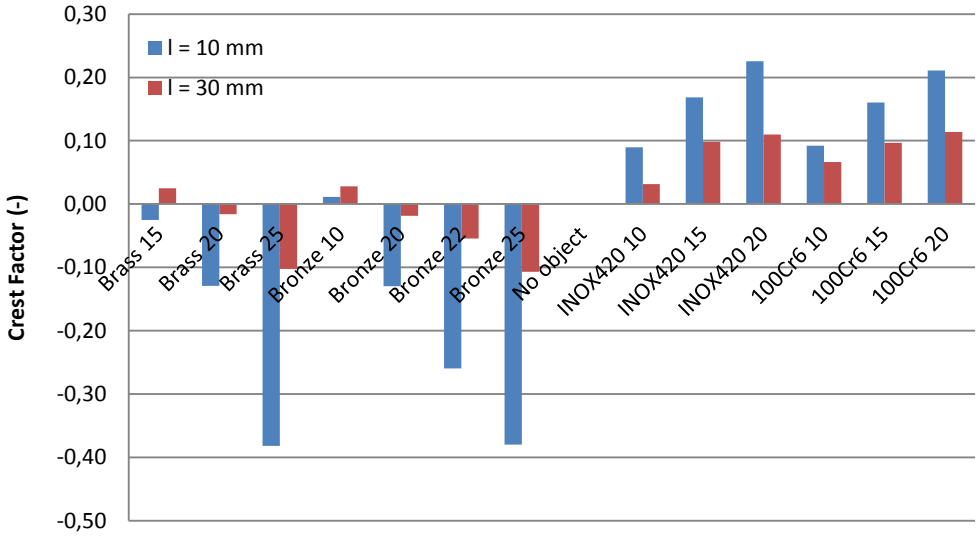

Fig. 5.28: Crest Factor value corresponds to different materials, sizes (in mm) and distances

Fig 5.29 shows crest factors from 5 different measurements of same objects which were placed into the same distance and pinpointed by the same way. The variances between individual measurements were minimal.

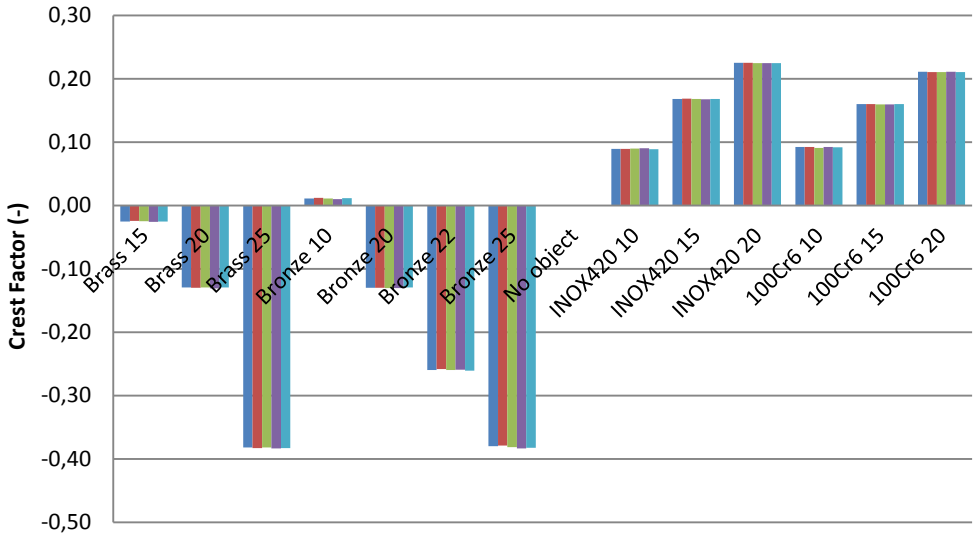

Fig. 5.29: Signal Crest Factor of different materials in the distance of l = 10 mm for 5 measurement under same conditions

Standard integral parameters offer a very simple and undemanding method how to distinguish ferrous and non-ferrous materials under specific conditions, however differentiation between individual materials cannot be done. Time domain does not offer any attractive options of signal processing, therefore the following work was dedicated to frequency domain processing.

5.3.2. Signal Processing in Frequency Domain

It was written at the beginning of chapter 5.3, processing in frequency domain offers FFT primarily. The procedure was similar to the previous experiment. First, a background signal without the presence of any tested objects is measured. Then, this signal is compared with the signals corresponding to the tested spheres. Presented results obtained using the Fourier transform are presented in Figures 5.30 – 5.40. Sampling frequency of the digitizer was 1MSample per second, the record was one second long.

Firstly the signal was filtered by the same FIR filter as using time domain processing. These filtered signals were after processed by DFT using a FFT algorithm (5.3) and (5.4), and were computed from number of samples N = 1048578, which is nearest powers of two from 1 Msamples. The phase spectra were calculated from a complex variable definition. All presented phase spectra were computed as a difference between the phase spectrum of the signal which corresponds to measurement without any target (background, no object) and the phase spectrum of the signal which correspond to measurement with a testing

target. For better presentation and comparison, the spectra of comparing signals which are presented are shifted by ±100 Hz. This is done for better presentation only.

Figures 5.30 and 5.31 shows the measured amplitude and phase spectra, together with polar graph, of the ferromagnetic AISI 52100 100Cr6 testing spheres of two different sizes (diameter of 10 mm and 20 mm). In the case of the multiple carriers, the frequency characteristic covers a wide range of *Response Function* in the same way as at chirp signal. Amplitude spectra which correspond to this material is greater at all frequencies than amplitude spectra of signal which correspond to no object present. This is caused by ferromagnetic material permeability which is much greater than one. In general, magnitude spectra are getting higher for all ferrous materials with increasing diameter of the sphere. Magnitudes on low frequencies increase more significantly than at higher frequencies witch can be caused by character of the *Response Function* and goes to its inductive limit. Phase shift difference shows that ferrous material shift the phase from positive values to negative. For greater diameter, absolute phase shift increasing but relative phase shift due to getting closer to inductive limit decreasing apparently. The difference between measured diameters of 10 mm and 20 mm is also in amplitude and phase spectra trend.

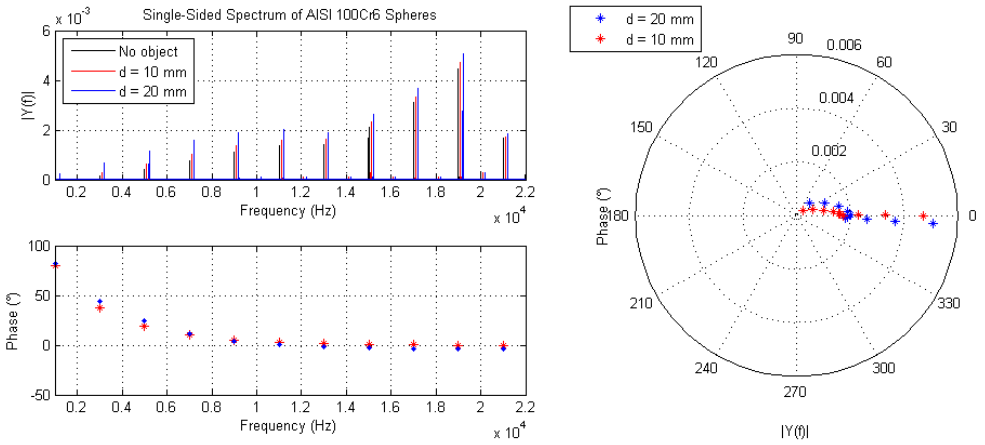

Fig. 5.30: Amplitude spectra, Phase spectra and polar graph corresponding to AISI 52100 100Cr6 sphere with diameters of 10 mm and 20 mm

Next presented ferromagnetic object (Fig. 5.31) is stainless steel AISI 420 which has similar electromagnetic properties as chrome steel 100Cr6 (see Tab 4.1). Amplitude and phase spectra are similar too. Unsurprisingly, in lower frequencies the signal amplitude spectrum of signal corresponding to the AISI 420 sphere increasing more than at higher frequencies similarly as for a 100Cr6 chrome steel sphere. A phase difference spectrum shows also the same trend.

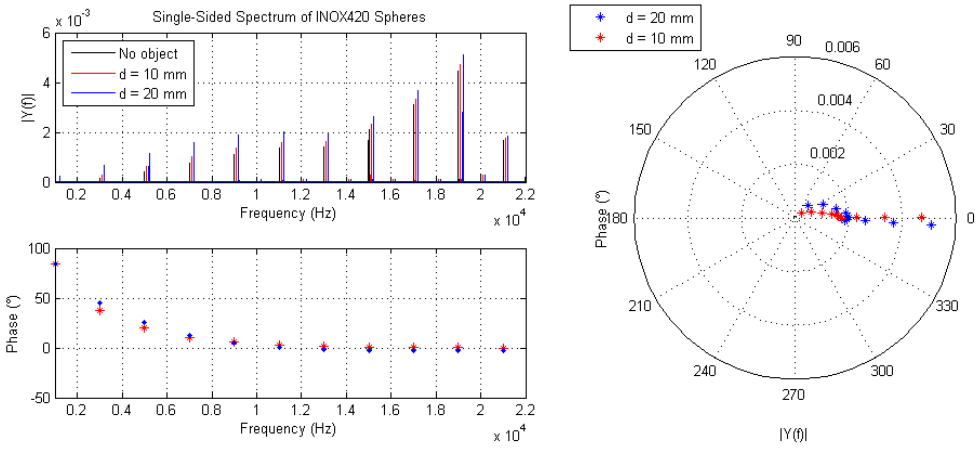

Fig. 5.31: Amplitude spectra, Phase spectra and polar graph corresponding to AISI 420 sphere with diameters of 10 mm and 20 mm

Amplitude spectra of both materials show noticeable increases at lower frequencies – this can be explained due to the small ferrous core which is inside the ATMID metal detector search head. Measurements confirm that the distinction between different similar ferromagnetic objects cannot be done easily. Comparison of both materials will be done in next section.

The first presented non-ferromagnetic material is brass. Brass spheres with diameter of 12 mm and 20 mm is presented in Fig. 5.32. An amplitude spectrum show essential difference from ferrous materials. At lower frequencies amplitude spectra rises with diameter of the target. This is due to the influence of the ferromagnetic core inside of the search head. However at higher frequencies (approx. 8 kHz) a different situation occurs. Non-ferromagnetic material begins to dominate. At higher frequencies the phase shift of the signal is larger and causes the suppression of the induced voltage. This causes drop of spectral lines at higher frequencies.

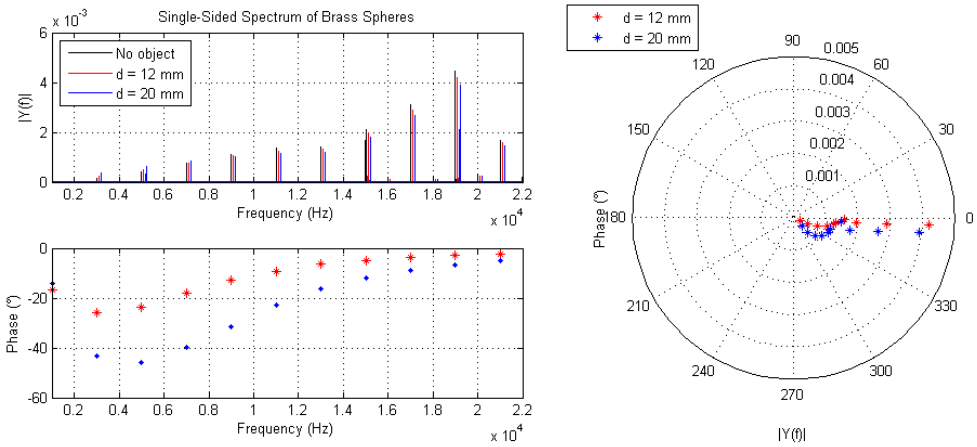

Fig. 5.32: Amplitude spectra, Phase spectra and polar graph corresponding to Brass sphere with diameters of 12 mm and 20 mm

Similar situation shows also the difference of phase spectra. As expected phase shift caused by non-ferromagnetic objects goes to negative values. At lower frequencies the phase difference between the signal which corresponds to non-ferrous material and signal which corresponds to the measurement without any target present is bigger as diameter of the sphere getting larger. At higher frequencies similar situation as for ferromagnetic material occurs; relative phase shift decreases and absolute phase shift gets bigger with larger diameter of spheres.

In Fig. 5.33 another non ferromagnetic material is presented. The results resemble situation between different ferrous materials, response of non-ferrous materials is similar to each other. Behavior of amplitude and even phase spectra is similar, which was expected. The *Response Function* changed minimally – the difference between response parameters α of the both materials is (thanks to similar conductivity, see Table 4.1), minimal. Comparison of all nonferrous materials together with ferrous materials is be presented in next section.

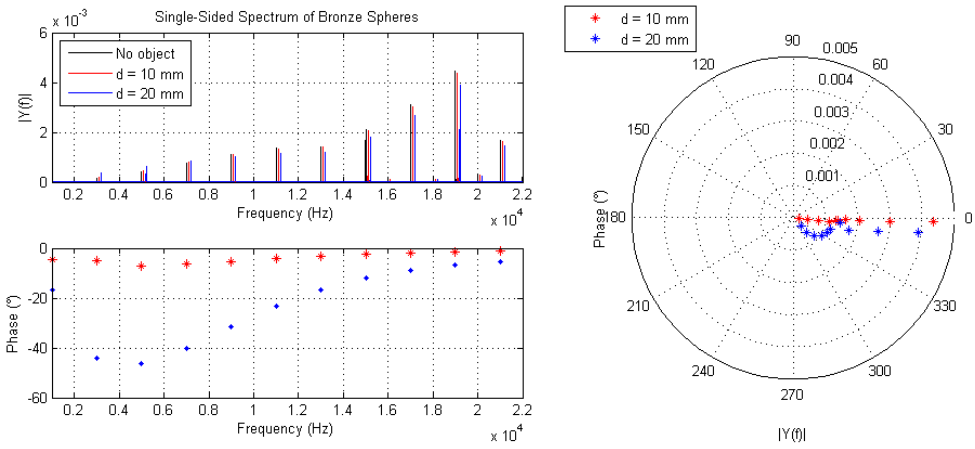

Fig. 5.33: Amplitude spectra, Phase spectra and polar graph corresponding to Bronze sphere with diameters of 10 mm and 20 mm

The last presented material is non-ferromagnetic stainless steel INOX 316. Behavior of the signal which corresponds to testing sphere with greater diameter is similar to other non-ferrous materials presented above. The amplitude of the received signal (induced voltage) is suppressed and the signal phase is shifted to the negative values. Sphere with smaller diameter has a minor response.

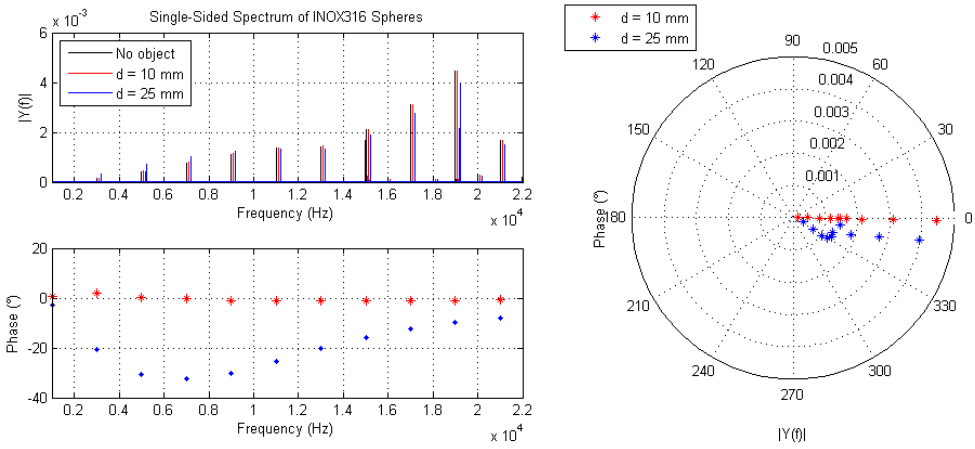

Fig. 5.34: Amplitude spectra, Phase spectra and polar graph corresponding to AISI 316 sphere with diameters of 10 mm and 20 mm

At lower frequencies the ferrous core dominates and induced voltage is greater than induced voltage without any object present. This is due to the low conductivity of INOX 316. At higher frequencies the influence of INOX 316 gets bigger. The phase shift has similar trend like all other non-ferrous materials. The

absolute phase shift in comparison to other two non-ferrous materials is due to lower conductivity smaller. It indicates lower sensitivity on small objects with low conductivity.

The measurement proves an apparent difference between ferromagnetic and non-ferromagnetic materials as it was expected. Ferromagnetic materials cause phase shift from positive to negative values and significant signal magnification at all carrier frequencies. Non-ferromagnetic objects cause negative phase shift and signal diminution at higher frequencies. The Ferromagnetic core in the search head predominate at lower frequencies over a low conductive non-ferromagnetic materials and it causes increasing of magnitudes of amplitude spectrum. At higher frequencies negative phase shift which is caused by non-ferromagnetic materials cause suppression of the transmitted field. It affects the shape of amplitude spectra.

Experiments show an applicability of the modified sinc signal and its benefit to apply all frequencies at once. It is possible to define the number of carrier frequencies and their position easily. Results of the measurement also showed lower sensitivity on low conducted materials.

By comparing of four different specimen with different diameters (d = 10 mm, 15 mm 20 mm and 25 mm) from ferrous chrome steel 100Cr6 it is evident that with increasing diameter the induced voltage increases uniformly. Differences between induced voltages getting smaller on higher frequencies this can be explained by approaching the Inductive limit of the *Response Function*. Phase spectra show differences in phases for individual the spheres. The difference increases with various diameters at higher frequencies especially. Spheres of larger diameter changes phase more than those of smaller diameter. Unforeseen phenomena occurs for diameter d = 10 mm. At low frequencies phase shift is greater than for all the larger spheres. Since the trend of its phase shift is different, at higher frequencies the phase shift, as would be expected, is lower. This phenomenon occurred even with repeated measurements and for similar ferrous materials.

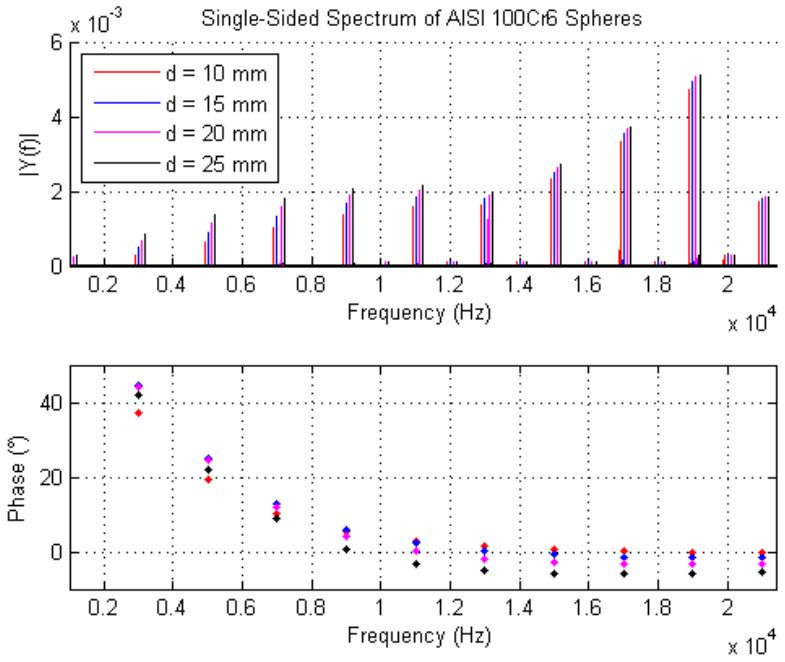

Fig. 5.35: Amplitude spectra and Phase spectra corresponding to AISI 52100 100Cr6 with diameters of 10 mm, 15 mm, 20 mm and 25 mm

The results of comparison of four different bronze spheres (diameters d = 10 mm, 13 mm, 20 mm and 22 mm) from a non-ferrous material is shown in Fig 5.35. The change of induced voltage has opposite trend, with increasing diameter of the sphere induced voltage decreases uniformly. It can be explained by negative phase shift. As already has been proven, non-ferrous materials change phase to negative values. Therefore the induced voltage which is induced when the coil is unbalanced is shifted and it cause drop in amplitude (chapter 2, Fig. 2.15). At lower frequencies absolute phase shift difference increasing greatly with diameter and getting smaller at higher frequencies thanks to character of the *Response Function*. This phase shift caused by non-ferrous is in contrast with ferrous materials. Phase shift, caused by different sizes of ferrous material, changes a little at lower frequencies.

From comparison (Figs 5.35 and 5.36) of different diameter sizes of ferrous and non-ferrous materials it follows that differentiation between ferrous and non-ferrous materials can be done. In addition thanks to the phase response and its trend object size estimation could also be done.

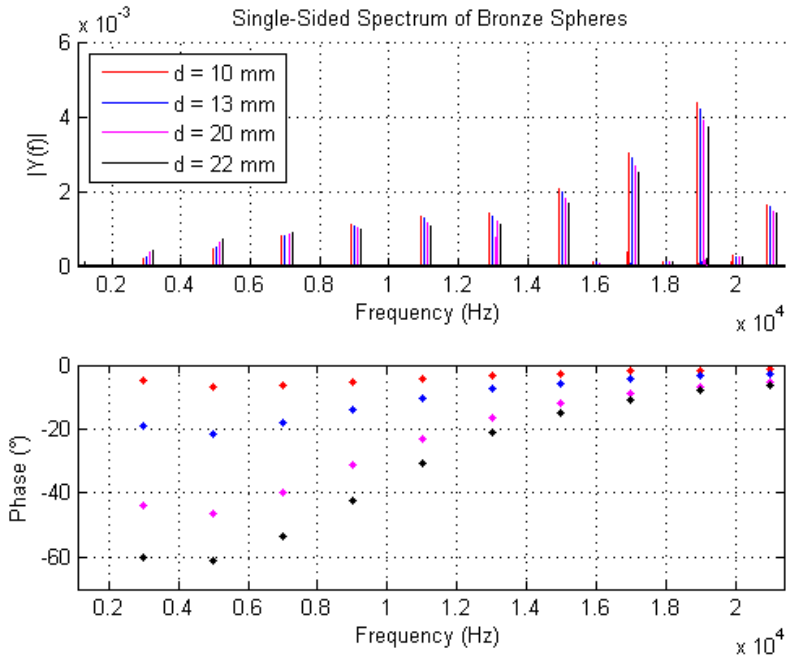

Fig. 5.36: Amplitude spectra and Phase spectra corresponding to bronze sphere with diameters of 10 mm, 15 mm, 20 mm and 25 mm

A closer comparison of similar materials is presented on the next two figures (Figs. 5.37 and 5.38). Since induced voltage is highly dependent on the position of the target, it is important for comparison of similar materials to keep the position of targets at the same position. All compared results were measured in the same position; exactly defined – in highest axis of sensitivity of the detector head at a distance of 50 mm from the detector. Presented results are processed using the same by from 1 Msamples/s. Spectra were computed from 1000 periods of the signal.

Fig 5.37 shows amplitude and phase spectra concerning two specimen from similar materials; INOX AISI 420 and AISI 52100 100Cr6 sphere with diameters of 20 mm. Phase difference corresponding to these materials is slightly larger than 1 degree at lower frequencies and slightly smaller than 1 degree at higher frequencies; difference between both materials is in the trend of the phase spectrum. Difference between the amplitude spectra is also minimal. The biggest difference is at the 10^{th} harmonic; at highest frequency. For better viewing X-Y chart is also presented (x-axis ~ magnitude, y-axis ~ phase).

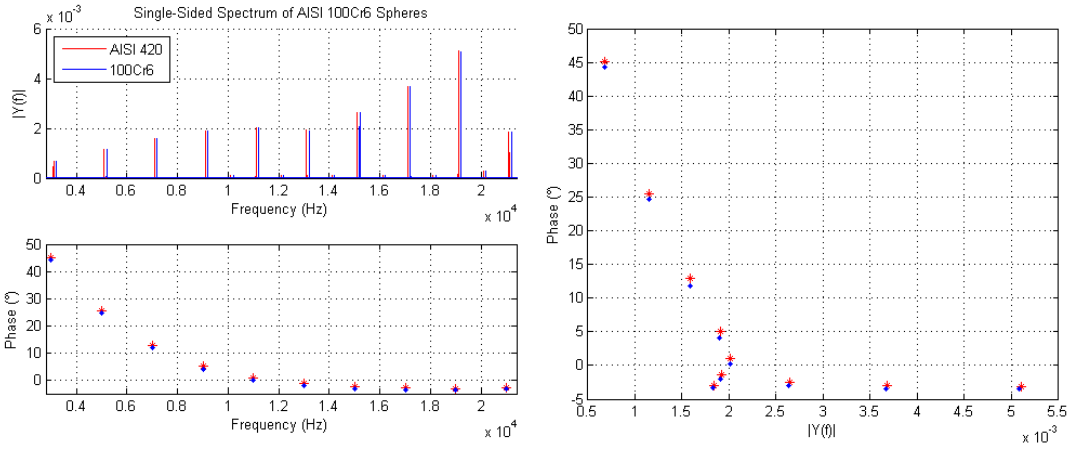

Fig. 5.37: Amplitude spectra, Phase spectra and X-Y chart corresponding to AISI 420 and AISI 52100 100Cr6 sphere with diameters of 20 mm

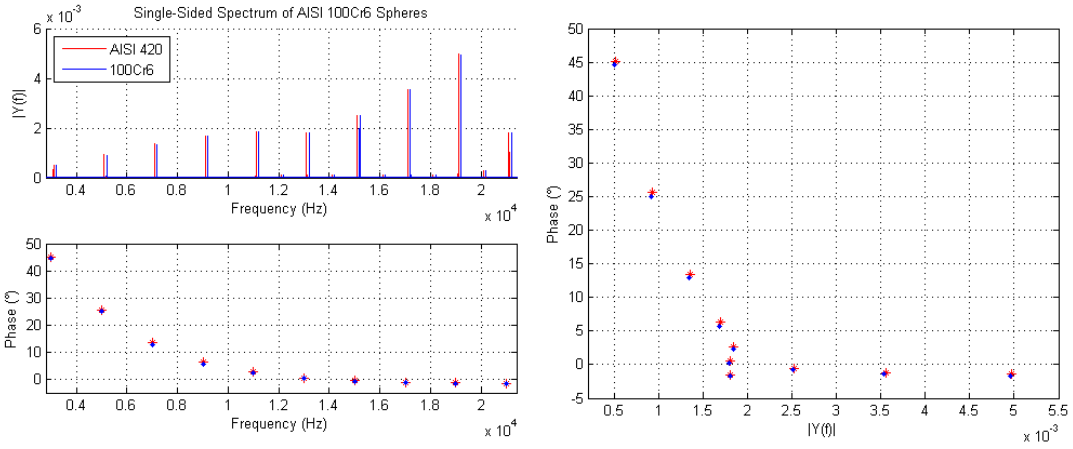

Fig. 5.38: Amplitude spectra, Phase spectra and X-Y chart corresponding to AISI 420 and AISI 52100 100Cr6 sphere with diameters of 15 mm

Fig 5.38 shows comparison of same two materials mentioned above but of different diameters, d = 15 mm. For smaller diameter phase shift difference between both materials decreasing. Phase shift of diameter d = 15 mm is halved in comparison with diameter d = 20 mm phase for both lower and higher frequencies. Phase difference is about 0.7 degree at lower frequencies and about 0.5 degree at higher frequencies. As in the previous case, the difference is in the trend of the phase spectrum. Amplitude spectra difference is bigger with increasing frequency.

A similar trend of difference between phase spectra is shown in Fig. 5.39 for spheres with diameter d = 10 mm. Phase difference is about 0.4 degree for lower frequencies and about 0.2 degree for higher frequencies.

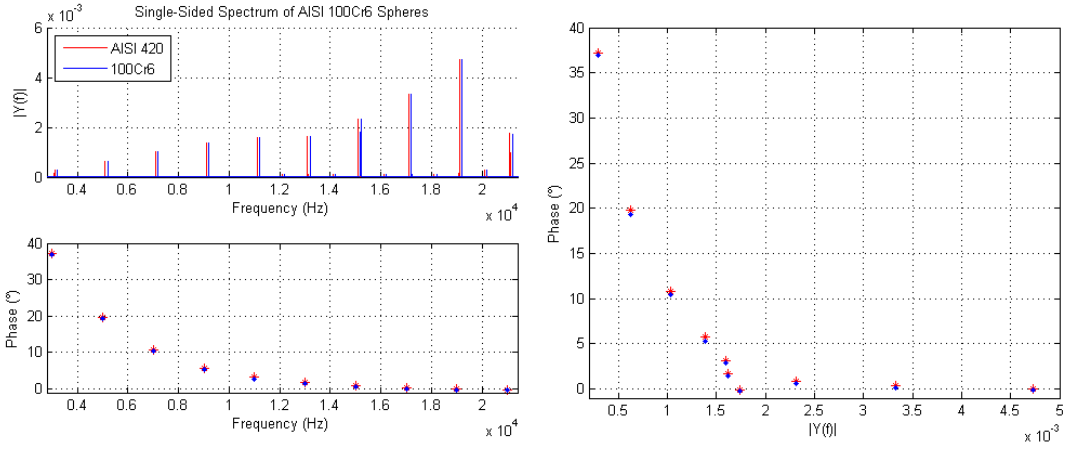

Fig. 5.39: Amplitude spectra and Phase spectra and X-Y chart of AISI 420 and AISI 52100 100Cr6 sphere with diameters of 10 mm

This results show that the differentiation between similar materials is more difficult when the size of the object become smaller.

When comparing non-ferromagnetic materials with similar electromagnetic properties (brass and bronze) similar situation occurs. Comparison of brass and bronze spheres with diameter of d = 20 mm is shown in Fig 5.40. The difference in the amplitude spectrum increases with increasing frequency. The phase spectra difference decreases with increasing frequency.

Phase difference at lower frequencies is about 1.5 degree for lower frequencies and only about 0.2 degree for higher frequencies. The trend of the phase shift depends on response parameter α. Response parameter α of brass is approx. twice as bigger as of bronze. It leads to a smaller change in phase. The change of the phase shift between materials with similar properties is decreasing with the smaller diameter similarly like for ferromagnetic materials.

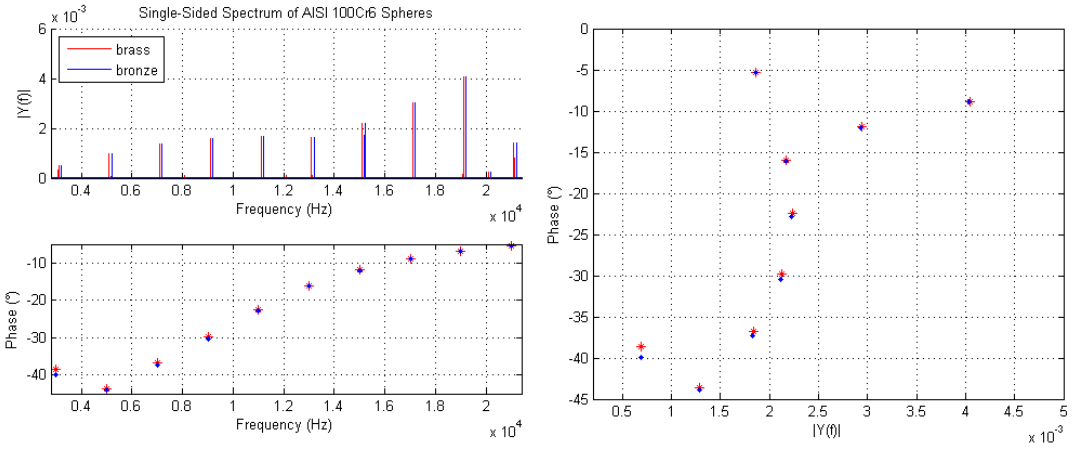

Fig. 5.40: Amplitude spectra and Phase spectra and X-Y chart of brass and bronze sphere with diameters of 20 mm

In general, experiment shows that the phase difference between similar ferromagnetic or non-ferromagnetic materials decreases with diameter. In addition at higher frequencies the difference between amplitude spectra of similar materials gets bigger in contrast to phase spectra difference. Phase difference between similar materials gets smaller with increasing frequency.

Based on the experimental results, use of sinc excitation signals allows possible identification and discrimination of the detected objects. The application of polyharmonic excitation signals bring an opportunity for better response in a wide range of frequencies, and therefore more extensive and complex set of data for the signal analysis is available. It is evident that thanks to the *Response Function* the discrimination between different materials by means of classifier can be done. Possible problems with the classification are represented by the stability of the chosen features, and the presence of unknown targets.

5.4. Summary

In this chapter an application of polyharmonic signal for metal detection and classification is presented. Step sweep sine-wave signal, chirp signal and sinc signal were investigated. Step sweep sine-wave signal confirms behavior of ferromagnetic and non-ferromagnetic materials for different frequencies which were presented in chapter 4.2. Chirp signal showed possibilities to apply a polyharmonic signal for metal detection. Several experiments were done and presented ([43] and [44]) before the author left this excitation signal due to usage of similar signal by Minelab company. Sinc signal thanks to its spectrum comes into consideration finally.

Since the signal can be generated by generator with DDS and its parameters can be easily defined it appeared as an ideal polyharmonic signal used for metal objects identification. Experiments showed that processing in the time domain standard integral parameters offer a simple method how to distinguish between ferrous and non-ferrous materials. It can be done if the induced voltage which corresponds to a detected object is strong enough. Therefore time domain does not offer any attractive methods for advanced identification of objects. Processing in frequency domain using FFT amplitude and phase spectra with multiple frequencies is obtained. It can be used for object identification and classification. Experiments showed that thanks to multiple frequencies, differentiation between even similar objects (in a way of electromagnetic response) can be done.

[43] Svatos, J. - Vedral, J., 2012: The Usage of Frequency Swept Signals for Metal Detection, *IEEE Transactions on Magnetics*, vol. 4, no. 48, pp. 1501-1504.

[44] Svatos, J., Vedral, J., Fexa, P., 2011. Metal Detector Excited by Frequency Swept Signals, *Metrology and Measurement Systems*, vol. XVIII, no. 1, pp. 57-68.

[45] Svatos, J., Vedral, J., Fexa, P., 2010. Metal Detector Excited by Polyharmonic Signals, *Applied Electronics*, pp. 339–342.

[46] Fexa, P., Vedral, J., 2012. DAC testing using impulse signals, *Metrology and Measurement Systems*, vol. XIX, No. 1, pp. 105-114.

[47] Kowalewski, M., Lentka, G., 2013. Fast High-Impedance Spectroscopy Method Using Sinc Signal Excitation, *Metrology and Measurement Systems*, vol. XX, no. 4, pp. 645-654.

[48] LECROY. Operational Manual HDO6000 High Definition Oscilloscopes, [online] Available at <http://cdn.teledynelecroy.com/files/pdf/hdo6000_oscilloscope_datasheet.pdf>.

[49] Svatos, J., Vedral, J., Novacek, P., 2012. Metal Object Detection and Discrimination Using Sinc Signal, *Baltic Electronic Conference*, Tallinn.

[50] Svatos, J., Vedral, J., Novacek, P., 2012. Sin(x)/x Signal Utilization in Metal Detection and Discrimination, Magnetic Measurement 2012, Book of Abstracts, pp. 46.

[51] Fexa, P., Svatos, J., Vedral, J., 2009. Dynamic Testing of Audio Codec, Electronic Devices and Systems, *IMAPS CS International Conference*, pp. 63-68.

[52] Fexa, P., Svatos, J., Vedral, J., 2009. High Resolution Audio Codec Test, *MEASUREMENT 2009 - Proceedings of the 7th International Conference on Measurement*, pp. 206-209.

[53] Vedral, J., Svatos, J., Fexa, P., 2009. Methods for Economical Test of Dynamic Parameters ADCs, *Metrology and Measurement Systems*, vol. XV, no. 1, pp. 161-170.

[54] Svatos, J. - Vedral, J. - Novacek, P., 2012. Sin(x)/x Signal Utilization in Metal Detection and Discrimination In: *Magnetic Measurements 2012*. Bratislava, Slovak University of Technology.

[55] Svatos, J. - Vedral, J. - Novacek, P., 2012. Metal Object Detection and Discrimination Using Sinc Signal, *BEC 2012 - Proceedings of the 13th Biennial Baltic Electronics Conference*, Tallinn Technical University, pp. 307-310.

6. Data Classification

Pattern classification or in short classification tries to solve a problem of identifying and assigning examined data to set of categories a new observation belongs. Assigning of examined data depends on the basis of a training data set containing observations whose category membership is known. An algorithm that implements identifying and assigning of examined data is known as a classifier. An algorithm should be robust to differences between examined and trained data. The term "classifier" sometimes also refers to the mathematical function, implemented by a classification algorithm that maps input data to a category [56]. Classifier assigns a class label to examined data based on measurements that are obtained from previous observations.

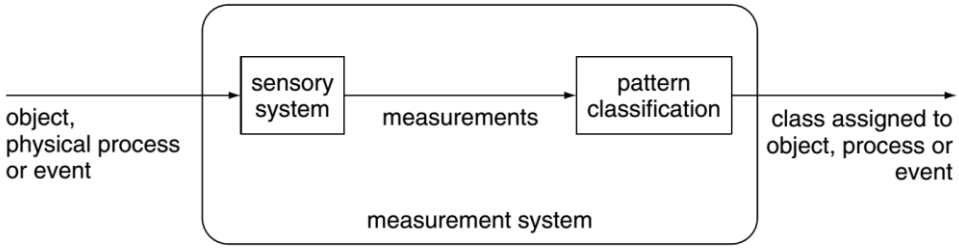

Fig. 6.1: Pattern classification [57]

There are two basic groups of classification methods; syntactic method and feature method. Syntactic methods are used in computer vision. Feature methods use a vector of features which characterize the properties of an object. Vector of features is usually represented by measured data or significant characteristics computed from measured data. Features can be of continuous or discrete value. Algorithm of pattern recognition can be defined on the basis of analyses of process (or its model) or can be trained – supervised learning [58].

Supervised learning is a learning task algorithm where the function is inferred from labeled training data (vector of features). The labels determine to which class the training data belong. A supervised learning algorithm analyzes the training data vector of features and creates a function, which can be used for mapping new measured data. An optimal function will allow the algorithm to correctly determine the class labels for the testing data [59].

Machine learning can be achieved by using various advanced statistical methods for classification tasks. These methods include Naive Bayes, k-Nearest Neighbors (KNN) and Support Vector Machines (SVM). More details about all methods can be found in [60].

Naive Bayes methods are based on Bayesian theorem (6.1) and are particularly appropriate when the dimensionality of the inputs is high. The Naive Bayes Classifier estimates for every class and every feature separately. Naive Bayes method is simple, but despite its simplicity can often outperform other sophisticated classification methods.

$$P(A/B) = \frac{P(B/A)P(A)}{P(B)}, \tag{6.1}$$

where $P(A)$, $P(B)$ is prior probability of A, B respectively and $P(B/A)$ is the conditional probability, the probability of A given that B is true.

KNN method is a non-parametric method which can work without training. It is based on the intuitive idea that close objects are more likely to be in the same category. The KNN algorithm is among the simplest of all classifying algorithms. The input consists of the k closest training examples in the feature space. The output is a class membership. The neighbors are taken from a data set for which the class of the data is known. This can be thought of as a training set for the algorithm, though no explicit training step is required. A shortcoming of the KNN algorithm is its sensitivity to the local structure of the data [61].

SVM method works based on construction of nonlinear decision boundaries. SVM creates decision plane (Hyperplane) which, in Feature space, separate training data optimally. Decision plane then separates sets of objects which have different class memberships. Because of the nature of the Feature space (Fig 6.2) in which these boundaries are found, SVM can exhibit a large degree of flexibility in handling classification [62]. Outline shows principle of SMV algorithm. Input data are transformed (mapped) to Feature space using mathematical function known as kernel.

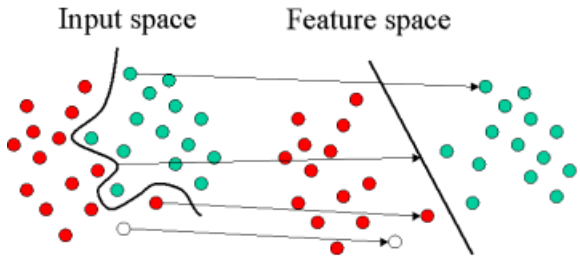

Fig. 6.2: Pattern classification [62]

Support vector models can be linear, polynomial, sigmoidal and radial basis function. Advantage of classifying the detected objects may be in the creation of database of patterns (different materials or even specific objects). This could help in discrimination or in identification of examined objects. The disadvantage of

using classification methods in metal detection and identification can be found in stability of the chosen features (multi frequency approach), in presence of untrained data/objects or in correct pinpointing of examined object – in a proper location of the highest axis of sensitivity in the middle of the detector head.

6.1. Data Preprocessing

Behavior of electromagnetic response for polyharmonic sinc signal, which consists of 10 significant frequencies, has been shown in chapter 5.3. Experiments with different ferromagnetic and non-ferromagnetic materials were done. In the case that Signal to Noise ratio is strong enough, a classification or an identification of examined objects can be done. Thanks to *Response Function* of each object there is a chance to distinguish ferromagnetic and non-ferromagnetic materials, small objects and large objects and even, with certain probability, different types of materials.

All data processing and classification was done using Matlab software with classification pattern recognition PRTools ver. 5. PRTools offers more than 300 user routines for traditional statistical pattern recognition tasks. It includes procedures for data generation, training classifiers, combining classifiers, features selection, linear and non-linear feature extraction, density estimation, cluster analysis, evaluation and visualization. PRTools works with three specific programming classes [63]:

- *Dataset*: is defined as a set of objects which are represented by vectors. Together with these vectors, additional information about individual objects, features, classes and the entire dataset is stored.
- *Datafile*: defines the way how to specific sets of raw objects can be transformed into a dataset.
- *Mapping*: stores the names of the routines that define the transformation of objects from one space to another. Moreover it stores the parameter values or information about space dimensions and class names.

Various designed procedures can be used with these specific classes to perform a pattern recognition and classification. The list of the most important procedures is introduced.

- *Preprocessing*: together with Matlab and various public open Matlab toolboxes, PRTools toolbox offer an extensive set of routines for raw data processing.
- *Feature extraction*: PRTools offers various routines such as Patch statistics, blob dimensions, various moments, histograms, 1-D and 2-D spectra and Harris points.

- *Feature spaces*: routines for scaling, feature selection (individual, forward, backward, floating, branch and bound), principal component analysis - PCA, linear discriminant analysis - LDA, Fisher mapping and more.
- *Density estimation*: various Gaussian models, mixture of Gaussians, Parzen and nearest neighbor density estimation.
- *Classifiers*: PRTools offers s large number of classifiers such as kNN, Gaussian models, nearest mean, SVM, adaboost, decision trees, feed-forward neural network and many others. PRTools offers combining classifiers also.
- *Evaluation*: In addition PRTools offers automatic cross validation based optimization of classifier parameters, learning curves, rejects options and many others.

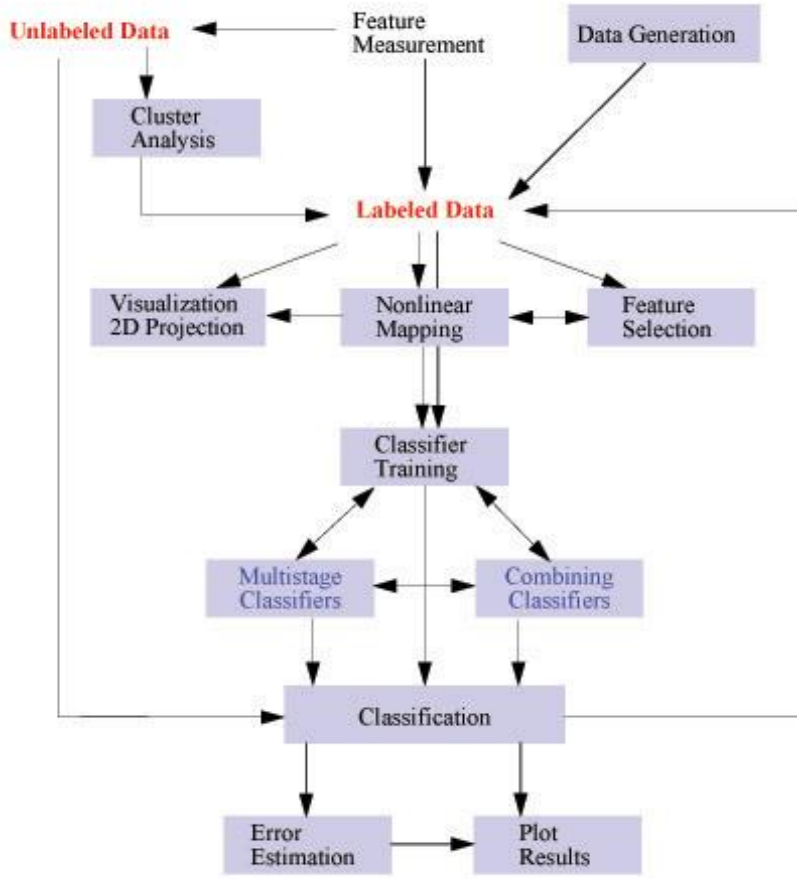

Fig. 6.3: PRTools toolbox [63]

Measured raw data must be preprocessed before a classification can be performed. The raw data obtained from individual experiments were digitized and stored at datasets. These datasets were used for further classification process. One dataset contains 20 individual measurements. Each measurement represents different size and materials. Measured materials are Brass, Bronze, INOX AISI 316 and AISI 420 and 52100 100Cr6. These materials were selected because of their use in other experiments made in Department of Measurement [63]. Spheres with diameter d = 10 mm, 12 mm, 13 mm, 15 mm, 20 mm, 22 mm and 25 mm were used together with testing piece (Fig. 6.4) from 52100 100Cr6 material which is used as testing object by Schiebel company.

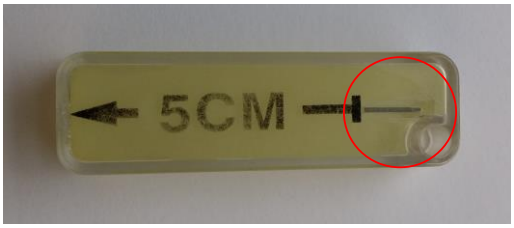

Fig. 6.4: Testing piece from 52100 100Cr6

To ensure that the data classification is done correctly, great amount of data must be collected and processed. To reduce amount of data and computing demands primarily, the decision has been made that the length of one measurement is 250000 samples. Sample rate 1Msamples/s has been used, i.e. one measurement has taken 250 ms and has consisted of 250 periods (1000 samples/period) for each individual target.

Total of 20 sets of measurements for classification were taken. Measurement of one set has been done as follows; target was placed under the coil in the distance of maximum 50 mm. Coil was placed to position where the signal of induced voltage was maximal. Target was pinpointed. Thereafter signal from the pinpointed target was measured four times. One set consists of 20 different materials and diameters described above. All targets were measured four times each. By following this measurement process 20 sets of raw data from 20 targets, where each target is measured four times, were obtained. The best way how to arrange all measurements in Matlab for future processing and classification is to save all measurements into a Nested structure.

At first, raw data have to be filtered. Since the frequency of measured data was from f_d = 1 kHz to f_h = 21 kHz a band pass digital filter has been used. Whereas a measured data from specific object were compared to data without object, a background (i.e. signal without any object present) signal was measured before every single set of measurement. Thereafter a discrete Fourier transform was computed from filtered raw data of each set and all targets.

As only amplitude and phase spectra at desired frequencies are relevant, the algorithm for maximum peak detection near significant frequencies was applied. The algorithm finds relevant spectral lines in amplitude spectrum and its corresponding phases. Thanks to that a set of 10 desired frequencies and corresponding 10 values of amplitude spectra and 10 values of phase spectra for each target and every measurement is obtained.

Preprocessed data was stored in nested structure (Fig. 6.5) for further processing and classification. Nested structure consist of *N* sets of measurement, where one set of measurement contains *M* numbers of measured samples where every sample was measured *K*-times. Every sample was stored in arrays of frequencies, magnitudes and phases at the end.

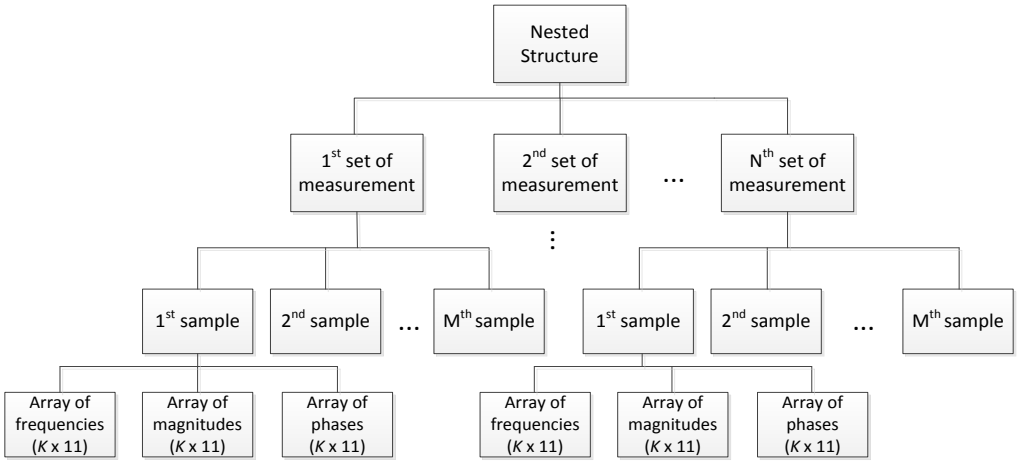

Fig. 6.5: Nested structure

As mentioned above, phase spectra were computed as the difference between signal with and without target. To suppress any interferences amplitude spectra were computed in a same way as a phase spectra, as a difference between signal with and without target. This way of approach is advantageous in areas where the background signal can change (for example in mineralized soils).

Data preprocessed and stored this way can be used for further classification of metal objects. Therefore all raw signals from detected/pinpointed object could be processed using the same method. Flow chart of preprocessing part of program is presented in Fig. 6.6.

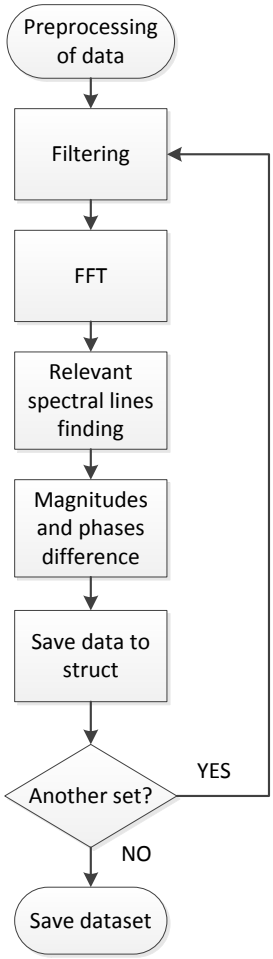

Fig. 6.6: Preprocessing flowchart

6.2. Support Vector Machines Classifier

At the beginning of this chapter several types of classifiers were outlined. Based on consultations and available literature, for example [57], [63] and [65], a decision has been made to use primarily Support Vector Machines (SVM) classifier. SVM classifier belongs to the category that learns from examples. The learning problem of classifiers can be defined as supervised or unsupervised; it means that the true class of the sample is known or unknown. Since the class of the samples is known, supervised learning is discussed only. As with any supervised learning model, a SVM must be learned firstly and then cross validated as a classifier. In this case it is assumed that a large number of examined data is available. Some part of the available data is selected from the group. These selected data are called training samples. Each sample is presented to the sensory

system which returns the measurement vector associated with that sample. The purpose of supervised learning is to use these measurement vectors of the samples to build a classifier [57].

There is one main method of representing data sets in PRTools. Let N_s be the number of samples in training set. Then each object of the sample is enumerated by $n = 1, 2, \ldots, N_s$ and have a measurement vector $\boldsymbol{z}_n$. The class of the n^{th} object is denoted by θ_n. The labeled training data T_s consist from a measurement vector and its class:

$$T_s = \{(z_n, \theta_n)\} \tag{6.2}$$

SVM classifier works based on construction of decision hyperplane as described at the beginning of this chapter. The best hyperplane means the one with the maximal margin between two classes. Margin means the maximal width of the borders parallel to the hyperplane that does not contain samples data. In contrast to other linear classifiers, which separates data based on findings one solution arbitrary selected from an 'infinite' set on solutions.

If the training data are linearly separable SVM can be expressed as follows. The equation of the hyperplane is defined by (6.3).

$$g(\boldsymbol{z}) = \boldsymbol{w} \cdot \boldsymbol{z} + b \tag{6.3}$$

Defined in [65] (6.3) can be rewritten for training data $\boldsymbol{z}_n$ labeled by $\boldsymbol{c}_n$ into two constraint hyperplanes (6.4) and subsequently into (6.5):

$$\begin{aligned} \boldsymbol{w} \cdot \boldsymbol{z}_n + b \;&\geq\; 1 \qquad \text{for} \qquad \boldsymbol{c}_n = 1 \\ \boldsymbol{w} \cdot \boldsymbol{z}_n + b \;&\leq\; 1 \qquad \text{for} \qquad \boldsymbol{c}_n = -1 \end{aligned} \tag{6.4}$$

$$\boldsymbol{c_n}(\boldsymbol{w} \cdot \boldsymbol{z}_n + b) \;\geq\; 1, \tag{6.5}$$

where $\boldsymbol{z}_n$ is training samples and are labeled by $\boldsymbol{c}_n = \pm 1$, algorithm defines best separating hyperplane by finding $\boldsymbol{w}$ and b that minimize $\|\boldsymbol{w}\|$ such that for all data samples.

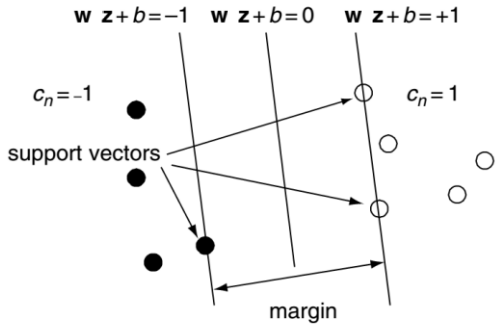

Fig. 6.7: Linear support vector classifier

Using Lagrange multipliers α_n, by multiplying each constraint in (6.5) equation for minimization is obtained (6.6) which is computationally simpler to solve.

$$L = \frac{1}{2}\left||w|\right| - \sum_n^{N_s} \alpha_n (c_n[\boldsymbol{w}\boldsymbol{z}_n + b] - 1) \tag{6.6}$$

Equation 4.32 should be minimized for $\boldsymbol{w}$ and b and maximized for Lagrange multipliers α_n. Computing partial derivative (6.7) and substituting into (6.6) one gets dual form (6.8).

$$\boldsymbol{w} = \sum_{n=1}^{N_s} \alpha_n c_n \boldsymbol{z}_n \qquad \text{and} \qquad \sum_{n=1}^{N_s} \alpha_n \boldsymbol{z}_n = 0 \tag{6.7}$$

$$L = \sum_{n=1}^{N_s} \alpha_n - \frac{1}{2}\sum_{n=1}^{N_s}\sum_{m=1}^{N_s} \alpha_n c_n \boldsymbol{z}_n \alpha_m c_m \boldsymbol{z}_m, \tag{6.8}$$

for $\alpha_n \geq 0$. This is a quadratic optimization problem, for which standard software packages are available. Only a few samples will have $\alpha_n > 0$ and the corresponding $\boldsymbol{z}_n$ are called support vector which lie on the margin and satisfy (6.5).

6.3. Data Classification

As data are preprocessed, optimal features and classification method must be chosen. At first 10 magnitudes and 10 phases at specific significant frequency obtained from FFT, are considered as features. This gives a 20-dimensional space for classification.

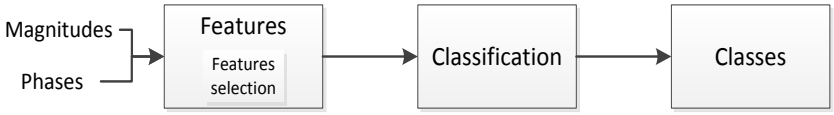

Fig. 6.8: Classification

Before the classification, it is necessary to determine into which classes to classify the measured data. From the experimental result presented in 5.3 it is evident, that an investigation of the object being ferromagnetic or not can be done. Therefore this classification should divide objects into two classes – ferrous and non-ferrous materials. Multiple frequencies and the fact that ferrous materials increase induced voltages and non-ferrous at higher frequencies decrease them, together with induced voltage phase change lead to the outcome that the classification can be done only by using elemental features (10 magnitudes and 10 phases; i.e. 20 dimensional problem).

To classify in individual materials classes, more complex approach and additional features must be considered. Experimental measured data shows that under ideal condition there is a chance to differentiate between different materials. Ideal conditions mean that the target is pinpointed accurately and induced voltage, which corresponds to detected target, has to be strong enough to be digitized properly. Magnitudes and phases together with additional features based on relations between magnitudes and phases should be used as features.

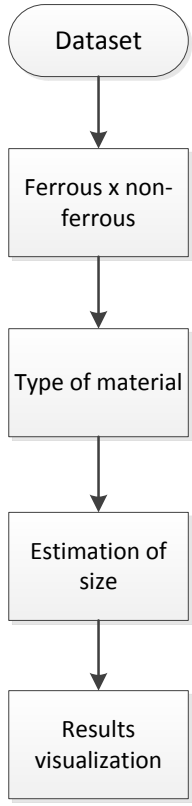

Fig. 6.9: Classification process

A size estimation of detected object should be considered as another possible classification. To identify the exact size of a target is almost impossible, but to estimate a size roughly, is possible thanks to different trends of magnitudes and phases spectra. As the classification has been done mainly by support vectors, following text will be focused mostly on it. However, the classifier is compared to other used classifiers.

Since classifiers with supervised learning are used, experimental data arranged in nested structure (Fig 6.5) must be separated into two groups. First group contained the training data and second group was used for testing data. There are many articles which deal with optimal number of training data. One of the proposed methods is the use of Learning curve. Use of Learning curves for optimal size of training data is described in [67]. Learning curve shows dependency of the model performance on the training data size. It depends on classification method, complexity of the classifier or how well can be the classes separated.

Learning curve in Fig. 6.10 shows optimal number of used training data in relation to the whole measured experimental data. This Learning curve shows dependency of classification success on training data size (classifying of non-ferrous object to its classes – materials).

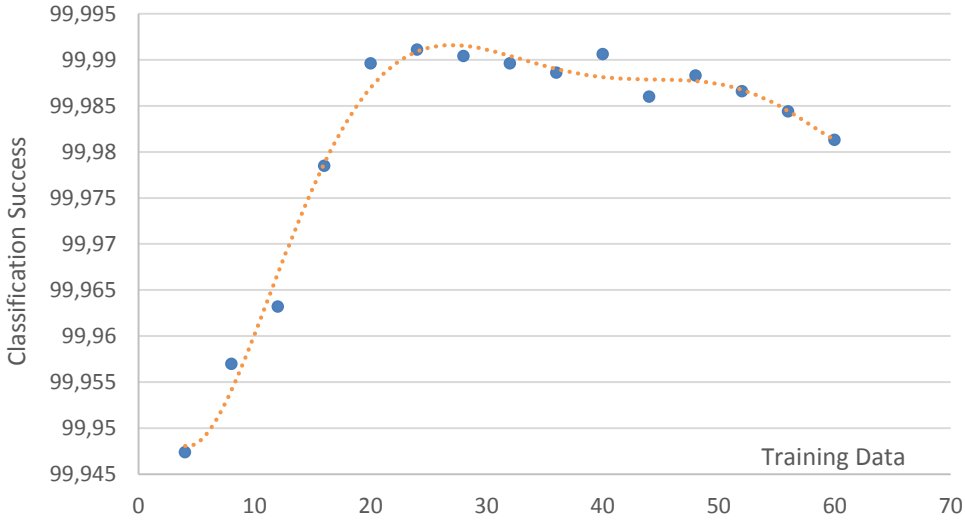

Fig. 6.10: Learning Curve

Optimal size of training data can be determined from the maximum of the Learning curve. For this case the number of training data is optimal for 24 sets.

Together with the size of training set, features for data classification must be determined. From the experimental results it is clear that differences between two classes (ferrous and non-ferrous material) are significant thus no more features for classification are needed. For classifying individual materials different approach must be used. Thanks to similar responses new features have to be found. These new features can be defined as certain relations between elemental features (10 magnitudes and 10 phases). When training the classifier only some of the most significant features can be taken for the training and testing to reduce the dimensionality. This is due to experimenting with these features, due to understanding features impact on classifying.

To reduce the dimensionality and to use most relevant features, Feature selection can be done. Feature selection decreases the dimensionality of data set by selecting only a subset of features. If the dimensionality is too large it may causes a decrease of performance. This is because some features may be irrelevant or redundant with respect to the classification process. Redundant features are those which provide no more information than the currently selected features, and irrelevant features provide no useful information in any context. Algorithms search for a subset of predictors that optimally model measured responses, subject to constraints, such as required or excluded features, and the size of the subset [68].

Algorithm combines a search technique for proposing a new feature subsets, together with an evaluation measure, which scores the different feature subsets. Advantage of Feature selection is to improve interpretability or shorter training times. It's also useful when datasets analysis is done, because Feature selection shows which features are important for a classification, and how are these features related.

Several feature selection algorithm like as *Branch and Bound* or *Pudil's floating feature selection* [57] are trying to solve the problem of selecting a subset from the N-dimensional measurement vector. Number of selected features can be defined by user. Optimal number of selected features has a positive effect on resulting classification. Various criteria can be used as a measure of the performance for evaluation of feature selection. These criteria are for example *inter-intra distance*, *Mahalanobis distances* or *1-Nearest Neighbor leave-one-out classification performance*. These criteria are described in many literatures for example in [57]. PRTools offers a large range of feature selection methods. Even the various evaluation criteria are implemented.

6.3.1. Classification of Ferrous and Non-ferrous Materials

Significant differences between ferrous and non-ferrous materials have been shown in chapter 5.3. Therefore classifier can be trained with corresponding magnitudes and phases from 24 training datasets. The values of phases in degrees are in different order than the values of magnitudes. This case, where features have different values, is not suitable for classification. Therefore values of magnitudes are multiplied by constant to get the values of magnitudes to the same order as values of phases.

To display the relation between selected classes a 2D scatterplot (Fig. 6.11) of the selected two features from the dataset can be used. Two features are selected for displaying the results of classifying. The Figure 2D scatterplot shows two features of two classes (ferrous – red and non-ferrous – blue) selected by *Branch and Bound* algorithm that uses *inter-intra distance* criteria. The displayed features are separated/classified with SVM classifier with linear kernel (red line). Same results can be obtained while using another algorithm (Pudil's floating feature) for the two selected features.

2D scatterplot helps to understand the relation between two (or more) classes and is used for better understandings of connection between assorted features.

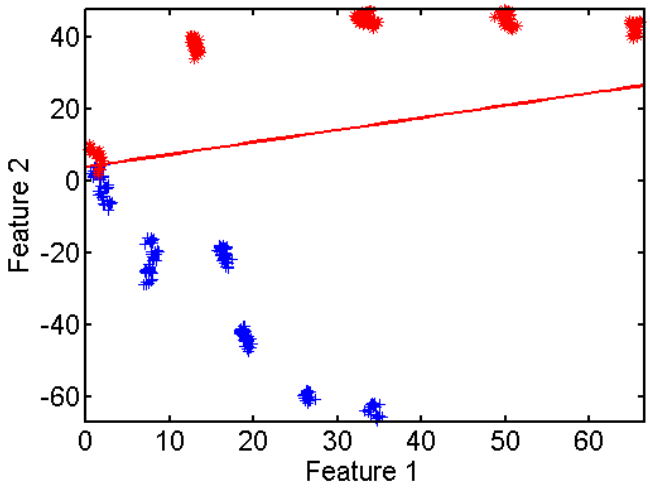

Fig. 6.11: 2D scatterplot of two selected features

All classifiers were trained from 6 measurements (i.e. 24 datasets) and tested on the different 14 measurements (i.e. rest of 80 datasets – 56 datasets). Compared classifiers are support vector classifier (SVC), k-Nearest Neighbors Classifier (KNNC) with optimized number of neighbors using the *leave-one-out error*, Linear Nearest Mean Classifier (NMC) and Naive Bayes classifier (naivebc). The

other classifiers are presented for comparison. Naive Bayes together with KNNC classifier, which were briefly described at the beginning of the chapter 5.4, are presented as an example of simple classifiers. KNNC gives good results for similar measured data but from its principle it isn't robust. Nearest Mean Classifier is standardly used classifier and it is used for comparison.

Results for experimental measures and datasets (as describes in 6.1.1) are displayed in Table 6.1.

Tab. 6.1: Comparison of various classifiers and its success rate in % for ferrous x nonferrous classes

Classifier	***SVC***	***KNNC***	***NMC***	***naivebc***
All features	100%	100%	94.44%	97.32%
Branch and Bound selected 2 features	97.92%	98.51%	94.74%	95.73%

From these classifying results it is evident that if the induced voltage, which corresponds to detected target, is strong enough and target is pinpointed correctly, thanks to multiple frequency approach, there is 100% chance to differentiate between ferrous and non-ferrous materials. If *Pudil's floating feature selection* algorithm is used to select optimal number of features, algorithm selects all 20 used features.

6.3.2. Classification of Individual Non-ferrous Materials

Classification of non-ferrous materials has to be done using different approach. Differences between individual measured non-ferrous materials are slight, especially for small diameters. Therefore to improve classification process additional features should be added. Added features do not need to have any physical nature and it can be defined using existing features. To improve the classification, ratio of magnitudes and phases of each 10 investigating frequency were added together with the differences between two subsequent values of phases (9 features). These features were selected based on results in chapter 5.3.

This adds 19 new features that can improve the separation of individual non-ferrous objects. Values of magnitudes as well as in previous case are multiplied by constant to get to the same order as values of phases. Classifiers were trained from non-ferrous object of the 6 measurements and tested on the different non-ferrous objects from 14 measurements.

2D scatterplot (Fig. 6.12) is used to display the relation between all three classes of the selected two features from the dataset together with a SVM classifier.

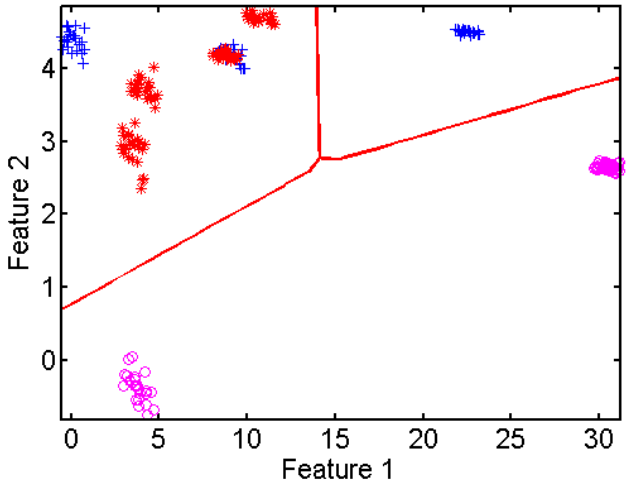

Fig. 6.12: 2D scatterplot of two selected features

Table 6.2 shows comparison of results for various numbers of features and for used classifiers.

Tab. 6.2: Comparison of various classifiers and its success rate in % for non−ferrous classes

Classifier	***SVC***	***KNNC***	***NMC***	***naivebc***
20 elemental features	89.46%	99.29%	50%	90%
All features	91.25%	99.29%	50%	90%
Branch and Bound selected 2 features	68.21%	91.61%	70.54%	86.25%

From Table 6.2 is evident that if only two features are used, classifying success of SVC is less than 70%. If 20 elemental features of all 10 investigated frequencies are used, classification success increases to 89.46%. Classification success increases again to 91.07% when all 39 features are used. However this does not mean that the increasing number of features (dimensionality) the error rate will decrease. With overall increase of dimensionality the error rate could be increasing again. The error rate's dependency on number of used features of individual non-ferrous materials is shown in Fig. 6.13.

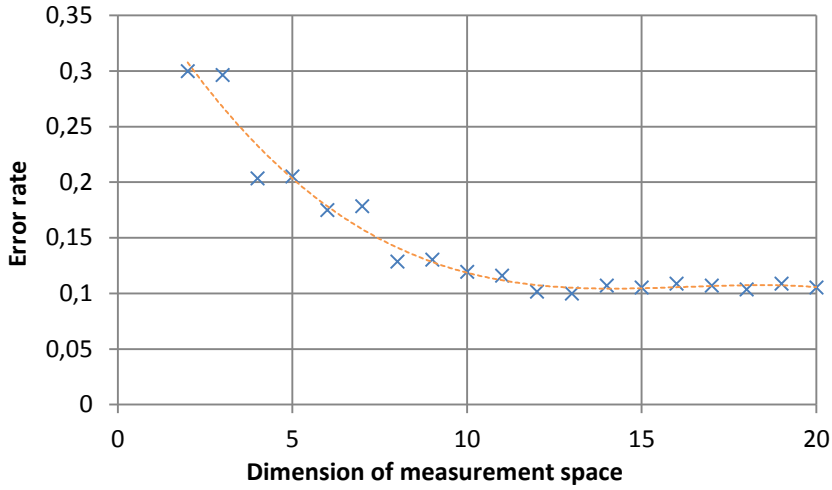

Fig. 6.13: Error rates versus dimension of measurement space

It is worth mentioning that KNNC has more than 99% success rate. This classifier gives good results for similar data i.e. when the target is in similar distance as data in training set and testing set is pinpointed in the same method. But it is known that this classifier gives worse results for various data, because it works on very simple learning algorithm.

6.3.3. Classification of Individual Ferrous Materials

Classification of individual ferrous materials must be done using similar or even the same approach as classification of non-ferrous materials. Thanks to small differences between individual materials, additional features should be also added. As the features, added in classification of non-ferrous materials, have been proven, the same features have been added for this classification. Therefore the classification has been done under the same conditions as classification of Individual Non-ferrous materials.

Fig 6.14 shows the relation between two ferrous materials using selected two features from the data set together with a SVM classifier.

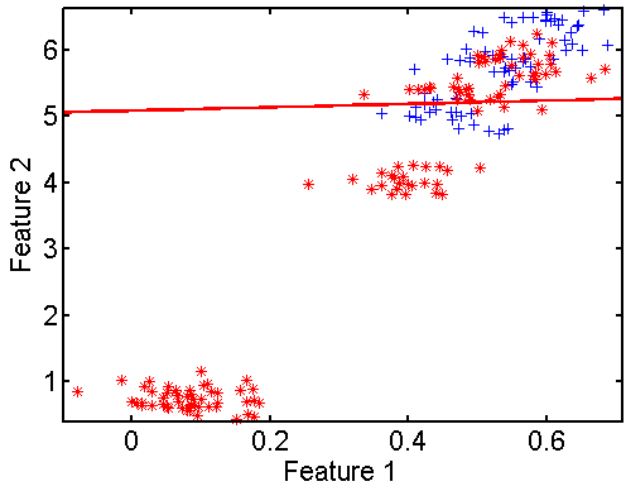

Fig. 6.14: 2D scatterplot of two selected features

Table 6.3 shows results for all tested classifiers and for various numbers of features. Results show similar trend as classifying non-ferrous materials.

Tab. 6.3: Comparison of various classifiers and its success rate in % for ferrous classes

Classifier	***SVC***	***KNNC***	***NMC***	***naivebc***
20 elemental features	94.42%	100%	50%	85.94%
All features	97.32%	99.33%	54.46%	86.16%
Branch and Bound selected 2 features	66.96%	86.16%	75%	78.35%

If only two features selected by *Branch and Bound* algorithm were used, SVC success rate was only 66.96%. The success rate increased to 94.42%, when 20 elemental features of 10 investigating frequency were used for classification. This confirms previous results that if multiple frequencies are used, there are more features for classification available and therefor better results can be achieved. Classification success increased to 97.32% if all defined features (39) were used.

KNNC shows that increasing number of features does not decrease error rate. Success rate is 100% for 20 features and 99.33% for 39 features. For comparison results of others classifiers are presented also.

For comprehensive overview of the error rates' dependency on number of selected features of individual ferrous materials is shown in Fig. 6.15.

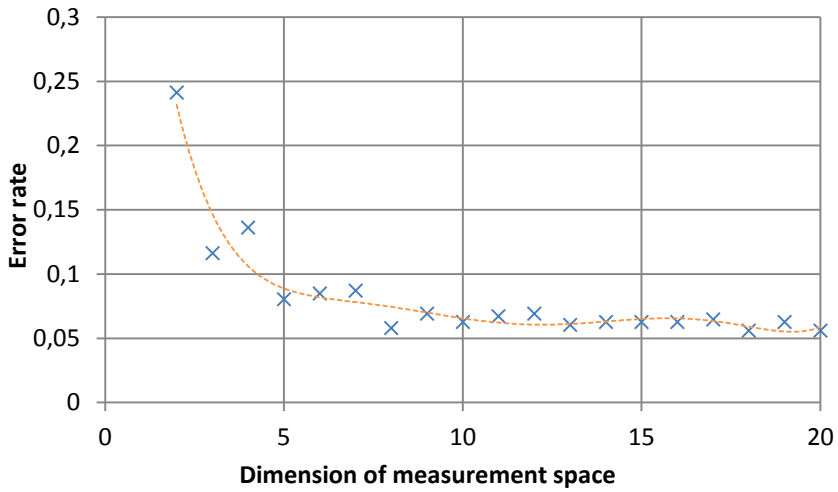

Fig. 6.15: Error rates versus dimension of measurement space

6.3.4. Objects Sizes Classification

The last classification which is presented is object size estimation. However the object size estimation can be done under specific condition. To determine the approximate size, rough distance from the located object should be known. How to estimate the depth of the located object is presented in [69] or [70]. Results presented here are about the same distance from the detector head.

As spheres with diameter from 10 mm to 25 mm and testing object (Fig. 6.4) were measured, classification into the three classes was chosen. The 1st class includes object sizes to 10 mm, the 2nd class includes object sizes from 11 mm to 20 mm and last class includes objects larger than 21 mm. Results presented in Table 6.4 confirm results obtained in previous subsections.

Tab. 6.4: Comparison of various classifiers and its success rate in % for different sizes of materials

	Classifier	***SVC***	***KNNC***	***NMC***	***naivebc***
Non-ferrous	All features	100%	100%	85.94%	100%
	Branch and Bound selected 2 features	100%	100%	87.5%	100%
	Pudil's floating optimum number of features	100%	100%	96.87%	100%
Ferrous	All features	99.55%	99.55%	88.84%	100%
	Branch and Bound selected 2 features	99.33%	100%	97.54%	98.88%
	Pudil's floating optimum number of features	99.78%	99.55%	88.84%	100%

There is possibility, thanks to multiple frequencies, to distinguish between different sizes of located ferrous and non-ferrous objects in given condition. As approximate depth of the object is not always known, it can be used only in specific cases.

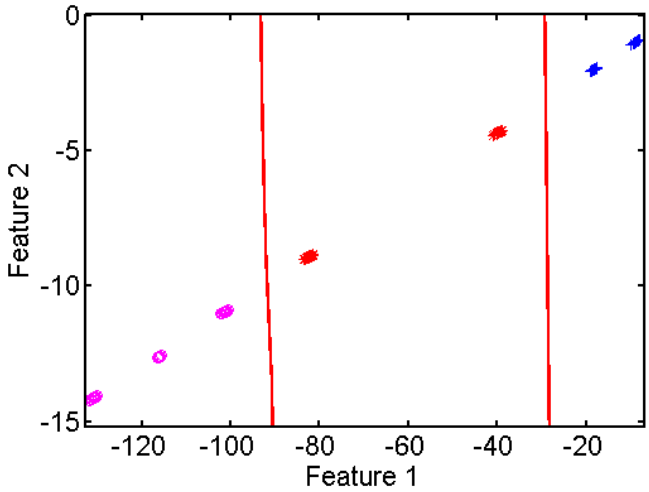

Fig. 6.16: 2D scatterplot of two selected features of non-ferrous materials

Fig 6.16 shows the relation between all three size classes of non-ferrous materials using selected two features from the dataset together with a SVM classifier. It is evident that even using only two features (selected by *Branch and Bound* algorithm), classification can be done successfully. This is shown also in Fig. 5.36. Differences between individual sizes are significant due to significant phase difference of the response.

Fig. 6.17 shows the same relation but for ferrous materials. Situation for ferrous materials is little different. As shown in Fig. 5.35 the differences between individual materials were not significant, especially in phase response. The values for diameters from 10 mm to 20 mm are similar. Apparent difference was in their trends. Due to added features (see 2D scatterplot, x-axis - difference between two subsequent values of phases and y-axis - ratio of magnitude and phase) classification by SVC (red line) is done adequately.

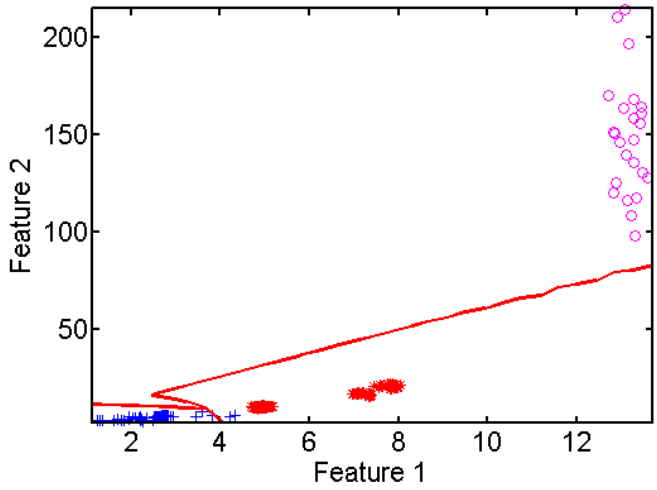

Fig. 6.17: 2D scatterplot of two selected features of ferrous materials

6.4. Summary

Support vector classifier was used for a measured data classification primarily together with other classifiers. Classifications of measured materials into ferromagnetic and non-ferromagnetic classes has been done as well as classification into individual materials. Classification into the object sizes also has been done. Experiments showed that if multiple frequencies – their magnitudes and phases are used as features for classification and new features (relations between existing ones) are added, successfully classification can be.

[56] Venkatesan, R., Ganesan, R., Selvakumar, A. A. L., 2012. A Survey on Intrusion Detection using Data Mining Techniques, International Journal of Computers and Distributed Systems, vol. 2, no. 1, pp. 54–58.

[57] Heijden, F., Duin, R.P.W., Ridder, D., Tax, D. M. J., 2004. *Classification, Parameter Estimation and State Estimation: An Engineering Approach using MATLAB*, John Wiley & Sons.

[58] Kraidl, M., 2001. *Diagnosticke systemy*, CVUT, Prague, ISBN: 80-01-02349-4.

[59] Mohri, M., Rostamizadeh, A., Talwalkar, A., 2012. *Foundations of Machine Learning*, The MIT Press.

[60] Hastie, T., Tibshirani, R., Freedman, J., 2009. *The Elements of Statistical Learning: Data Mining*, Inference, and Prediction, Second edition, Springer.

[61] Hofmann, M., Klinkenberg, R., 2014. *Rapid Miner: Data Mining Use Cases and Business Analytics Applications*, CRC press.

[62] StatSoft, Inc. (2013). Electronic Statistics Textbook. Tulsa, OK: StatSoft. [online] Available at < http://www.statsoft.com/textbook/>.

[63] Delft University of Technology, 2014. [online] Available at <http://prtools.org/>.

[64] Ripka, P., Janosek, M., Novacek, P., 2010. Depth estimation of metal objects, *Proc. Eurosensors XXIV*, Linz, Austria, pp. 280-203.

[65] Weston, J., Mukherjee, S., et all, 2000. *Feature Selection for SVM*, The UCL Department of Computer Science, London's Global University, London, UK.

[66] Mathworks, 2014. [online] Available at <http://www.mathworks.com/help/stats/support-vector-machines-svm.html>.

[67] Beleites, C. and Neugebauer, U. and Bocklitz, T. and Krafft, C. and Popp, J., 2013. Sample size planning for classification models. *Anal. Chim. Acta*, vol. 760, pp. 25-33.

[68] Mathworks, 2014. [online] Available at <http://www.mathworks.com/help/stats/feature-selection.html>.

[69] Das Y., McFee J. E., Chesney, R. H., 1985. Determination of Depth of Shallowly Buried Objects by Electromagnetic Induction, *IEEE Trans. on Geoscience & Remote Sensing*, vol. 23, no. 1, pp. 60-66.

[70] Das Y., McFee J. E., Toews, J., Stuart, G. C., 1990. Analysis of an Electromagnetic Induction Detector For Real-Time Location of Buried Objects, *IEEE Trans. on Geoscience & Remote Sensing*, vol. 28, no. 3, pp. 278-288.

7. Conclusion

The main goal of this dissertation was to analyze and to verify possibilities of using polyharmonic excitation signals to improve the identification of located metal objects. Since the eddy current metal detectors remain the most commonly used type of metal detectors in archeology, treasure hunting, mine clearance or in security, all the experiments were done on this type of detector only. Although eddy current metal detectors have discrimination ability, thanks to different phase shifts of induced voltage which corresponds to detected metal materials, there is still an uncertainty how to avoid undesirable metal materials or what kind of target has been found. This is due to the fact that some of them causes similar phase shift of the induced voltage. For this reason the dissertation was focused to improve their identification ability.

The main shortcoming of present day detectors and their discrimination ability lies in the fact that the majority of them use only one frequency excitation signal for detecting and identifying objects. Thus the information about the detected object is contained in one frequency. However, the operator needs more information to detect and identify object. This led the author of this dissertation to an idea to use multifrequency signals.

Considering the partial list of the dissertation objectives each part of it is fulfiled.

- *Analysis of the system properties excited by a polyharmonic signals (see chapter 4.2 for details)*

  Behavior of electromagnetic induction has been explained by a *Simple circuit model*. *Response Function* $G(\alpha)$ has been defined. It has been shown that in *Simple circuit model Response Function* of the object/target depends on its electromagnetic properties and frequency. Theoretical analysis for a homogenous sphere, which represents well a common small object, has been studied in more detail. It has been shown that induced voltage can be expressed as a sum of infinite geometric series and frequency dependent terms. This expression can be divided into its real and imaginary part; Geometry dependent term - real part and *Response Function* – complex part. Under certain conditions and for a *Dipole Approximation* higher orders can be neglected and only the first term is relevant. Furthermore in a quasi-static approximation the *Response Function* depends only on objects properties (μ, σ, a) and on operating frequency f of the detector but not on its position. *Response Function* of non-ferromagnetic objects is similar to the *simple circuit model*. Non-ferromagnetic materials shift the phase to negative values only (from 0° to −90°) in contrast to ferromagnetic materials which have phase shift to positive values as well (from +90° to −90°). Therefore differentiation between ferrous

and non-ferrous objects can be done thanks to its phase response but not by using one frequency. Measuring by one frequency only may result in a negative value for some frequencies for both types of materials. However, the phase of the *Response Function* depends as on objects properties and also on operating frequency. Thanks to the multiple frequencies, which polyharmonic signal contains, there is an opportunity to measure a wide band of the *Response Function* and better characterize the detected object.

- *Verification of the system properties using an excitation by a multiple frequency signals (see chapter 5.1 for details)*

For all experiments ATMID metal detector search head has been used. The behavior of the ATMID search head configuration was verified on the experimental coil. Due to ATMID coil parameters, operating frequencies of the detector were at frequency range from 1 kHz to 25 kHz. Parameters of the coil were described in detail in chapter 4.3. For *Response Function* verification a multifrequency step sweep sine-wave signal and polyharmonic chirp signal were used. Step sweep sine-wave signal confirms expected response of ferromagnetic and non-ferromagnetic materials for different frequencies which were described. Experiments showed differences between ferrous and non-ferrous materials and its sizes not only in their phase shift but also in amplitude of induced voltage. Chirp signal and its signal processing in frequency domain showed possibilities how to use of polyharmonic signal for metal detection. Thanks to amplitude and phase spectra one gets response of the target in a wide band. More experiments with the chirp signal were not conducted because of usage of similar technique by Minelab company. Another polyharmonic signal which comes into consideration was sinc signal.

- *Experimental measured data processing in time and frequency domain (see chapter 5.3 for details)*

All experimental data were measured using the sinc signal as the excitation signal. The sinc signal thanks to its spectrum with easily defined numbers and positions of individual frequencies, which are appropriate for further spectral analysis of the *Response Function*, was shown to be as a perspective excitation polyharmonic signal. Another advantage of the sinc signal lies in a possibility to generate it by any generator with DDS. Thanks to that it appeared as an ideal polyharmonic signal used for metal objects identification. Several experiments have been done using such excitation signal. Results were processed in both time and frequency domain. Spheres of different diameters and from different ferrous and non-ferrous materials were used as specimens. In time domain the sinc signal does not offer any attractive methods for advanced identification of objects. This is due to the fact that in

time domain individual frequencies cannot be examined separately but only the signal as a whole. Experiments showed that Crest factor can be used as a simple method how to distinguish between ferrous and non-ferrous materials. However, this method can be used only if the response from the detected object was strong enough. The capability of differentiation of objects is decreasing with increasing of distance or with decreasing of diameter. In frequency domain signal processing by means of DFT using FFT algorithm were done. Thanks to that amplitude and phase spectra with multiple frequencies are obtained. The *Response Function* of the detected object over a wide band of frequencies. This response has been used for further object identification. Experiments show that thanks to multiple frequencies approach, differentiation between even similar objects (in a way of electromagnetic response) can be done.

- *Classification of measured data into classes (see chapter 6.3 for details)*

As part of the work, classifications of ferromagnetic and non-ferromagnetic materials were done based on experimental measured data as well as classification of individual ferrous and non-ferrous materials and estimation of the size of the classified object. For data classification support vector classifier was used primarily together with other classifiers. Measured data showed that if multiple frequencies (its magnitudes and phases) are used as features and new features (relations between existing ones) are added, the classification can be done successfully. Efficiency of the classification decreases with increasing distance between the detector and target and if the size of the targets is getting smaller.

A standard single tone method offers the greatest sensitivity thanks to possibility of using a synchronous demodulator. Special synchronous demodulators offer signal to noise ratio up to 120 dB, compared with polyharmonic signal method where synchronous demodulation cannot be done. Polyharmonic signals have to be digitized. Signal to noise ratio of such measure chain, which is composed of preamplifier and analogue to digital converter, does not reach usually more than 90 dB. Detailed analysis is presented at the chapter 5.4.

Single tone methods shortcoming is in that an information about detected object is contained only in phase shift. Therefore single phase measure itself is not sufficient to state whether the object is ferromagnetic or non-ferromagnetic or even what type of material is made of. Advantage of polyharmonic methods is based on multiple frequencies approach. Thanks to multiple frequencies a response of detected object is a wide band. In this case the information about

detected object is contained in phase and amplitude spectra. It enables better identification of detected object.

Together with presented methods several other methods were examined. In time domain it was correlation methods and fitting methods. In frequency domain Hilbert transformation method was tested. All of these methods didn't give any relevant results. Finally, it must be noted, that although in general, classification or identification of an object cannot be done successfully, it still might be possible to extract some valuable additional information from the response of the detected object for the operator, such as if detected object is ferromagnetic or non-ferromagnetic.

7.1. Future Research

There were new multi-frequency methods and processing algorithms being developed. The next step, experimental measurement in order to acquire data under realistic conditions, should be accomplish.

At first, measurement under a different ground conditions can be done to verify usage of polyharmonic signal sinc to detect buried objects in various environments. The focus should be put on some specific objects such as mines. Based on these measurements a database of templates can be created to provide objects classification (for example mine or debris) or identification (mine type). From this database there should be enable to collect a useful characterization of the detected object (mine).

Secondly, the classification by support vector machine classifier can be done using other nonlinear kernels such as polynomial. Together with nonlinear kernel, adding another new features to improve the classification ability of the classifier can be considered.

8. List of Publications

8.1. Related with Thesis

8.1.1. Publications in Journals with Impact Factor

[1] Svatos, J. (70%) - Fexa, P. (15%) - Vedral, J. (15%): Metal Detector Excited by Frequency Swept signal In: Metrology and Measurement Systems. 2011, vol. 18, no. 1, p. 57-68. ISSN 0860-8229. *Times Cited: 3*

[2] Svatos, J. (50%) - Novacek, P. (45%) - Vedral, J. (5%): Sin(x)/x Signal Utilization in Metal Detection and Discrimination In: Magnetic Measurements 2012. Bratislava: Slovak University of Technology, 2012, p. 46. ISBN 978-80-227-3770-8. *Times Cited: 0*

[3] Svatos, J. (80%) - Vedral, J. (20%): The Usage of Frequency Swept Signals for Metal Detection In: IEEE Transactions on Magnetics. 2012, vol. 4, no. 48, p. 1501-1504. ISSN 0018-9464. *Times Cited: 1*

[4] Svatos, J. (80%) - Vedral, J. (15%) – Kriz, M. (5%): Application of Unconventional Polyharmonic Signals for Eddy Current Based Metal Detection and Discrimination In: Metrology and Measurement Systems. In review. 2014. *Times Cited: 0*

8.1.2. Publications in ISI

[1] Svatos, J. - Fexa, P. - Vedral, J.: Metal Detector Excited by Polyharmonic Signals In: Applied Electronic 2010. Pilsen: University of West Bohemia, 2010, p. 339-342. ISBN 978-80-7043-865-7. *Times Cited: 0*

[2] Novacek, P. - Svatos, J.: Intelligent Metal Detector In: Key Engineering Materials: Transtech Publications, 2013, p. 133–136. ISSN 1013-9826. *Times Cited: 0*

8.1.3. Other Publications

[1] Svatos, J - Vedral, J.: Using of Frequency Swept Signals for Metal Detection, In: 20th International Conference on Soft Magnetic Materials, Book of Abstract, Kos Island, 2011, p. 144, ISBN 978-960-9534-14-7. *Times Cited: 0*

[2] Svatos, J. - Vedral, J. - Nováček, P.: Summary of Non-traditional Methods for Metal Detection and Discrimination In: Eurosensors XXVI - 2012 - The 26th European Conference on Solid-State Transducers, Kraków: Wydawnictwo Politechniki Krakowskiej, 2012, p. 298–301. ISSN 1877-7058. *Times Cited: 0*

[3] Svatos, J. - Vedral, J. - Novacek, P.: Metal Object Detection and Discrimination Using Sinc Signal In: BEC 2012 - Proceedings of the 13th Biennial Baltic Electronics Conference, Tallinn Technical University, 2012, p. 307-310. *Times Cited: 0*

[4] Novacek, P. - Svatos, J.: Intelligent Metal Detector In: IC-MAST - 2012 - 2nd International Conference on Materials and Applications for Sensors and Transducers, Abstracts Book. Athens: National Technical University, 2012, p. 145. *Times Cited: 0*

[5] Svatos, J.: Software for Metal Object Detection In: Graphical Development Environment Labview In: International Masaryk Conference for Ph.D. Students and Young Researchers. Praha. 2013. *Times Cited: 0*

8.2. Non-related with Thesis

8.2.1. Publications in Journals with Impact Factor

[1] Vedral, J. (55%) - Fexa, P. (30%) - Svatos, J. (15%): DAC Testing Using Modulated Signals In: Metrology and Measurement Systems. 2011, vol. 18, no. 2, p. 283-293. ISSN 0860-8229. *Times Cited: 3*

[2] Vedral, J. (70%) - Svatos, J. (20%) - Fexa, P. (10%): Methods for Economical Test of Dynamic Parameters ADCs In: Metrology and Measurement Systems. 2009, vol. 15, no. 1, p. 161-170. ISSN 0860-8229. *Times Cited: 1*

8.2.2. Publications in ISI

[1] Vedral, J. - Svatos, J. - Fexa, P.: Economical Test of Internal ADC in Embedded Systems In: XIX IMEKO World Congress 2009 – Fundamental and Applied Metrology, Lisbon: Instituto Superior Técnico/Instituto de Telecomunicações Portugal, 2009, p. 702-705. ISBN 978-963-88410-0-1. *Times Cited: 1*

[2] Fexa, P. - Svatos, J. - Vedral, J.: High Resolution Audio Codec Test In: MEASUREMENT 2009 - Proceedings of the 7th International Conference on Measurement. Bratislava: Institute of Measurement Science, 2009, p. 209. ISBN 978-80-969672-1-6. *Times Cited: 0*

[3] Svatos, J. - Fexa, P. - Vedral, J.: Methods of Education Electronic Measurement Circuits and Systems at FEE CTU In: Applied Electronic 2009. Pilsen: University of West Bohemia, 2009, p. App. 9-App. 12. ISBN 978-80-7043-781-0. *Times Cited: 3*

[4] Fexa, P. - Svatos, J. - Vedral, J.: FM and QAM Signals for ADC Testing In: Applied Electronic 2010. Pilsen: University of West Bohemia, 2010, p. 359-362. ISBN 978-80-7043-781-0. *Times Cited: 0*

[5] Vedral, J. - Svatos, J. - Fexa, P.: Using of AM and FM Signal for ADC Testing In: I2MTC International Instrumentation and Measurement Technology Conference. Austin, Texas, 2010, p. 508-511. *Times Cited: 0*

8.2.3. Other Publications

[1] Fexa, P. - Svatos, J. - Vedral, J.: Dynamic Testing of Audio Codec In: Electronic Devices and Systems, IMAPS CS International Conference 2009 Proceedings. Brno: VUT v Brně, FEI, 2009, vol. 1, p. 63-68. ISBN 978-80-214-3933-7. *Times Cited: 0*

[2] Vedral, J. - Svatos, J. - Fexa, P.: Laboratory of Analog Signal Processing and Digitizing at FEE CTU in Prague In: XIX IMEKO World Congress 2009 – Fundamental and Applied Metrology, Lisbon: Instituto Superior Técnico/Instituto de Telecomunicações Portugal, 2009, p. 15-19. ISBN 978-963-88410-0-1. *Times Cited: 0*

[3] Vedral, J. - Svatos, J. - Fexa, P.: Comparative Testing of Dynamic Parameters DACs with Multi-Tone Signals In: IMEKO Symposium TC-4, TC-19 & IWADC Instrumentation for the ICT Area. Košice: Technical University of Košice, 2010. p. 75-80. *Times Cited: 0*

[4] Svatos, J – Kriz, M.: Education methods of analogue to digital converters testing at FE CULS In: 13th International Scientific Conference on Engineering for Rural Development 2014. Latvia University of Agriculture, 2014, p. 571–576, ISSN 1691-3043. *Times Cited: 0*